





Narrow absorption lines from intervening material in supernovae

I. Measurements and temporal evolution

Santiago González-Gaitán¹, Claudia P. Gutiérrez^{2,3}, Joseph P. Anderson^{4,5}, Antonia Morales-Garoffolo⁶, Lluís Galbany^{3,2}, Sabyasashi Goswami^{1,6}, Ana M. Mourão¹, Seppo Mattila^{7,8}, and Mark Sullivan⁹

¹ CENTRA, Instituto Superior Técnico, Universidade de Lisboa, Av. Rovisco Pais 1, 1049-001 Lisboa, Portugal
e-mail: gongsale@gmail.com

² Institut d'Estudis Espacials de Catalunya (IEEC), Gran Capità, 2-4, Edifici Nexus, Desp. 201, E-08034 Barcelona, Spain
e-mail: cgutierrez@ice.csic.es

³ Institute of Space Sciences (ICE, CSIC), Campus UAB, Carrer de Can Magrans, s/n, E-08193 Barcelona, Spain

⁴ European Southern Observatory, Alonso de Córdova 3107, Casilla 19, Santiago, Chile

⁵ Millennium Institute of Astrophysics MAS, Nuncio Monsenor Sotero Sanz 100, Off. 104, Providencia, Santiago, Chile

⁶ Department of Applied Physics, School of Engineering, University of Cádiz, Campus of Puerto Real, E-11519 Cádiz, Spain

⁷ Tuorla Observatory, Department of Physics and Astronomy, University of Turku, FI-20014 Turku, Finland

⁸ School of Sciences, European University Cyprus, Diogenes Street, Engomi, 1516 Nicosia, Cyprus

⁹ School of Physics and Astronomy, University of Southampton, Southampton, SO17 1BJ, UK

ABSTRACT

Narrow absorption features in nearby supernova (SN) spectra are a powerful diagnostic of the slow-moving material in the line of sight: they are extensively used to infer dust extinction from the host galaxies, and they can also serve in the detection of circumstellar material originating from the SN progenitor and present in the vicinity of the explosion. Despite their wide use, very few studies have examined the biases of the methods to characterize narrow lines, and not many statistical analyses exist. This is the first paper of a series in which we present a statistical analysis of narrow lines of SN spectra of various resolutions. We develop a robust automated methodology to measure the equivalent width (EW) and velocity of narrow absorption lines from intervening material in the line of sight of SNe, including Na I D, Ca II H&K, K I and diffuse interstellar bands (DIBs). We carefully study systematic biases in heterogeneous spectra from the literature by simulating different signal-to-noise, spectral resolution, slit size and orientation and present the real capabilities and limitations of using low- and mid-resolution spectra to study these lines. In particular, we find that the measurement of the equivalent width of the narrow lines in low-resolution spectra is highly affected by the evolving broad P-Cygni profiles of the SN ejecta, both for core-collapse and type Ia SNe, inducing a conspicuous apparent evolution. Such pervading non-physical evolution of narrow lines might lead to wrong conclusions on the line-of-sight material, e.g. concerning circumstellar material ejected from the SN progenitors. We present thus an easy way to detect and exclude those cases to obtain more robust and reliable measurements. Finally, after considering all possible effects, we analyse the temporal evolution of the narrow features in a large sample of nearby SNe to detect any possible variation in their EWs over time. We find no time evolution of the narrow line features in our large sample for all SN types.

Key words. supernovae:general, ISM: lines and bands, ISM: dust and extinction

1. Introduction

The light emitted by astrophysical sources detected from Earth is subject to interaction with matter that lies along the line of sight between the source and the observer. Studying the effects of this line of sight material on the background light source gives information on the nature of that material, whether it is close to the light source, e.g. circumstellar material (CSM), within galaxies, i.e. the interstellar medium (ISM), or between galaxies, i.e. the intergalactic medium (IGM). It is important to understand these processes: CSM for stellar mass loss and ISM and IGM for galaxy enrichment and evolution. At the same time, this intervening material is also extremely important for un-

derstanding the light sources themselves as it absorbs the light, especially dimming it at optical wavelengths and re-emitting it at longer wavelengths. It thus impacts on our understanding of the brightness and properties of the emitters.

This material in the line of sight may be composed of dust and gas. Dust grains are a product of stellar evolution and responsible for the effect of absorption and reddening of optical starlight (e.g., [Draine 2011](#)). Molecular gas is known to exist, e.g. in the form of hydrogen (H₂) and of carbon monoxide (CO) ([Dame et al. 2001](#)) but also in the form of diffuse interstellar bands (DIBs) which trace as-yet-unidentified molecules (e.g. [Lan et al. 2015](#)). On the other hand, the atomic gas phase component of the inter-

vening material is mostly composed of hydrogen. Nevertheless, a fraction of metals is also present and provides valuable information on the chemistry, ionization state and gas temperature of the line-of-sight matter. These different species will absorb the light at characteristic wavelengths, generating detectable absorption lines in the spectroscopic observations.

Optical interstellar absorption lines in the form of sodium, calcium, potassium and DIBs have long been observed in spectroscopic binaries (e.g., Heger 1919a,b; Young 1922), in early-type stars (Struve 1928; Wilson & Merrill 1937; Merrill 1937; Sanford 1937; Evans 1941), in novae (Merrill 1935), in galaxies (e.g. Heckman & Lehnert 2000), in active galactic nuclei (e.g. Baron et al. 2016) and in supernovae (SN; e.g. Penston & Blades 1980). In contrast to material moving at high velocity, as is the case for SN ejecta, these intervening lines will appear much narrower than the characteristic P-Cygni profiles of fast-expanding material. Today, narrow interstellar lines are routinely detected in the optical spectra of a great number of astrophysical transients (e.g., Galazutdinov 2005; Megier et al. 2009; Chen et al. 2010; Park et al. 2015). The relation of the strength of these lines with colour excess and extinction has been studied in depth (e.g. Merrill & Wilson 1938; Spitzer 1948; Buscombe & Kennedy 1968; Hobbs 1974) providing empirical relations between the amount of dust extinction and strength of the gas lines (e.g., Richmond et al. 1994; Munari & Zwitter 1997; Turatto et al. 2003; Poznanski et al. 2012; Murga et al. 2015), with caveats for the sodium line since it saturates (Munari & Zwitter 1997; Poznanski et al. 2011). Alternative lines like potassium (e.g. Hobbs 1974; Munari & Zwitter 1997; Galazutdinov 2005; Phillips et al. 2013) and DIBs (Kos & Zwitter 2013; Phillips et al. 2013; Krelowski et al. 2019) have been claimed to be superior extinction tracers.

SNe offer a particularly good laboratory to investigate the material in the line of sight as they are bright and are found in many different environments. On the other hand, understanding this material is also key to understanding SN progenitor systems and their explosions, as it can give us information on stellar evolution and mass loss. Indeed, the study of narrow line-of-sight lines in transient objects has increased during the last few years, partly due to the detection of time-variable absorption features in high-resolution spectra. While intermediate-luminosity red transients embedded in dusty cocoons show clear signs of sodium line strength evolution (Byrne et al. 2023), the only SN coming from the core collapse of a massive star showing this evolution is the broad-lined type Ic, SN 2012ap (Milisavljevic et al. 2013), with changes in the strength of the DIBs but no variations in the sodium lines. The authors conclude that the material producing these variations is nearby, and the SN interacts with it. More surprisingly, a handful of type Ia SNe – the thermonuclear runaway of white dwarfs in binary systems – have shown evolving sodium lines in high-resolution spectra: SN 2006X (Patat et al. 2007), SN 1999cl (Blondin et al. 2009), SN 2007le (Simon et al. 2009), SN 2013gh (Ferretti et al. 2016), and SN 2014J with time-varying potassium instead of sodium (Graham et al. 2015). This has significant implications for the debate surrounding the SN progenitor system: it has been suggested that such variable lines could originate from the CSM ejected by the progenitor system, in principle favouring the single degenerate scenario of a binary system com-

posed of a white dwarf and a main-sequence or red giant (e.g. Moore & Bildsten 2012). However, double degenerate models composed of two white dwarfs could potentially also exhibit CSM characteristics (Raskin & Kasen 2013; Shen et al. 2013; Levanon & Soker 2019). Such CSM claims are further emphasized with the observation of a statistical excess of blueshifted (vs redshifted) sodium absorption lines in high-resolution SN Ia spectra (Sternberg et al. 2013; Maguire et al. 2013; Phillips et al. 2013; Clark et al. 2021), that may also be related to other SN properties such as ejecta velocity and SN colour (Foley et al. 2012a).

On the other hand, measurements of narrow lines from intervening material in SN Ia spectra of lower resolution have also shown intriguing correlations between line strength and intrinsic SN properties such as the nebular velocity shifts (Förster et al. 2012) and the late colour decline rate (Förster et al. 2013), arguing again for a possible interaction of nearby material with a sub-group of SNe Ia. This has been recently confirmed by Wang et al. (2019) also with low/mid-resolution spectra who additionally find possible line evolution in the interacting SNe Ia.

A significant caveat of the above studies is that lower resolution and signal-to-noise ratio (S/N) spectra may affect or even prevent proper measurements. Can low and mid-resolution spectra be used to infer narrow line equivalent widths and velocities? Can weaker lines such as DIBs and potassium reliably be detected in such spectra? Can the presence of the high-velocity, broad features from the SN ejecta interfere with the narrow line measurements? Are there any biases that could simulate an apparent evolution or blueshift? Given the large amount of SN spectra gathered in the literature and the scarcity of methods to investigate the material in the line of sight of the SN, the capability to robustly use these spectra for narrow lines studies could provide powerful, statistically meaningful results on the presence and distribution of these species in the intervening matter.

In order to investigate narrow lines, we use here simulations and a large sample of observed SNe from the literature that consists of more than 1000 objects of different types –including SNe Ia, SNe II (classical plateau and linearly declining hydrogen-rich SNe), stripped-envelope SNe (SESNe) with SNe Ic, SNe Ib and SNe IIb, and interacting SNe including SNe IIn, SNe Ibn and SNe Icn. The spectra and simulations include various spectral resolutions that allow us to test several different possible biases in the measurements of equivalent widths and velocities of narrow line-of-sight lines. After defining the limitations of our technique, we also look into the likelihood that these lines in SN spectra evolve over time. In forthcoming papers, we will investigate the differences in these lines for various SN types, SN properties and environmental characteristics.

The paper is organised as follows. Section 2 introduces the lines from intervening matter analysed in this study. We present the data sample in Section 3 and the automated line measurement in Section 4. The systematic biases are presented in Section 5, while the evolution analysis and discussion are in Section 6. We conclude in Section 7.

2. Line-of-sight absorption lines

The properties of the ISM of a SN host galaxy and, more specifically, the environment where the SN exploded – or of the CSM ejected by the progenitor prior to explosion

– can be studied with spectroscopy. The spectral resolution, usually given by $R = \lambda/\Delta\lambda$ reveals the capacity of the instrument to resolve narrower lines; we define here high-resolution spectra as those with $R \gtrsim 10000$ (or $\Delta v < 30\text{km/s}$; Appenzeller 1986) and mid-resolution as $5000 < R < 1000$ (or $30\text{km/s} < \Delta v < 60\text{km/s}$). In nearby objects exploding in reddened environments, it is possible to detect narrow lines close to the host galaxy’s rest-frame line wavelength, but also due to the MW close to the observer-frame line wavelength, at a variety of spectral resolutions and signal-to-noise ratios, as will be shown later (sections 5.2 and 5.3).

We outline here the main optical absorption lines that can be measured and utilised to investigate the ISM and the extinction towards SNe.

- Sodium (Na I D) lines are very prominent and the typical tracers of the ISM. They were discovered in the solar spectrum by Fraunhofer in 1814. They are the doublet from the fine structure splitting of the excitation states of neutral sodium at $\lambda = 5891.58\text{Å}$ for D₂ and $\lambda = 5897.56\text{Å}$ for D₁. Neutral sodium has an ionization potential of 5.14 eV (Morton 2003).
- Calcium (Ca II H&K) lines were also seen by Fraunhofer in sunlight and, similarly, they correspond to the doublet of the fine structure splitting of the excitation states of the singly ionized calcium at $\lambda = 3934.8\text{Å}$ for K and $\lambda = 3969.6\text{Å}$ for H, with an ionization potential of 11.87 eV.
- Potassium (K I) lines were first detected by Dunham (1937). This resonant doublet from the fine structure splitting of the neutral potassium excitation states occurs at $\lambda = 7664.90\text{Å}$ for K₁ and $\lambda = 7698.97\text{Å}$ for K₂. Neutral potassium has an ionization potential of 4.34 eV.
- The diffuse interstellar bands (DIBs) were first discovered in stellar spectra by Heger (1922). Today, hundreds of DIBs from unidentified molecules in the ISM have been discovered (see Herbig 1995). Proposed carriers include polycyclic aromatic hydrocarbons (PAHs), fullerenes and other hydrocarbons ions and molecules (Salama et al. 1999; Kroto et al. 1985; Motylewski et al. 2000). We choose here three of the strongest and more isolated DIBs at $\lambda = 4428.2, 5780.5, 6283.8\text{Å}$.

Table 1 summarizes these narrow lines and their characteristics. We also include the “integration window”, a velocity interval around the central wavelength in which the line will be measured (see section 4.1). It is related to the strength of the line and therefore the wavelength range it may cover.

SNe in low-reddening environments may only display the strongest line-of-sight lines, which normally are the Na I D absorption features. If the strength of the absorption line is very low, it indicates negligible material in the line of sight and very low reddening. Figure 1 shows the location of the narrow Na I D features for some low-redshift ($z < 0.1$) SNe observed with a low (top panels) and high (bottom panels) resolution instrument. In SNe II (left panels), the narrow Na I D lines are on the top of the He I $\lambda 5876$ broad line from the ejecta at early phases, but after 30-40 days, they are around the peak of the broad Na I D emission line (from the SN). In SESNe (middle panels), they are between the He I/Na I D and the Si II/He I or H α (in SNe Iib), while

Table 1. Narrow spectral features from the intervening medium considered in this study.

Line	Wavelength (Å)	Ionization potential (eV)	Integration window (km/s)
Na I D	5889.95 5895.92	5.14	± 1000
Ca II H	3969.60	11.87	± 900
Ca II K	3934.80	11.87	± 900
K I 1	7664.90	4.34	± 600
K I 2	7698.97	4.34	± 600
DIB	4428.20	–	± 750
DIB	5780.50	–	± 600
DIB	6283.80	–	± 750

in SNe Ia (right panels), the narrow Na I D features are between the Si II lines. The effect these broad lines have in the narrow lines will be further discussed in Section 5.

In high-resolution spectra, the narrow Na I D lines can be resolved. It is possible to detect four lines in the spectra (see, for example, bottom panel of Figure 1), two from the MW ($\lambda 5890$ and $\lambda 5896$) and two from the host galaxy ($\lambda 5890 \times (1+z)$ and $\lambda 5896 \times (1+z)$, where z is the SN redshift), as long as a single cloud component is present. For low-resolution spectra, only two lines can be detected (one that corresponds to the MW ($\lambda 5893$, on average) and another related to the host galaxy ($\lambda 5893 \times (1+z)$). When the SN is very nearby ($z < 0.04$; e.g. SN 1987A), the MW and the host galaxy lines can be blended, and just a single narrow absorption line is visible. These cases are not included in the current analysis (see the selection criteria in Sections 3 and 5).

The narrow line-of-sight lines play an important role in estimating the reddening in the line of sight of SNe. Theoretically, this is somewhat expected as the line equivalent width (EW) of a given gas species X is given by:

$$EW_X = \int (1 - e^{-\tau_X(\lambda)}) d\lambda, \quad (1)$$

where τ_X is the optical depth, which is a function of the column density of the species, N_X , multiplied by the absorption coefficient, κ_0 . In turn, the gas column density depends on the gas-to-dust ratio, f_{gd} , the mass fraction of the gas, f_X , and the ionization fraction, f_{ion} . For low optical depths, $EW_X \propto \tau_X \propto N_X$, so that:

$$EW_X \propto \tau_X = \kappa_0 N_X = \kappa_0 (1 - f_{ion}) f_X f_{gd} N_{dust}, \quad (2)$$

where the dust column density, N_{dust} , is directly proportional to the extinction A_V :

$$EW_X \propto \kappa_0 (1 - f_{ion}) f_X f_{gd} A_V \quad (3)$$

As the optical depth increases, the line profile becomes saturated, and the equivalent width does not increase linearly with column density. Indeed, the strength at the central wavelength stalls whereas the Doppler broadening increases, so that $EW_X \propto \sqrt{\ln N_X}$. At even larger optical

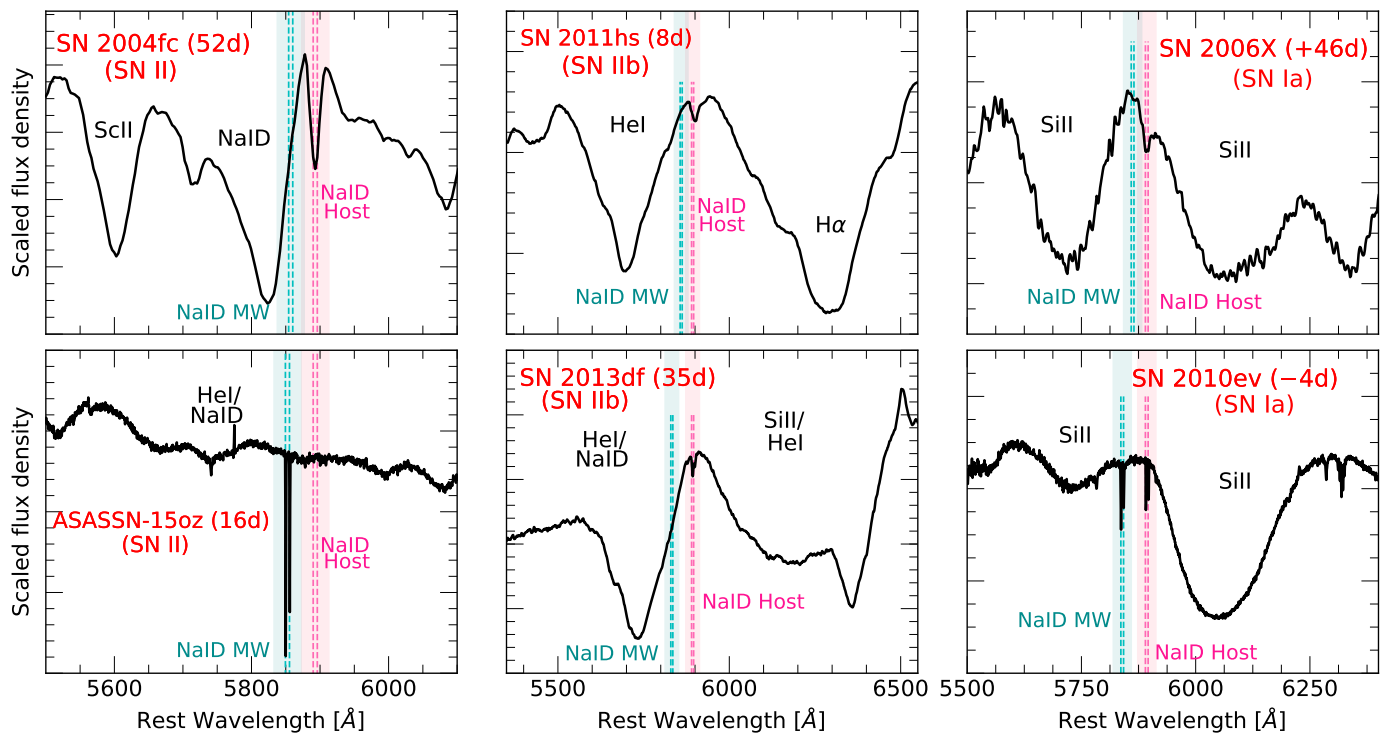


Fig. 1. Location of the narrow NaID absorption lines in SNe II (left), SESNe (middle) and SNe Ia (right panel). The names and phases with respect to the B -band maximum in their observed light curves are marked in each inset. Low-resolution spectra are presented in the top panels (pseudo-resolution – see Section 3 – of $R_p = 1951, 3087$ and 3869 from left to right), while higher-resolution spectra ($R_p = 11877, 9306$ and 14879 from left to right) are at the bottom. The vertical dashed lines indicate the position of the NaID for the MW (cyan) and the host galaxy (magenta), with the integration window of ± 1000 km/s shown in shaded areas.

depths, the collisional broadening dominates and $EW_X \propto \sqrt{N_X}$.

The linear relation between EW and A_V at low optical depths (eq. 3) depends strongly on other factors that are quite uncertain and vary substantially in our MW. For example, the low ionization potentials of the gaseous metals (below the Hydrogen ionization potential of 13.6 eV, see Table 1) mean that they are easily photo-ionized, changing the ionization fraction. Multiple gas clouds in the line of sight can also create several spectral components whose varying velocities cannot be disentangled in mid- and low-resolution spectra and thus contribute to the saturation of the line.

Despite these uncertainties in the theoretical relation, it has been shown empirically, as mentioned above, that the strength of the narrow NaID intervening lines correlates with dust extinction, based either on nearby stars (e.g., Munari & Zwitter 1997), SNe (Turatto et al. 2003; Sollerman et al. 2005) or large samples of extragalactic sources whose light is absorbed in the MW gas and dust (Poznanski et al. 2012; Murga et al. 2015). The trends are limited by the large dispersion and a distinct saturation for EW values larger than 0.5 \AA in low-resolution data (Munari & Zwitter 1997; Poznanski et al. 2011), and 1.8 \AA in higher resolution spectra (1 \AA for NaID₂ and 0.8 \AA for NaID₁; Poznanski et al. 2012) respectively. Poznanski et al. (2011) suggested that the EW estimated from low-resolution spectra is a bad estimator of $E(B - V)$, while Phillips et al. (2013) argued that the NaID gives an overabundance of $E(B - V)$ for several SNe Ia and the DIB at 5780 \AA is a better tracer of reddening than NaID. Indeed, Baron et al.

(2015) demonstrate that eight different DIBs correlate well with extinction for a large sample of extragalactic objects from the Sloan Digital Sky Survey.

In the context of SNe, the presence of the high-velocity, wide features from the SN makes the measurement of the EW difficult (see section 5.4). Additionally, time-variable NaID absorption lines detected in a few SNe Ia (Patat et al. 2007; Blondin et al. 2009; Simon et al. 2009) also complicate their use as reddening tracers. However, considering their easy identification and the scarcity of other methods to constrain dust extinction along the line of sight, their use is still widespread. That is why a robust methodology and a careful study of systematic biases, as the one presented here, are needed.

3. Sample

The data analysed in this paper consists of a large heterogeneous sample from the literature obtained through large web compilations such as SUSPECT (Richardson et al. 2001), WISEREP¹ (Yaron & Gal-Yam 2012), the Open Supernova Catalog² (Guillochon et al. 2017), and from individual journal publications. It contains SNe Ia from the thermonuclear runaway of white dwarfs in binary systems, including the peculiar 91bg-like, 91T-like, 02es-like and Iax; it contains hydrogen-rich SNe (SN II) from the core-collapse of massive stars that have retained their hydrogen envelopes, including both old light-curve classifications, SNe IIP (plateau) and SNe IIL (fast-decline); it con-

¹ <https://www.wiserep.org/>

² <https://sne.space/>

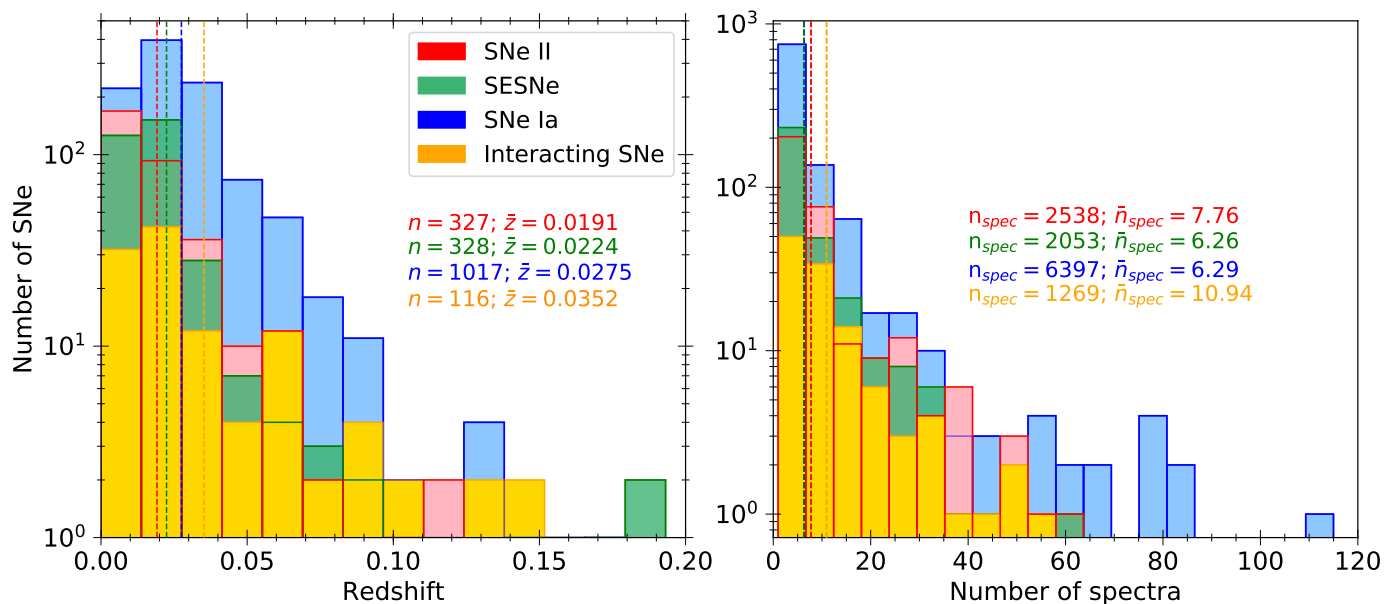


Fig. 2. **Left:** Distribution of heliocentric redshifts for the 1719 SNe included in our sample. **Right:** Histogram of the number of spectra per SN.

tains stripped-envelope (SESNe) from the core-collapse of massive stars that have lost their outer layers: I Ib with hydrogen shown only initially in their spectra but not later on, Ib without hydrogen throughout their evolution, Ic without hydrogen nor helium in their spectra and Ic-BL with broad lines from a central engine; and it contains various transients related to stellar outbursts and death of massive stars with clear signs of interaction with circumstellar material like SNe IIn, SNe Ibn, SNe Icn, and SN impostors, collectively called here "SNe-int".

This dataset consists of 12257 spectra of 1788 SNe observed between 1937 and 2023. 2538 of these spectra correspond to 327 SNe II, 2053 spectra to 328 SESNe, 1269 spectra to 116 SNe-int and 6397 spectra to 1017 SNe Ia. The sample also includes 174 spectra with mid- and high-resolution. Most of them are from SNe Ia. Only 19 are from SESNe, and 60 are from SNe II. All spectra are corrected for MW extinction with the maps of [Schlafly & Finkbeiner \(2011\)](#) and brought to the rest frame. Due to the heterogeneous nature of the sources, this sample is not complete, neither in volume nor in magnitude. The sample details can be found in [Table A1](#) in the Appendix.

Figure 2 (left panel) shows the redshift distribution of our sample. The mean redshift value is 0.026, while the median is 0.019. The nearest object is SN 1987A with a redshift of 0.00001, while the farthest object is IPTF-13ajg with a redshift of 0.74. In the right panel of Figure 2, we present the distribution of spectra per object. 720 SNe have at least two spectra, 873 SNe have at least three spectra, and 937 SNe have between 3 and 10 spectra. The objects with the most data are the type Ia SN 2005cf (115), SN 2006X (85) and SN 2001V (82). On average, we have 6.7 spectra per SN. For the sample of SNe II, the average is 7.6, 6.4 for SESNe, and 6.4 for SNe Ia.

To give a better idea of the spectral quality of this large and diverse sample, we show in the top panel of Figure 3 the average resolution of all spectra, where we define this resolution as the average sampling around 10,000 km s⁻¹ of the narrow line (in this case Na I D): $\Delta v_{\text{res}} = \Delta \lambda_p c / \lambda_{\text{rest}}$ and

we also show the corresponding pseudo-resolution, $R_p = \lambda_{\text{rest}} / \Delta \lambda_p$, in the upper axis. $\Delta \lambda_p$ is the wavelength sampling provided in the spectral files instead of the full-width half-maximum of unresolved lines, which characterizes an instrument resolution. This is why we call R_p a pseudo-resolution, which is only a proxy for the real spectral resolution of the instrument. In particular, some spectra have higher wavelength spacing without meaning the spectral resolution is better. This is especially true for many old SN spectra from years before 1995 that have a narrower spacing data format but are not of particularly high resolution. These represent most of the first peak shown in the distribution, although some real high-resolution spectra are also present. Other peaks in the distribution are mostly but not exclusively populated by the spectra of large surveys with its instruments and their characteristic wavelength spacing: the supernova group at the Harvard-Smithsonian Center for Astrophysics³ (CfA; e.g. [Blondin et al. 2012](#); [Modjaz et al. 2014](#); [Hicken et al. 2017](#)), the UC Berkeley SN group⁴ (Berkeley; e.g. [Silverman et al. 2012a](#); [Shivvers et al. 2019](#); [Stahl et al. 2020](#)) and Carnegie Supernova Project⁵ (CSP; e.g. [Folatelli et al. 2013](#); [Gutiérrez et al. 2017](#); [Stritzinger et al. 2023](#)) are the most characteristic ones.

On the bottom panel of Figure 3, we also show the average S/N in the same wavelength regime calculated with the inverse of the root mean square (RMS) of the difference between the original spectrum and a smoothed spectrum with a cosine kernel. The distribution is exponentially falling with a mode around 30 and a median of 150.

With the aim of doing a systematic analysis and decreasing the bias in our sample, we will define several criteria for our data selection (see [Table 2](#)) that will be discussed in the next sections.

³ <https://lweb.cfa.harvard.edu/supernova/SNarchive.html>

⁴ <https://heracles.astro.berkeley.edu/sndb/>

⁵ <https://csp.obs.carnegiescience.edu/data>

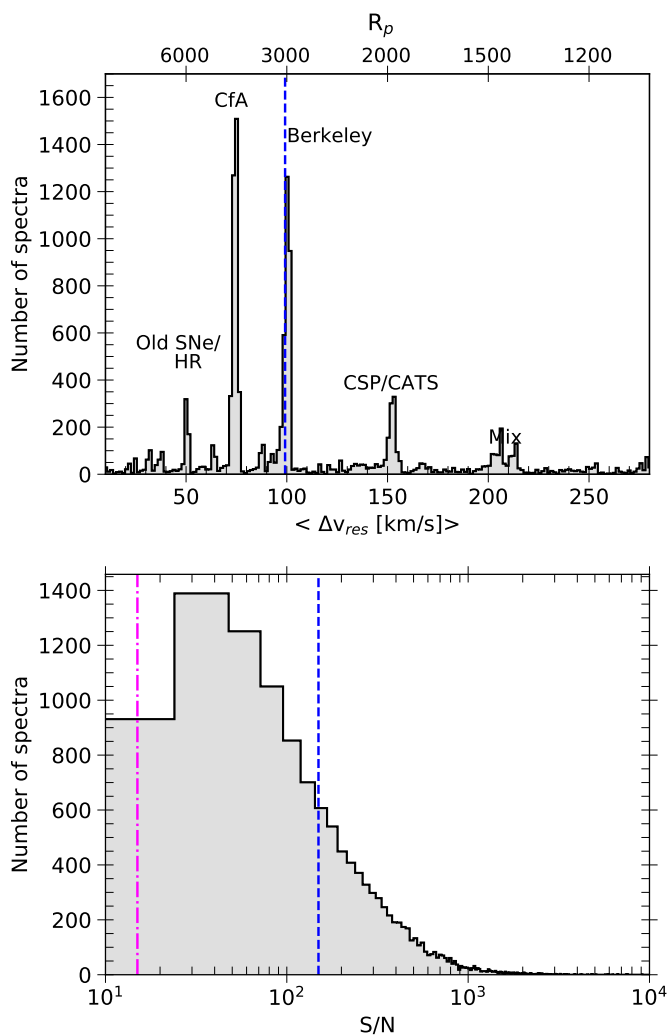


Fig. 3. Distribution of average velocity resolution (top) around the sodium doublet and signal-to-noise (bottom) for all spectra in our sample. Vertical blue dashed lines show the median values of the distributions ($\Delta v_{\text{res}} = 99.2$ km/s and $S/N = 155$).

4. Automated line measurement

In this section, we outline the automated methodology we have developed to measure EWs and velocities in a diverse set of spectra.

4.1. Equivalent width measurement

To measure the equivalent width of the various line-of-sight narrow lines from the host galaxy and/or the MW, we use a fully automated code inspired by Förster et al. (2012). First, a continuum is found by defining several nodes around the centre wavelength of the narrow line with separations between 50 and 2000 km s⁻¹. The nodes are evenly spaced (in velocity space), and the flux at each node is obtained by smoothing locally the spectrum with a cosine kernel.

Once the continuum is defined, we measure the EW:

$$\text{EW} = \sum_i \frac{c_i - f_i}{c_i} \Delta\lambda = \sum_i 1 - \frac{f_i}{c_i} \Delta\lambda, \quad (4)$$

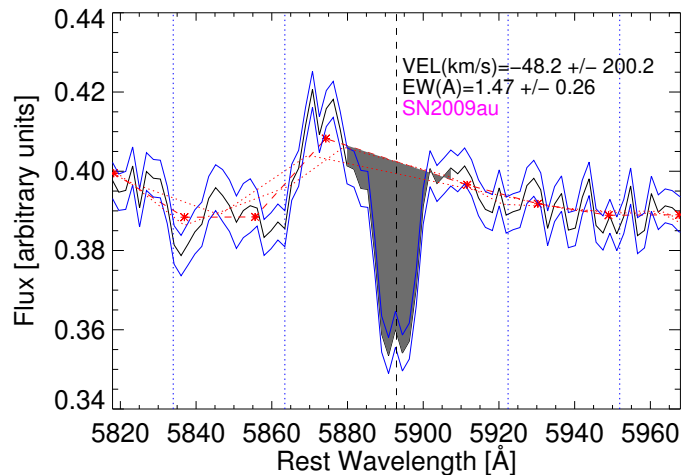


Fig. 4. SN 2009au (SN II) spectrum around the Na I D lines. The black line is the spectrum, the blue lines are the estimated flux errors, the red stars are the nodes, and the red dashed line is the continuum crossing the nodes. Red dotted lines represent the continua at $\pm 25\%$ of the node separation being considered. The grey-shaded area is the integrated line within ± 1000 km/s. The black dashed vertical line is the central wavelength of the line. The other vertical blue dotted lines indicate other wavelengths where we measured EW and whose dispersion provides a systematic uncertainty.

where the flux at each pixel, f_i , is compared to the continuum at that pixel c_i , and $\Delta\lambda$ is the wavelength separation between pixels in Å.

We sum the area under/over the continuum in a fixed velocity range around the central wavelength, similar to Förster et al. (2012). The velocity interval changes for each line that we consider and is given in Table 1. These intervals were estimated by a visual inspection of the spectra with the most pronounced narrow features, e.g. SN 2013fc (Kangas et al. 2016) or SN 2003cg (Elias-Rosa et al. 2006); it is largest for the stronger Na I D (± 1000 km s⁻¹) which includes two lines. We note that the EW measured in this way sums all contributions in the given range, meaning that, in principle, more than one feature could be present. Additionally, it is important to remember that emission lines are taken into account giving possible negative values of EWs. The net sum should be close to zero when there is only noise.

The error associated with the EW of a single spectrum has four components: i) the flux error, σ_f , which is calculated from the RMS between the flux and the continuum outside the range of the line (but within ± 10000 km/s), and an average of this outside error is assumed within the range of the line (see solid blue lines in e.g. Figures 4 and C.2); ii) the error in the continuum, σ_c , which comes from the dispersion obtained when assuming a difference of $\pm 25\%$ in the node separation that determines the continuum (see red dotted lines in Figures 4 and C.2); iii) the error in the integration window for which we re-calculate the EW at $\pm 25\%$ of the range given in Table 1 for each line; and iv) a systematic error, σ_{sys} , from the dispersion obtained when measuring the line at eight different positions where no line is expected (see vertical blue dotted lines in Figures 4 and C.2) and the EW should be zero. The first two sources of error are propagated in Eq. 4 to obtain the error on the EW, and together with the latter, they are added in quadrature.

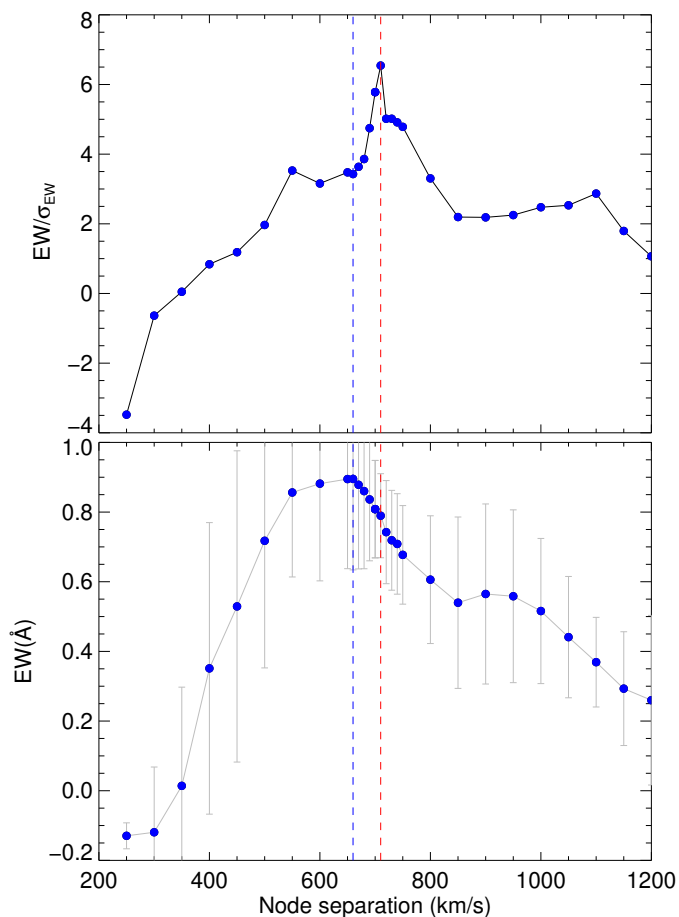


Fig. 5. Measured equivalent width, EW, over measured uncertainty, σ_{EW} , (**top**) and equivalent width (**bottom**) for a spectrum of SN 2014J around the K I 7665Å (see Figure C.2) as a function of the node separation defining the continuum. The maximum EW is shown with a blue dashed vertical line, whereas the maximum $|EW|/\sigma_{EW}$ is shown with a red line.

The node separation for the continuum plays a crucial role in this technique (see Figures 4 and C.2), so the optimal separation is found by maximizing the absolute value of the signal-to-noise of the EW (see Figure 5). This is done by calculating the EW for various node separations in bins of 50 km s^{-1} and through a secondary loop in bins of 10 km s^{-1} centred at the highest $|EW|/\sigma_{EW}$ found in the first iteration. The absolute value is used to make sure that we do not necessarily force positive values on the EW. We also require that the profile of the narrow line intersects with the continuum within the velocity window considered.

To verify the accuracy of the automated method, we compare the results obtained by measuring the EW of Na I D manually using IRAF (Tody 1986, 1993) and with our automatic software. Figure 6 shows the comparison for a sub-sample of 1145 low-resolution spectra and 23 high-resolution spectra. The methods give consistent results with a median absolute deviation of $0.01 \pm 0.22 \text{ \AA}$.

4.2. Velocity measurement

The velocity measurement is trickier compared to the EW: for weak or absent lines, it cannot be done, while for stronger lines, there might be multiple components that

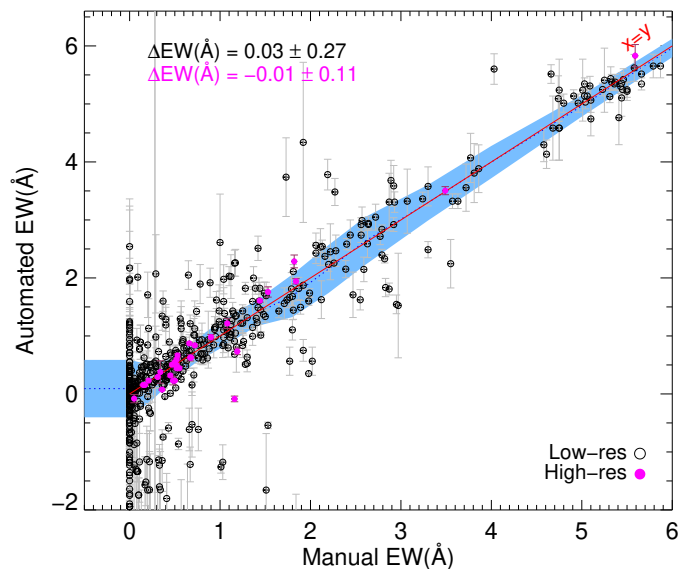


Fig. 6. Comparison of the EW of Na I D doublet measured manually and with our automatic software for a sub-sample of 1145 low-resolution spectra (empty circles) and 32 high-resolution spectra (purple circles). The red line shows a $x = y$ match. The blue shaded area represents the median scatter between the two measurements per EW bin. The median and deviation of the full sample are indicated at the top of the plot. The median error from the automatic method is 0.11 \AA . Below zero in the manual measurement, we show in blue the median and absolute median deviation, $-0.04 \pm 0.47 \text{ \AA}$, of the automated measurements for spectra where no line was found visually.

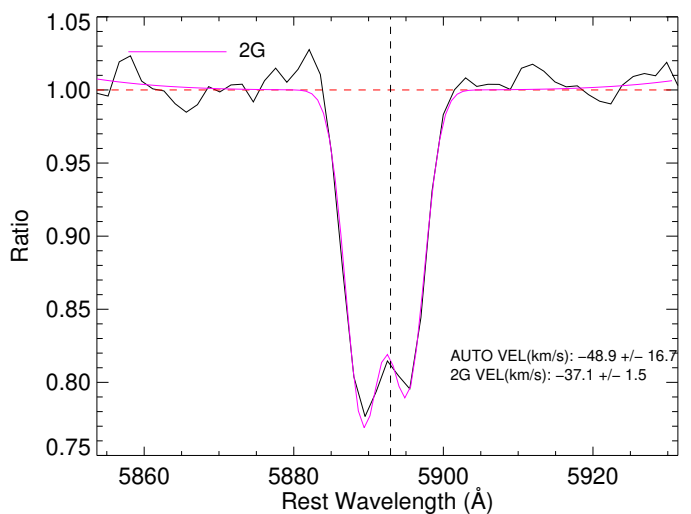


Fig. 7. Example of a double Gaussian fit (purple) for the host galaxy sodium doublet within a spectrum of SN 2002bo (black). The wavelength separation between both Gaussians is kept fixed. In this case, the fitted velocity is $-37.1 \pm 1.5 \text{ km/s}$ compared to $-48.9 \pm 16.7 \text{ km/s}$ (without the uncertainty floor of 35 km/s) obtained with the flux-weighted wavelength average. The vertical dashed line is the mean rest-frame centre of both lines, and the red horizontal dashed line marks the continuum.

are only resolvable with high-resolution spectroscopy. Obtaining an unbiased estimate of the velocity similar to the EW is perhaps impossible, but we attempt two approaches. The first is model independent and consists simply of a line-weighted average wavelength of the area under/over

the continuum measured above (grey shaded areas in e.g. Figure 4) compared to the rest wavelength of the line:

$$v(\text{km/s}) = \frac{c}{\lambda_{\text{rest}}} \left[\frac{\sum_i (1 - f_i/c_i) \lambda_i}{\sum_i (1 - f_i/c_i)} - \lambda_{\text{rest}} \right], \quad (5)$$

where c is the speed of light in vacuum and λ_{rest} the restframe wavelength of the line.

The first source of uncertainty stems from the wavelength calibration, which may vary substantially across our heterogeneous sample and is impractical to check individually given the lack of, e.g. sky spectra. Instead, we measure the emission lines from the gas phase of the environment, sometimes present in SN spectra, and calculate the average velocity dispersion between those lines. We obtain a characteristic dispersion of 35 km/s (see Appendix A), which we take as an uncertainty floor from the wavelength calibration. Additional sources of uncertainty come from re-measuring the velocities when i) the flux error is added/subtracted to the original flux, ii) when the continuum is changed by $\pm 25\%$, and iii) when the integration window is changed by $\pm 25\%$.

This simple technique works well when the narrow line is relatively symmetric but otherwise suffers from several biases. For example, in the case of the NaID, if one of the two doublet components is stronger, the flux-weighted wavelength will be affected, as seen for SN 2002bo (see Figure 7). The bias may be even stronger in the case of multiple components with different velocities.

Another approach, commonly used in the literature, consists of a parametric profile fitting with, e.g. one or multiple Gaussians. For this, one has to assume the number of components (i.e. number of Gaussians), which one may not be able to distinguish in the case of low-resolution spectra. In Figure 7, we show a fit with two Gaussians with a fixed wavelength separation of 6 Å between the two sodium lines and a common Gaussian width. We directly fit the ratio of the flux-to-continuum using the continuum obtained in the previous section. For this particular case, the line-weighted average estimates a slightly bluer velocity because of the stronger line of the doublet. A comparison of the automated EW and flux-weighted velocity measurements of the sodium doublet with the values obtained from a double Gaussian fit is shown in Figure 8. The match of the EWs is remarkable, while there is a larger dispersion for the velocity – still consistent within the large uncertainties. This dispersion is mostly driven by cases where the EW is very weak, and the measurement of the velocity becomes very uncertain for both methods. Spectra with stronger lines (see green points) agree better and present lower uncertainties. The two approaches are overall quite consistent, and we use our automated technique as our primary method but compare, when necessary, with the Gaussian approach.

4.3. SN average of multiple spectra

In the case where multiple spectra of a SN are available, and no evolution is expected or found (see section 6), one can get a better estimate of the EW and velocity of the intervening line by averaging the individual values found in the previous sections (sections 4.1 and 4.2). Nonetheless, given the heterogeneous set of spectra taken with different instruments and with different underlying SN ejecta throughout

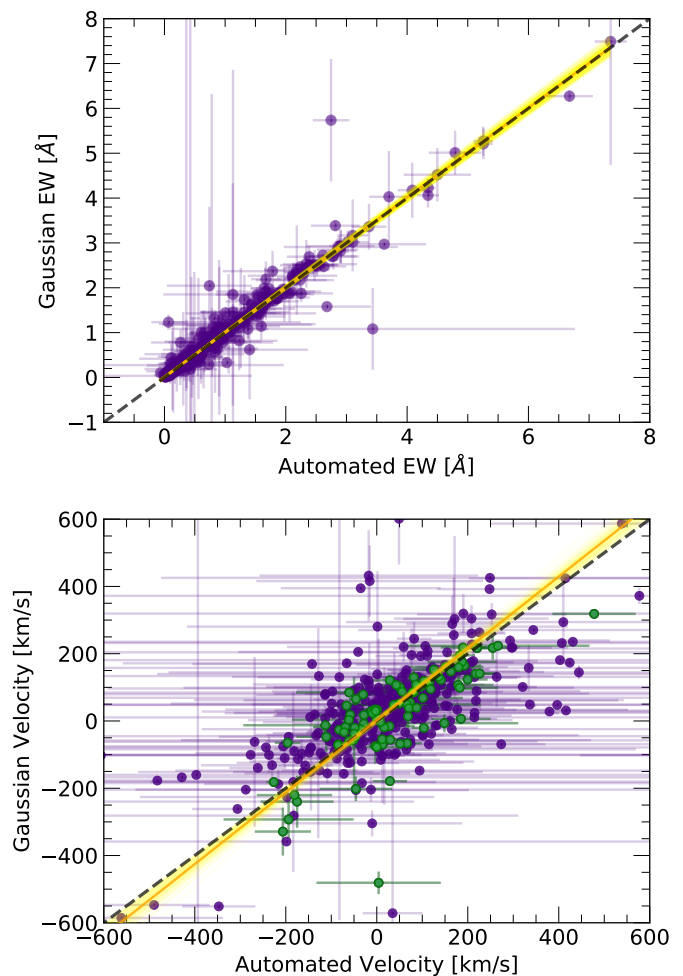


Fig. 8. Comparison of EWs (**top**) and velocities (**bottom**) measured with the automated technique and a double Gaussian fit for NaID with the wavelength separation fixed. Each plot shows the corresponding best linear MCMC fit (LINMIX_ERR; Kelly 2007) as a solid orange line and the variance with respect to the fit line in yellow. The $x = y$ line is indicated in dashed green lines. In the bottom plot, the green points show that cases for which the $\text{EW}/\sigma_{\text{EW}} > 1.3$ and $\text{EW} > 0.5$ have lower uncertainties and agree better within the two methods. The uncertainties here do not include the uncertainty floor of 35 km/s.

the SN evolution, we find that a better approach consists of taking the median of the individual flux-to-continuum ratios to generate a stacked ratio with higher signal-to-noise. This approach is similar to the work done by Poznanski et al. (2012) for NaID measured in galaxy spectra. We show an example of 12 stacked flux-to-continuum spectra of SN 2003cg around the DIB-5780 Å line in Figure 9. After the stacking, the EW and velocity are calculated in the same way as for individual spectra. To measure the corresponding error of this stacked value, we do a bootstrap with 100 iterations in which the same number of flux-to-continuum spectra are randomly taken from the original sample (some spectra may be repeated or missing in each iteration), and the EW and velocity are measured each time. The final asymmetric uncertainties are given by 16% and 84% of the distribution. The blue lines in Figure 9 contain the 1σ bootstrap realizations for illustration purposes. As for individual spectra, we also include the systematic er-

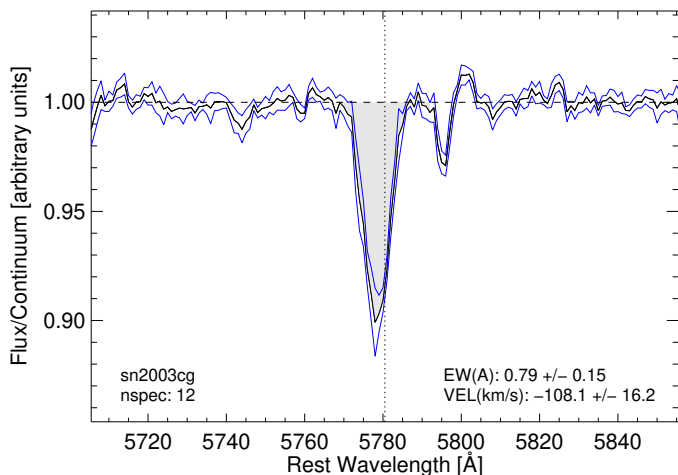


Fig. 9. Stacked flux-to-continuum ratios of 12 spectra of the SN Ia SN 2003cg around the DIB-5780 Å line (black) with the 1σ uncertainty from 100 bootstrap realizations (blue). The EW and velocity values measured with the automated technique (grey shading) are shown in the plot. The vertical dotted line indicates the wavelength of the line.

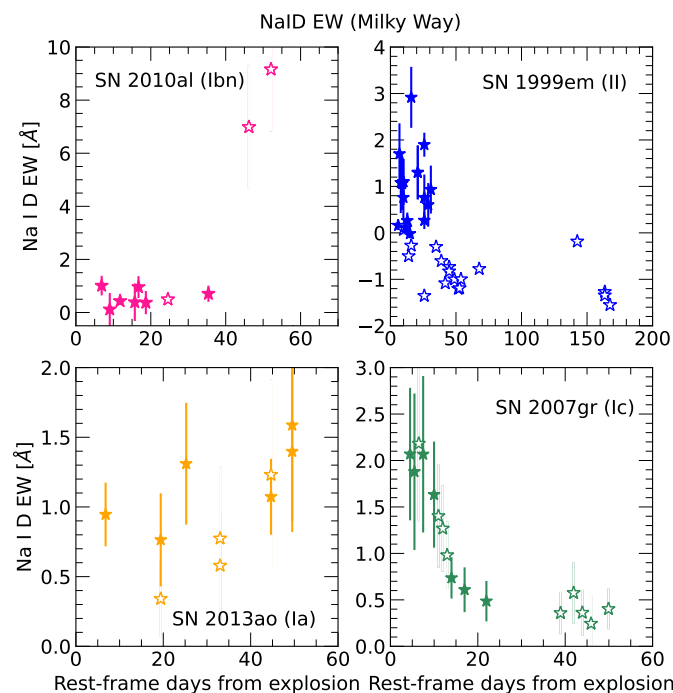


Fig. 10. Na I D EW measured at different epochs since explosion for the MW narrow line-of-sight line. Each panel shows the SN name and its type. Open symbols show all available measurements whereas filled symbols are the ones passing the cuts (see section 5).

rors from the continuum, the integration window and the dispersion of measuring the line at other wavelengths. A comparison of the EW measured from stacked spectra with the median or weighted averages of individual EW measurements is shown in Figure C.1.

5. Spurious temporal evolution of narrow lines and systematic biases

Although the methodology laid out in the previous section correctly measures the EW of narrow lines of spectra of various resolutions, there are some general caveats inherent to the use of low-resolution spectra that we investigate further. Some of these biases become evident when studying the behaviour of the narrow lines over time: we see a conspicuous evolution of the EW for some SNe. In particular, in Figure 10, we show the evolution of the Na I D EW for the MW line for different SN types measured with the automated technique. All objects show variations in their EWs; however, in SN 1999em and SN 2007gr, a constant decrease is striking. Narrow intervening lines from the MW are expected to be generally constant as a function of time since they come from material in our own Galaxy that does not interact with the SN; therefore, variations in their EWs suggest the interference of external factors. A similar, albeit more extreme, behaviour was observed for the narrow lines from the host galaxy (see section 5.4). This is worrying since it can lead to false physical interpretations like interaction with circumstellar material. These results motivate us to explore the possible biases that affect the strength of the narrow line-of-sight lines. They are described in detail in the following subsections.

5.1. Redshift

In order to ensure that the narrow Na I D absorption line from the MW and the host galaxy are separately resolved (i.e., to ensure they are not blended), we set a lower limit cut at 0.004 on the redshift of our sample (independently of the spectral resolution). This eliminates a small number of very nearby SNe (see Table 2). As will be shown later in section 5.4, the redshift also plays an important role in the location of the broad lines of SNe with respect to the narrow intervening lines affecting their measurement.

5.2. Spectral resolution

In this section, we explore the impact of varying spectral resolutions in measuring the EW and velocity of the lines from intervening matter. We pick high-resolution spectra ($\Delta v_{\text{res}} < 50 \text{ km s}^{-1}$) and smooth them with a cosine kernel (see Section 4) with increasing velocity windows to simulate lower resolutions (Figure C.3). We try velocity windows spanning 50-500 km s^{-1} , which conservatively cover our sample's average velocity resolutions (see Figure 3). As long as the continuum is relatively flat (Section 5.4), we find excellent agreement in the measured EW and velocity of the line-of-sight line for all resolution windows with the original high-resolution values. This is shown in Figure 11 for several SNe of different Na I D line strengths. We highlight that the uncertainties in the EW become larger, as expected, for worse resolutions. Therefore, no cut on the resolution is applied to our sample.

5.3. Signal-to-noise

We now evaluate the performance of the automated technique when subject to varying S/N ratios in the spectral range of the narrow line. The S/N, as explained in sec-

Table 2. Number of SNe and spectra after various cuts.

Cut	SNe Ia		SNe II		SE SNe		SNe-int*		Total		Comment
	N_{SN}	N_{spec}	N_{SN}	N_{spec}	N_{SN}	N_{spec}	N_{SN}	N_{spec}	N_{SN}	N_{spec}	
None	1017	6397	327	2538	328	2053	116	1269	1788	12257	–
$z > 0.004$	988	5759	285	1890	303	1694	110	1177	1686	10520	Section 5.1
$S/N > 15$	988	4171	285	1515	303	1099	110	834	1686	7619	Section 5.3
$m_c < 0.002 \text{ \AA}^{-1}$	701	2466	214	809	233	856	98	439	1246	4570	Section 5.4 [†]
$N_{\text{sp}} > 1$	400	2165	140	735	142	765	71	412	753	4077	Section 5.6

* These include interacting SNe: SNe IIn, Ibn and Icn.

[†] Values for NaID. The exact cuts and number of SNe/spectra changes according to line species.

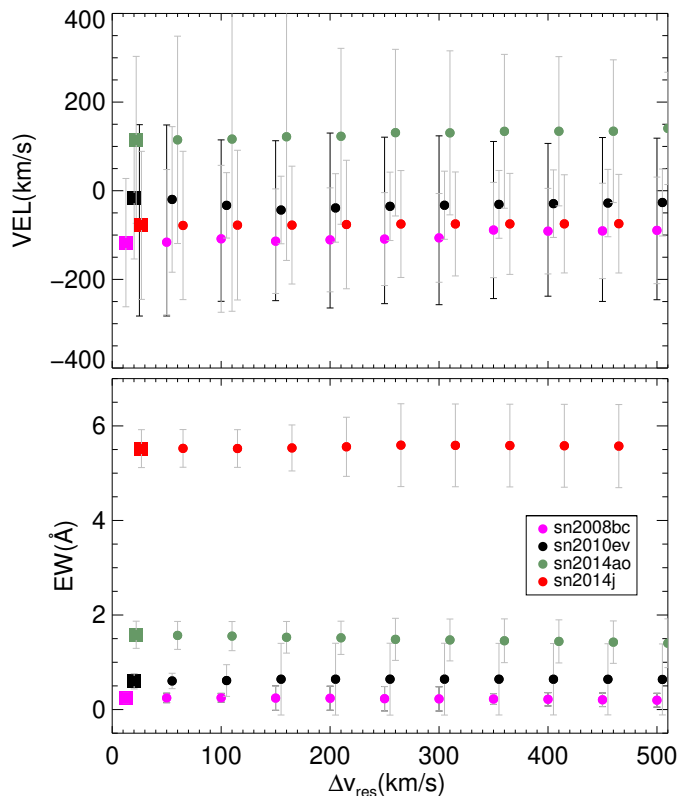


Fig. 11. Measured velocity (**top**) and equivalent width (**bottom**) of NaID as a function of the decreasing simulated resolution, Δv_{res} for the SN 2010ev spectra shown in Figure C.3 (black) and also for smoothed high-resolution spectra of SN 2008bc (purple), SN 2014ao (green) and SN 2014J (red). The squares show the original high-resolution values of each SN.

tion 3, is estimated by calculating the RMS of the observed spectrum with respect to a smoothed version. We perform a simulation by taking spectra with high signal-to-noise and randomly perturbing them according to various decreasing S/N ratios (see Figure C.4). For each given S/N, we do 10 simulations and take the mean and standard deviation to show the effect in Figure 12. The measured EWs are remarkably consistent with decreasing S/N, and the uncertainties measured by the automated code (dashed error bars) are always larger than the standard deviation (solid error bars) of the simulations. Nevertheless, we do see that for weak lines (e.g. those in the spectra of SN 2002an and SN 2007oc), the average EW starts to increase at very low S/N, albeit always within the errors. Because of this, we add a conservative additional minimal S/N cut of 15 that rejects around 1500 spectra (see Table 2).

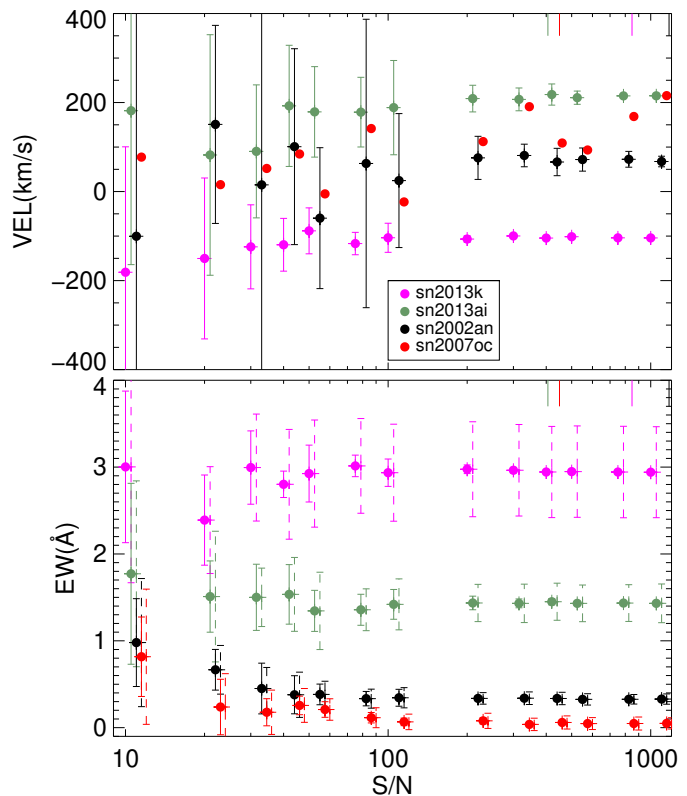


Fig. 12. Measured equivalent width (**bottom**) and velocity (**top**) as a function of the S/N for the perturbed SN 2002an spectra shown in Figure C.4 (black) and also for perturbed spectra of SN 2013K (purple), SN 2013ai (green) and SN 2007oc (red). The points are the mean of 10 different simulations for a given S/N, and its associated error bars are the standard deviations (SN 2007oc has too large errors on the velocities and are thus not shown). The dashed error bars of the EW are the mean of the errors calculated from the automated technique. Upper right ticks show the S/N of the original unperturbed spectra.

The recovered velocities are also consistent, but we note that, as expected, there is a large dispersion for weak lines as there is not much line flux to obtain the flux-weighted average wavelength. However, the uncertainties on the velocities are always much larger than the standard deviations of the simulated spectra (measured uncertainties are larger than 300 km s^{-1} and are not shown in the Figure).

5.4. Broad line interference

When measuring the narrow line-of-sight lines in individual spectra of SNe and investigating their evolution, it be-

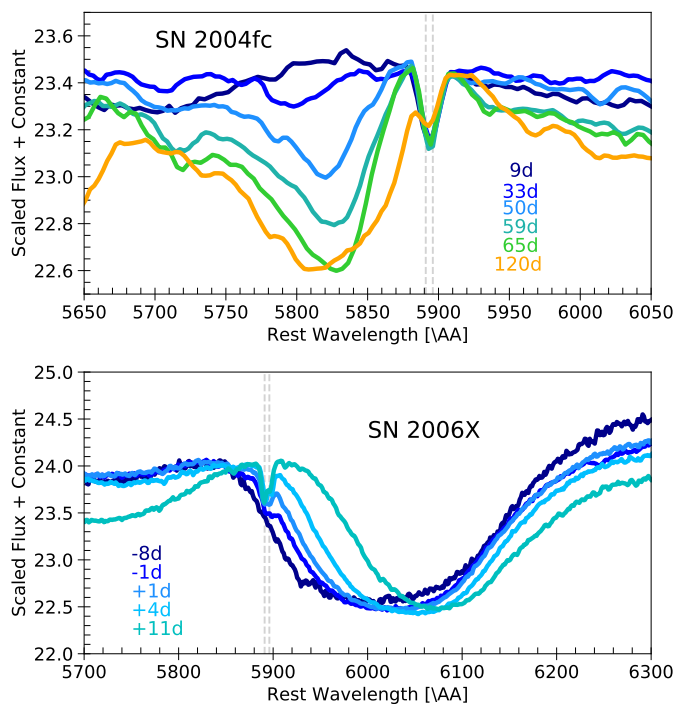


Fig. 13. Optical spectral evolution of SN II 2004fc (**top**) and SN Ia 2006X (**bottom**) around the Na I D doublet. An apparent evolution of the narrow line is seen for both cases that coincide with the P-Cygni profile evolution of Na I D at the left of the narrow line and of Si II at the right of the narrow line, respectively.

comes evident that several objects have a seemingly temporal change in the strength of Na I D. Particularly for SNe II, there is often a strong apparent decrease in the EW as a function of time, but variations can also be seen for SNe Ia (see, e.g. Figure 13). Upon closer examination of the SN spectra, these changes appear to be strongly linked to the appearance and evolution of the emission and absorption components in the P-Cygni profile of the broad Na I D (for SNe II) and Si II 6355 Å (for SNe Ia). If the variations are connected to the development of broad lines (see Gutiérrez et al. 2017 for the appearance and evolution of P-Cygni lines in SNe II), they do not constitute real intrinsic variations. In that case, one will infer a wrong evolution and, more generally, EW measurements that depend on the underlying profile and are thus not a reliable reflection of the column density of the intervening material.

To investigate such bias in more detail, we create a simple simulation in which we input fake narrow lines into various differing P-Cygni profiles and calculate the recovered EW. For these simulations, we take both observed optical spectra of seven SNe II, three SNe Ia, and five SESNe, together with two SN radiative transfer models: the delayed-detonation model of SNe Ia (Blondin et al. 2015), and the m15mlt3 for SNe II (Dessart & Hillier 2011; Dessart et al. 2014). Most of the selected observed SNe do not show evident narrow Na I D lines; however, when the lines are clearly detected, they are removed from the spectra by interpolating the continuum to the line wavelengths so that we can then add simulated lines of our choice.

Once the spectra are clean from the Na I D lines, we smooth them using a moving average box by convolution

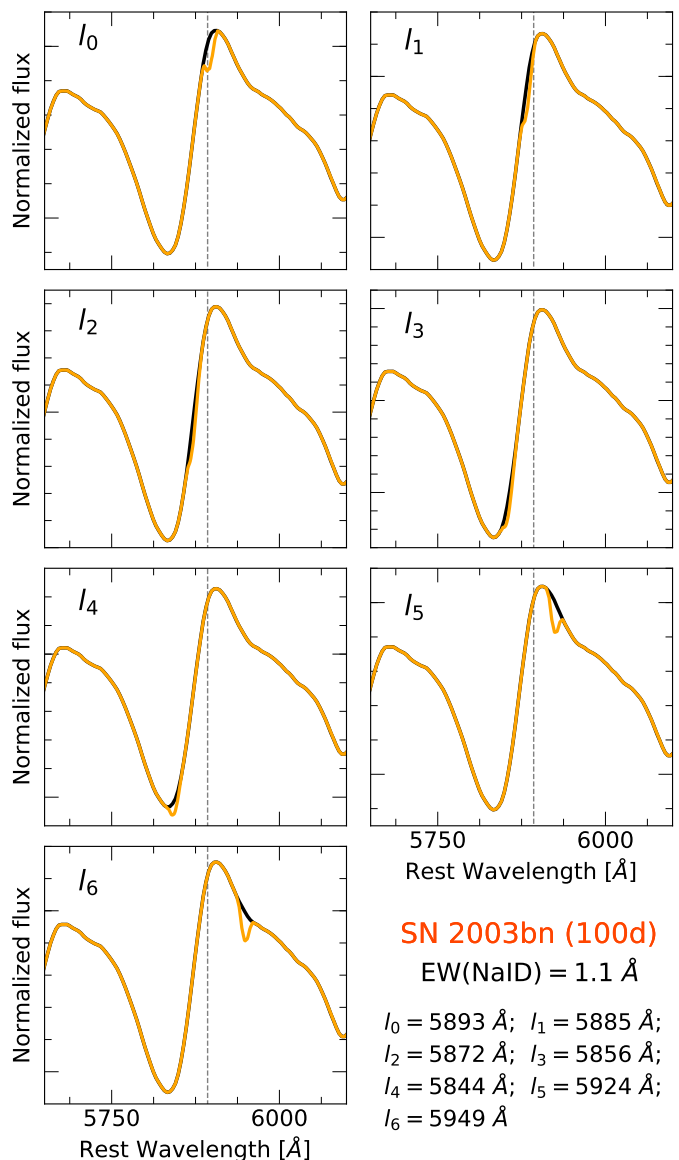


Fig. 14. Narrow Na I D lines artificially placed at various locations for SN 2003bn. Here, we added the narrow Na I D lines with low resolution (single line). The location of the narrow line is presented in the different panels.

with a cosine kernel. Although most spectra have a good S/N, the smoothing process provides easier identification of the continuum and the narrow lines. Following the smoothing, the spectra are normalised at the average position of the narrow lines ($\lambda 5893$). In parallel, we generate narrow Na I D absorption features with similar characteristics to those observed in SN spectra. These features are created for two cases: i) for low-resolution spectra that assume the Na I D doublet is blended and just one single feature is detected, and ii) for high-resolution spectra that produce the Na I D doublet (two resolved lines). For the two cases, we test different strengths of the narrow line.

To see the effect of the narrow lines in the SN spectra, we add the narrow Na I D feature at different locations offset from the central wavelength in all SN types to simulate different ejecta velocities and redshifts. Figure 14 shows the type II SN 2003bn spectra at 100 days from explosion centred on the broad Na I D P-Cygni profile with the added

narrow NaID feature at different locations. Here, the narrow NaID features were added for low (single line) resolution spectra. As one can see, the strength of the narrow NaID lines at low-resolution visually changes depending on the location in the spectrum; for example, at l_2 and l_3 , the line looks weaker. This same procedure of adding the narrow lines at different positions was also done for other observed SNe and for the aforementioned SN Ia and SN II models.

When we then calculate the EW of these simulated narrow lines, we find significant changes and a non-intrinsic evolution, as can be seen for observed and modelled spectra of SNe II in Figure 15. It is evident that as the P-Cygni profile of NaID develops with time during the SN photospheric evolution, the narrow line measurement is deeply affected: the EW we measure is lower and drops as a function of the steepness of the underlying continuum. Not only does this affect the EW measured for the narrow line, but it may also affect the photospheric or nebular line from the SN, e.g. producing an apparent redshift in the broad NaID emission line at late times in CC-SNe (> 100 days from explosion; see Figure C.5). This effect depends on the SN cosmological redshift and ejecta expansion velocity, which determine the location of the narrow line with respect to the P-Cygni profile. At different locations, the inferred behaviour changes accordingly. However, if we do the same simulations for high-resolution narrow lines, we do perfectly recover the EW, no matter the underlying P-Cygni profile.

Similarly, we show in Figure 16 the results for a simulation of SESN models and observed spectra. We also find that the NaID P-Cygni profile of the SN ejecta may swallow portions of the narrow line at later epochs in low-resolution spectra and consequently induce smaller measurements of the EW. Regarding SNe-int, there are no available models in the literature, and simulating narrow lines on top of a few objects will misrepresent a very heterogeneous class. Nonetheless, we expect –and visually confirm– the effect to be smaller, since strongly interacting SNe generally do not show prominent P-Cygni profiles.

Although less pronounced than SNe II, SNe Ia can also exhibit an apparent evolution from contamination by the broad ejecta features. This is seen for observed and simulated spectra (see Figure 17). In this case, the P-Cygni profile of SiII 6355 Å at early times, has very high expansion velocities, and part of it may reach the rest wavelength of the narrow NaID; later as the ejecta slows down, the narrow line is no longer engulfed by the absorption of the P-Cygni profile, and the EW is well recovered. The exact behaviour naturally depends strongly on the expansion velocity that moves different parts of the broad line into the narrow NaID, and the effect will be stronger for higher-velocity objects (bottom panel of Figure 13). Again, this is not seen for high-resolution spectra.

It is thus no surprise that using low-dispersion spectra, Wang et al. (2019) find the evolution of NaID lines in high-velocity SNe Ia when not properly considering this effect. Their evolution is strikingly similar to our simulated case shown in Figure 17. Therefore, variations in the strength of NaID narrow lines in SNe Ia at early times are not always indications of circumstellar interaction. In most cases, when low-resolution spectra are used, variations are produced by the interference of SN broad lines; in this case, by the SiII line.

Having seen the clear important bias of the interference of the broad line in the measurement of the narrow lines, is there a way to identify these dubious cases? Since the bias stems basically from a steep continuum from the P-Cygni profile, we can measure for a given spectrum the average absolute slope of the inferred continuum, m_c , from the automatic method (see Section 4.1) by doing:

$$m_c = \frac{1}{\langle f_c \rangle} \frac{1}{N} \sum_i^N \frac{|f_c^{i+1} - f_c^i|}{\lambda_c^{i+1} - \lambda_c^i}, \quad (6)$$

where the sum is over all N nodes of the continuum within $\pm 50\text{Å}$ of the line, and $\langle f_c \rangle$ is a normalization average of the continuum flux in the same range. The normalized slope continuum $m_c[\text{Å}^{-1}]$ is a measure of the steepness of the line in the immediate vicinity of the narrow line. Such slopes clearly reflect the presence of underlying broad profiles, as can be seen in Figures 15 and 17. The discrepancy with the real simulated EW increases for larger continuum slopes, as can also be seen in Figure 18. We find that a cut of continuum slopes of $m_c < 0.002 \text{ Å}^{-1}$ ensures deviations of less than 30% in the EW measurement for all simulated cases. We strongly encourage such a cut in m_c for the EW measurement of narrow lines in mid and low-resolution spectra.

5.5. Slit size and orientation

The stability of the strength of narrow lines could be affected by different external instrumental factors (besides the resolution and S/N), such as the size and orientation of the slit used for spectroscopy or the amount of host-galaxy light entering into the slit. These factors could introduce changes in the EWs that could be easily confused with intrinsic variations, given the diversity of instruments and observing conditions. To estimate the effect of some of these potential biases in the strength of the narrow lines, we measure the EW of the NaID lines in different environments and with different simulated slits. For this aim, we use data obtained with MUSE at the Very Large Telescope (VLT) as a part of the All-weather MUSE Supernova Integral field Nearby Galaxies (AMUSING, Galbany et al. 2016a) collaboration.

To evaluate the effect of the amount of host-galaxy light entering the slit, the impact of the slit orientation and its size, we define six different positions, with four distinct slit angles for each location (0, 45, 90 and 135 degrees with respect to the horizontal West-East axis) and two widths for the slit, one of 1'' and another one of 1.5''. The length of the slit is taken to be 15''. Figure 19 shows an example of the procedure for NGC 988, the host galaxy of the type II SN 2017gmr. As one can see, the chosen positions are distributed along the galaxy, from outer regions to the centre. We note that position 1 actually includes the SN 2017gmr in the slit, making this a particularly good study case. We then integrate all spectra within a rectangular aperture of the slit dimension. The resulting profiles centred on the narrow NaID lines are presented in Figure 20 for all different slit orientations and positions. We show the profiles obtained using the slit of 1'' width on the left panels and the slit of 1.5'' on the right panels. The average and standard deviations of the NaIDEWs for every position, displayed in each panel, show small differences (the largest deviation for the slit size is $\sim 3\%$ and for orientation is $\sim 13\%$ at

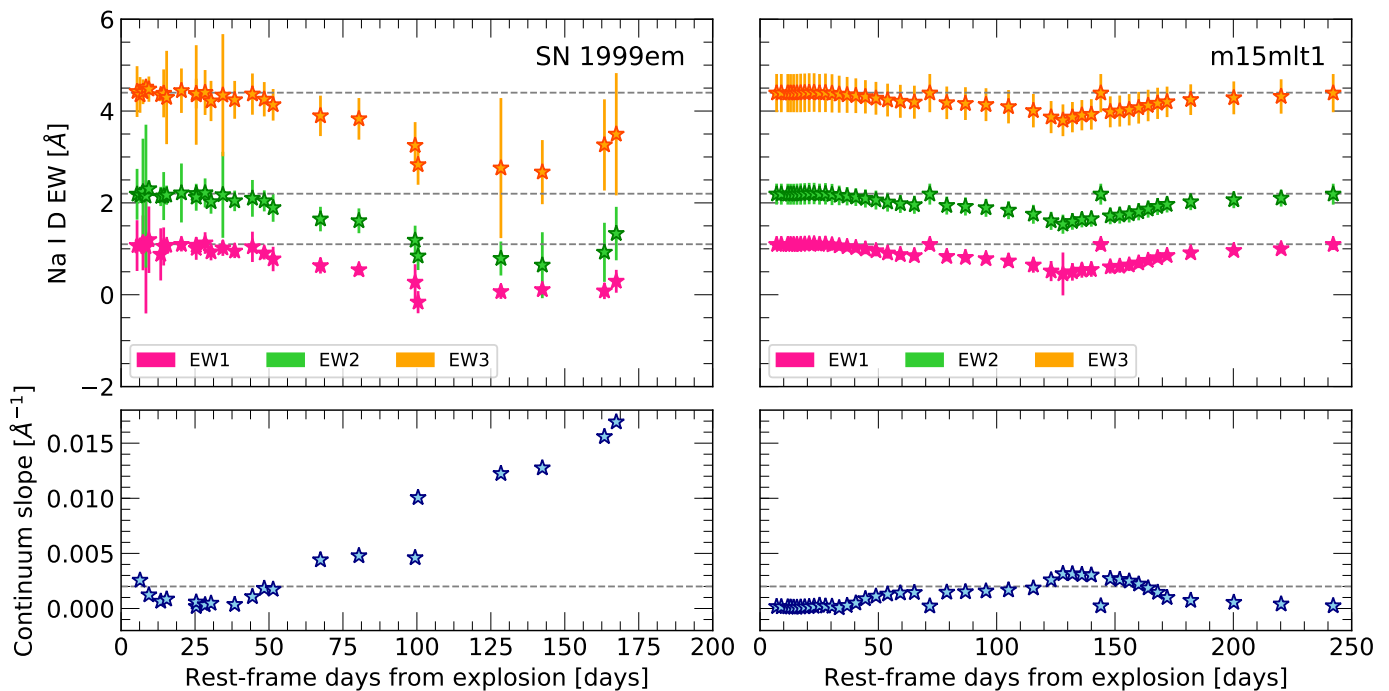


Fig. 15. EW measurements for simulated intervening Na I D lines located at rest-frame ($z_0 = 5893 \text{ \AA}$) on top of real sodium P-Cygni profiles from observed spectra of SN 1999em (left) and on top of simulated spectra of Dessart & Hillier (2011) (right). Horizontal lines show the EW expected from the simulated narrow Na I D line: $EW1 = 1.1 \text{ \AA}$, $EW2 = 2.2 \text{ \AA}$ and $EW3 = 4.4 \text{ \AA}$. The measured continuum slope at around 5893 \AA is presented in the bottom panel. The horizontal line shows the cut applied in this study: a maximum continuum slope value of 0.002 \AA^{-1} .

position 3). Although positions 2-6 do not enclose a supernova, we expect the effect of just integrated host light to be an upper limit on the EW since the light contribution of the SN will dominate. In fact, position 1 with the SN does present only minor changes of less than 3% with slit size and orientation. Similar results were also found using several other galaxies targeted by AMUSING, particularly the largest error associated with these components is about 0.20 \AA , which is generally always lower than the uncertainty estimate of our automated technique and thus not a major concern henceforth.

5.6. Minimum number of spectra

In this section, we evaluate how the automated measurement of the EW changes with the number of spectra used in the stacking procedure of section 4.3. We take non-evolving SNe with more than 20 spectra, passing the previous cuts (in particular, the continuum slope). We then explore the effect of using 1 to 15 spectra for calculating the EW. For each number of spectra used, we draw 50 random combinations of spectra and calculate the median and standard deviation, as shown in Figure 21. Besides the dispersion of all draws, we also show the typical median uncertainty obtained from our method with dashed error bars. The bottom plot shows that the uncertainties are conservative when using more than 2-3 spectra. The standard deviation indicates a high dispersion in the measured values for one and sometimes two spectra, even beyond the measured uncertainties. The bottom panel of Figure 21 shows that this underestimation can reach a factor of 2-10 when using only one spectrum. We thus prefer to discard SNe with only one

spectrum because of the large dispersion of $1 - 2 \text{ \AA}$ of some cases.

Our final set of spectra and SNe is considerably reduced after the four cuts (see Table 2): redshift, signal-to-noise in the spectra, continuum slope, signal-to-noise in the EW and minimum number of spectra. However, we believe these cuts provide a clean sample suitable for the automated measurement of narrow lines.

6. Na I D EW evolution analysis and discussion

The evolution of narrow lines from intervening material has been largely studied in the literature, and variations in the EW have been reported for various transients (e.g. Byrne et al. 2023; de Jaeger et al. 2015). Such observations have important implications for the presence and possible interaction with circumstellar matter or nearby patchy interstellar clouds. In high-resolution spectra of SNe Ia, SN 2006X (Patat et al. 2007), SN 2007le (Simon et al. 2009), SN 2013gh (Ferretti et al. 2016), and SN 2014J (Graham et al. 2015) showed changes in the EWs and profiles of the narrow intervening features. In the previous section, we showed with simulations that the EW measurement of narrow lines in high-resolution spectra is not affected by systematic biases; therefore, changes in profiles and intensities presented in these works probably represent true changes in the absorption of material in the line of sight of those SNe. On the other hand, we have shown that variations in low-resolution spectra should be analyzed with care. In particular, the effect of the varying morphology of the underlying ejecta P-Cygni profile must be considered. Wang et al. (2019) found variable Na I D absorption lines in low-

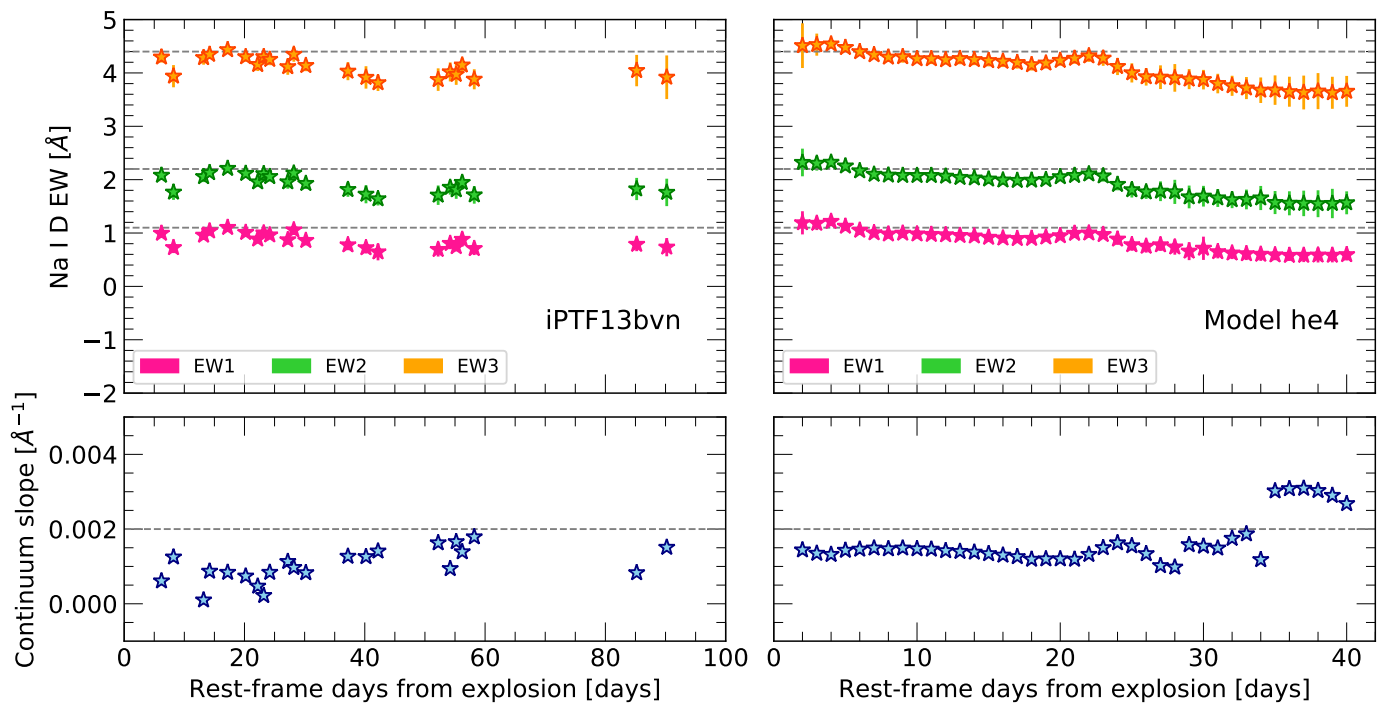


Fig. 16. Same as Figure 15, but for SESNe. Simulated narrow Na I D lines on top of observed spectra of iPTF13bvn (left) and on top of modeled spectra of Dessart et al. (2020) (right).

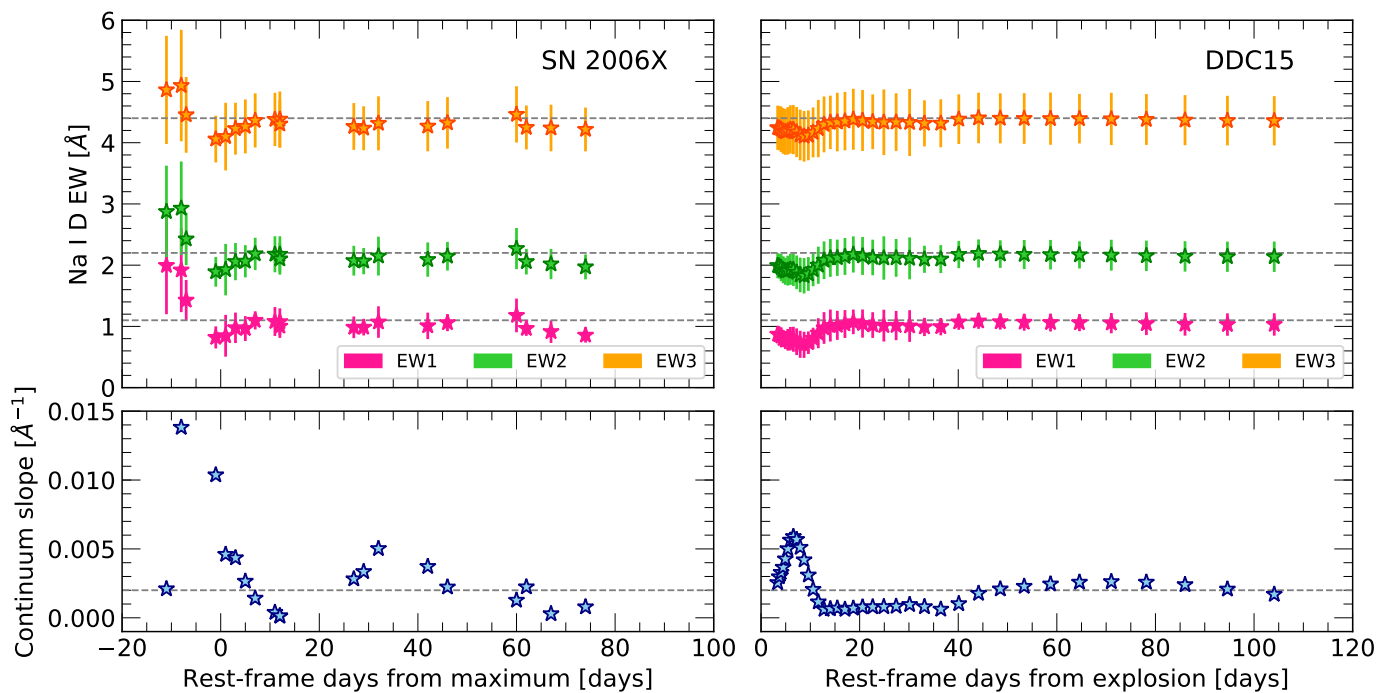


Fig. 17. Same as Figure 15, but for SNe Ia. Simulated narrow Na I D lines on top of observed spectra of SN 2006X (left) and on top of modeled spectra of Blondin et al. (2015) (right).

resolution spectra of high-velocity SNe Ia at early phases. We found a similar behaviour at similar phases in our low-resolution simulation: a decrease in the EW, followed by an increase, finally settling onto a constant evolution. As shown in Figure 17, the changes in the EW are closely related to the slope of the continuum. When a continuum cut is considered, the variability in most objects disappears.

This does not mean that the variability of the narrow absorption lines in low-resolution spectra cannot be real, but we suggest that careful cuts must be considered before performing such analysis and drawing conclusions.

After including the cuts described in previous sections (see summary in Table 2), we evaluate the behaviour of the strength of the narrow Na I D absorption lines as a function

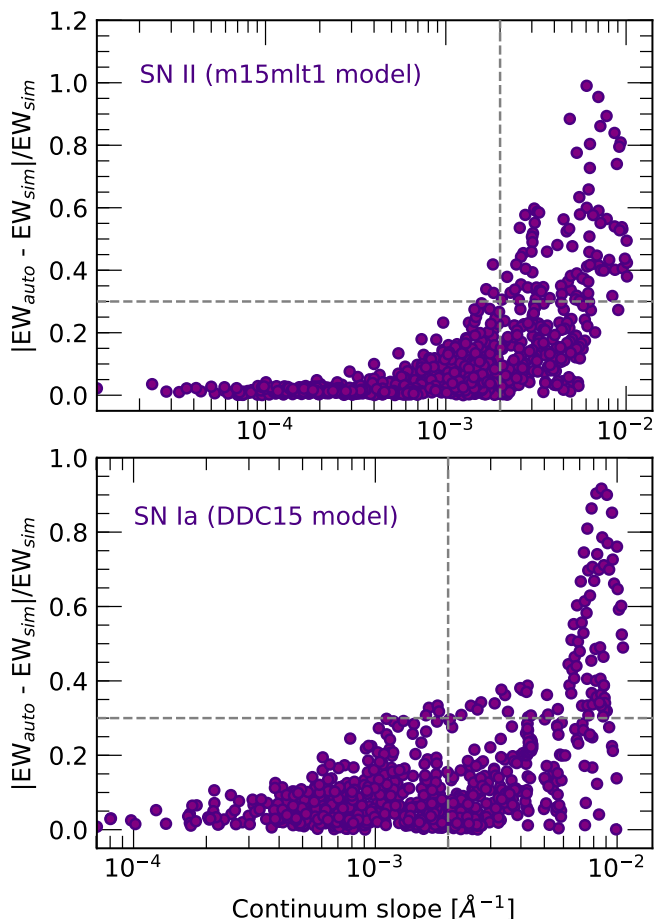


Fig. 18. Fractional residual of measured EW to simulated EW ($|EW_{\text{auto}} - EW_{\text{sim}}|/EW_{\text{sim}}$) as a function of the continuum slope around the Na I D line for simulated spectra of SNe II (top) and SNe Ia (bottom). EW measurements include simulated line-of-sight Na I D lines at 6 different positions around the central wavelength and for three different simulated narrow EW strengths. The vertical dashed line is our adopted cut to eliminate spectra with too large a continuum slope, i.e., a big underlying broad line profile, eliminating cases with more than 30% residuals (horizontal dashed lines).

of time. Since EW measurements from an individual spectrum can be unreliable (Section 5.6), we require at least two spectra per epoch range for a given SN; we then stack them and recalculate the EW (see Section 4.3). For this analysis, we explore various possibilities, using at least two or at least three spectra per SN in intervals of 10 to 20 days. While stacking SN spectra in time intervals will wash out shorter timescale variations, it ensures that we can study the time evolution of the EW with our methodology and low-resolution spectra. Once the spectra are stacked, we look at the evolution of the narrow lines both statistically and individually. Particularly, we focus on the EW of the line because it is more robust than the velocity (see section 4.2).

6.1. Statistical evolution of EW

We study the main SN types, SNe Ia, SNe II, SESNe and SNe-int, for statistical signs of evolution. Finding population-wide signs of evolution could give us important

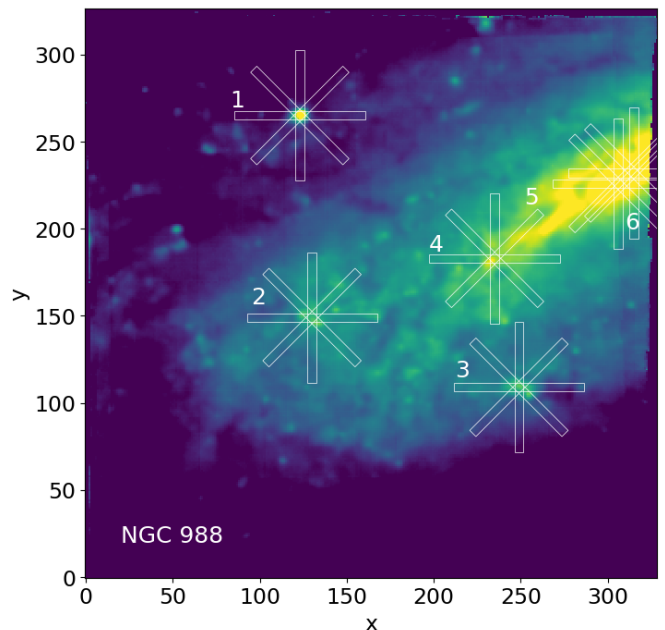


Fig. 19. MUSE image of the galaxy NGC 988. This synthetic image is created by collapsing the MUSE data cube across the full wavelength range of the observation. Orientation is North-up, East-left. The white rectangles mark four slit angles (0, 45, 90 and 135 degrees) at six different positions, labelled with numbers from 1 to 6. The width of the slit is 1'' in this case, but the tests are also performed for a 1.5'' slit.

insight into the progenitor systems and nearby material of a given population. For instance, a large number of SNe II are known to be subject to very early interaction with CSM (e.g. [Bostroem et al. 2023](#); [Martinez et al. 2023](#)) that could perhaps be revealed in the narrow absorption line evolution. SNe-int are by definition subject to interaction with nearby material and thus good candidates to observe evolution in the narrow absorption lines, as is the case for SN 2011A ([de Jaeger et al. 2015](#)); however, the line is often absent despite strong CSM interaction (e.g. [Ofek et al. 2010](#); [Pastorello et al. 2018](#)). To investigate this, we require a common reference epoch for each group. We use the maximum *B*-band dates obtained through multi-wavelength light-curve fits with spectrophotometric templates of each SN type (see Appendix B). The epochs are normalized to this reference epoch and put in rest-frame. All spectra of a given SN in time intervals of, e.g. 10 days, are stacked, and the EW is measured. We investigate the evolution of the σ -deviations per epoch interval i with respect to the all-epoch stacked EW measurement of each SN, i.e. \overline{EW} , so that:

$$\delta\sigma_i = \frac{EW_i - \overline{EW}}{\sqrt{\sigma_{EW_i}^2 + \sigma_{\overline{EW}}^2}}. \quad (7)$$

Figure 22 shows the evolution of the distribution of these deviations for the Na I D lines of the four SN types considered. In general, we can see that there is no large evolution of these groups within the uncertainties. For SESNe, there seems to be a decrease after 50 days post maximum, although this is likely due to low-number statistics. Simi-

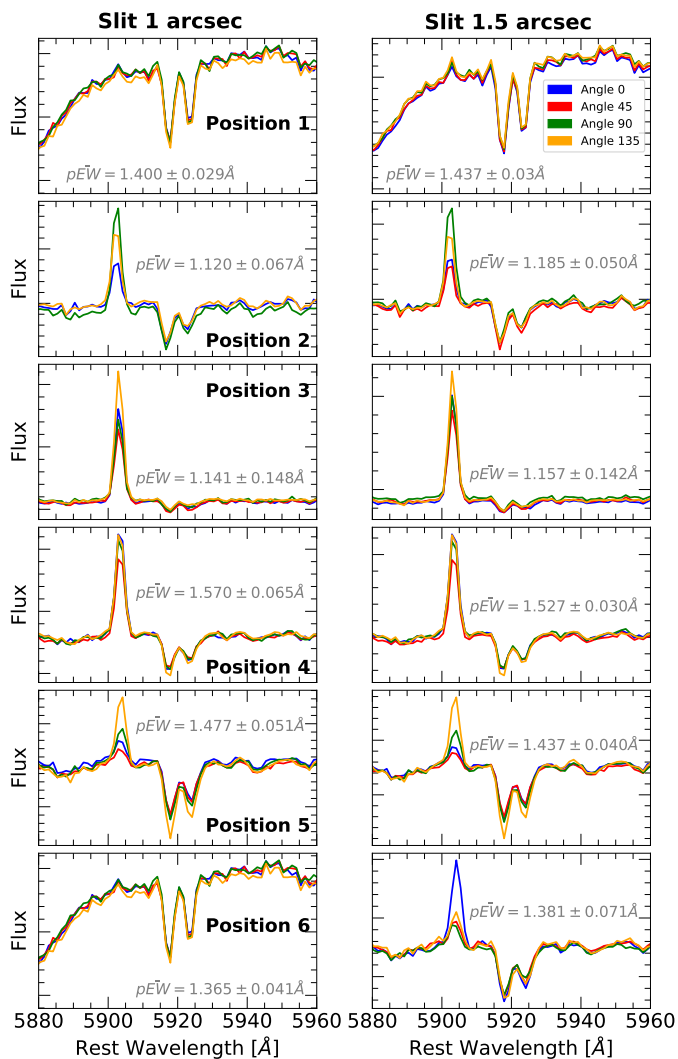


Fig. 20. Spectra around the Na I D line-of-sight line for six slit positions of the MUSE cube shown in Figure 19 and with four orientations with respect to the horizontal W-E orientation shown in colours: blue (0°), red (45°), green (90°) and yellow (135°). The left panels are for the $1''$ and the right panels for the $1.5''$ slits. The measured EWs and velocities are always consistent within the uncertainties for the different slit orientations and apertures. We note that the emission line to the left of Na I D absorption lines is the nebular He I at restframe 5875 \AA .

larly, SNe Ia appear to increase within 30 and 50 days post maximum, but with a small number of SNe at these epochs, this is mainly driven by one SN (SN 2012dn), as we will see in the next section. SNe-int also have very low statistics making any conclusion rather difficult. When investigating the evolution with different epoch intervals between 10-15 days and also requiring a minimum of three spectra per SN per interval instead of two, we obtain similar results.

Additionally, we also investigate narrow lines from other species, such as Ca II and K I finding no evidence of evolution. However, it is possible that smaller sub-groups might show signs of changes in time. Given the small statistics after all our cuts, we leave this for a future investigation. In the next section, we analyse the evolution of individual well-sampled SNe.

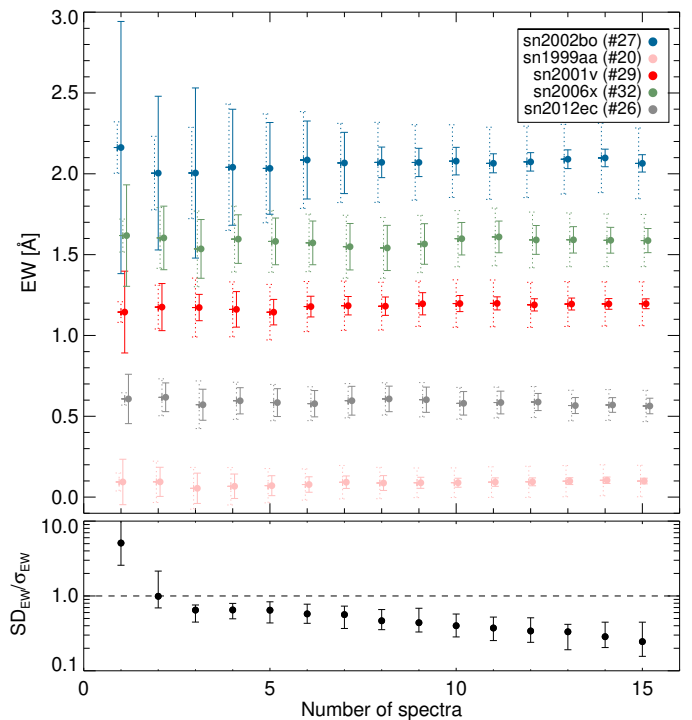


Fig. 21. **Top:** Median and standard deviation of equivalent width measurements from multiple spectra randomly taken from the numerous sets of spectra of five SNe: SN 1999aa, SN 2001V, SN 2002bo, SN 2006X and SN 2012ec, as a function of the number of spectra used for the measurement. The solid error bars represent the standard deviation, while the dashed error bars are the median error calculated by the automated technique. **Bottom:** Average ratio of the standard deviation to the calculated uncertainty from the automated technique for nearly 30 SNe with more than ten spectra. The error bars show the dispersion.

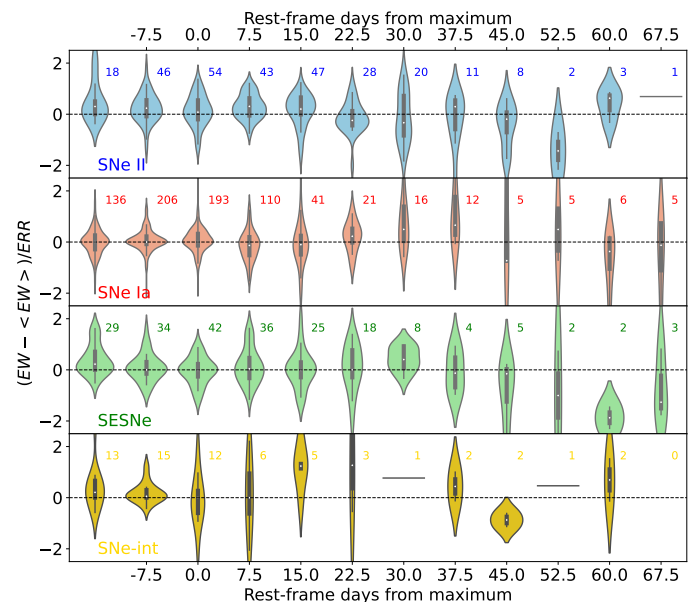


Fig. 22. Na I D Violin plots of Na I DEW evolution for each SN type (from top to bottom: SNe II, SNe Ia, SESNe and SNe-int) showing the mean and extreme of the distribution (white point in the box and edges of central vertical lines) and a kernel density probability estimation (coloured area). The number of SNe within each distribution at each epoch is indicated above each bin. We require at least two spectra per SN in intervals of 15 days for stacked EW measurements.

6.2. Individual evolution of EW

To analyze the evolution of the EW of narrow absorption lines for individual objects, we take the stacked EW of a minimum of two spectra in intervals of 10 days, as in the previous section. Besides a visual inspection, we apply two methods to identify possible candidates for evolution automatically:

- **Linear slope:** we fit the EW of all intervals of each SN to a simple line with a Bayesian fit from which the posterior distribution gives us the probability for the slope to be different from zero (Kelly 2007). A significantly non-zero slope ($p > 95\%$) indicates that there is a general monotonic trend in the evolution of the SN.
- **Cumulative sum:** to try to capture more complicated evolution, we also do a cumulative sum analysis (CUSUM, Page 1954) that monitors deviations from a target, in this case, the EW value obtained from the stack of all the spectra (at all epochs) of a given SN, \overline{EW} . Then the algorithm measures accumulated deviations, chosen here as a drift of half the uncertainty on the stacked EW, $0.5\sigma_{\overline{EW}}$, to both positive and negative directions, so that:

$$\begin{aligned} H_0 &= 0 \\ L_0 &= 0 \\ H_i &= \max\left[0, H_{i-1} + (EW_i - \sigma_{EW_i}) - (\overline{EW} + 0.5\sigma_{\overline{EW}})\right] \\ L_i &= \min\left[0, L_{i-1} + (EW_i + \sigma_{EW_i}) - (\overline{EW} - 0.5\sigma_{\overline{EW}})\right] \end{aligned}$$

where H_i and L_i indicate the positive and negative cumulative deviations updated at each time step i . We also take into account the uncertainty in each individual EW_i . This measures the cumulative deviations starting from the earliest epoch interval of the SN and increasing in time. In order to not give higher weight to the initial time bins, we also start the algorithm from the latest epoch interval going in decreasing time steps. The final cumulative H and L are the average of both sequential cumulative deviations. SNe with more than two cumulative deviations above the error on the stacked EW are considered viable candidates.

Figure 23 shows these two methods applied to the measurements of SN 2006X (SN Ia) and SN 2014G (SN II) after the cuts (filled black points). Doing a Bayesian linear fit to the stacked EWs per epoch interval (red points) results in a slope consistent with zero for SN 2006X and no significant points in the cumulative deviation analysis. SN 2014G, on the other hand, has a slope with a probability of 93.7% to be non-zero and one significant cumulative deviation point. Both of these SNe are considered to be not evolving in time according to our diagnostics. However, it is important to observe that if we were to do our analysis on all data points without cuts (empty black points), these SNe would have non-zero slope probabilities of 88.4% and 100%, with 4 and 12 significant cumulative deviation points, respectively. Both SNe would be considered to have an evolution. This shows the importance of our cuts, particularly the continuum slope that prevents strong blending with the broad P-Cygni profile (see Section 5.4).

When analysing various narrow lines for all SNe after cuts and stacking at least two spectra per 10 or 15-day intervals, we find that very few SNe are tagged as possibly evolving according to our two diagnostics. For every case, we ensure that no equivalent evolution is seen for the same lines of the MW and inspect them visually. The few SNe tagged (e.g. SN 2001N, SN 2012dn) have few points in the nebular phase with stronger EW. However, these are a very small number and, in some cases, still noisy after stacking per interval. In the case of SN 2012dn, a 03fg-like "super-Chandra" SN Ia (Chakradhari et al. 2014; Taubenberger et al. 2019), the narrow Na I D at ~ 40 days after the maximum gets mixed with features due to iron-group elements and it is difficult to disentangle the two.

SNe known to show variation in their lines with high-resolution spectra, e.g. SN 2006X, SN 2007le, SN 2013gh or SN 2014J, are not picked up by our cuts, but we have predominantly low-resolution spectra for which such small variations remain within the uncertainties. We have no access to high-resolution spectra for SN 2006X, SN 2013gh and only one for SN 2007le. For SN 2014J, if we restrict our analysis to the 10 high-resolution spectra we have and do not make any cuts on the continuum slope, we find no evolution of the EW for Na I D and no evolution of the three spectra that cover the wavelengths of K I. Graham et al. 2015 found evolution in K I lines in other spectra of even higher resolution ($R > 100000$). In the case of the type II in SN 2011A (de Jaeger et al. 2015), we do see the increase in EW with time that they report. Nonetheless, with only 5 spectra after cuts (and only two stacked points per 15-day interval), the linear slope is not significantly positive, and the stacked EW of all spectra is too influenced by the late spectra with increasing EW, such that no significant deviation points are found.

We conclude that the current dataset, after all our cuts and with our methodology, is consistent with no variation in the EW of narrow lines over time within the uncertainties. More subtle variations are naturally possible but necessitate better sampling and, foremost, higher spectral resolution.

7. Conclusions

In this paper, we have presented a statistical analysis of the evolution of narrow line-of-sight lines from intervening material (Na I D, Ca II H&K, K I, DIBs) visible in nearby SNe. We have analyzed over 11000 spectra of more than 1600 SNe with various resolutions. To quantify the properties of these narrow lines, we developed a robust automated methodology allowing for the estimation of their EWs and velocities. When searching for possible EW evolution, we found systematic variations in the Na I D line from the MW and the host galaxies. Changes in the Na I D depth from the MW narrow interstellar lines are in principle not expected because the material in our own Galaxy is at sufficiently large distances from the SN. The strength of the narrow absorption lines in low and mid-resolution spectra may thus be affected by different external factors that we explore: the signal-to-noise of the spectra, the spectral resolution, the slit size and orientation, the number of spectra used and most importantly, the interference of the broad P-Cygni lines from the SN. We found that these biases, particularly those associated with presence of the broad lines, induce a conspicuous apparent evolution (variability) over time in many SNe. For instance, in SNe II, the narrow sodium line

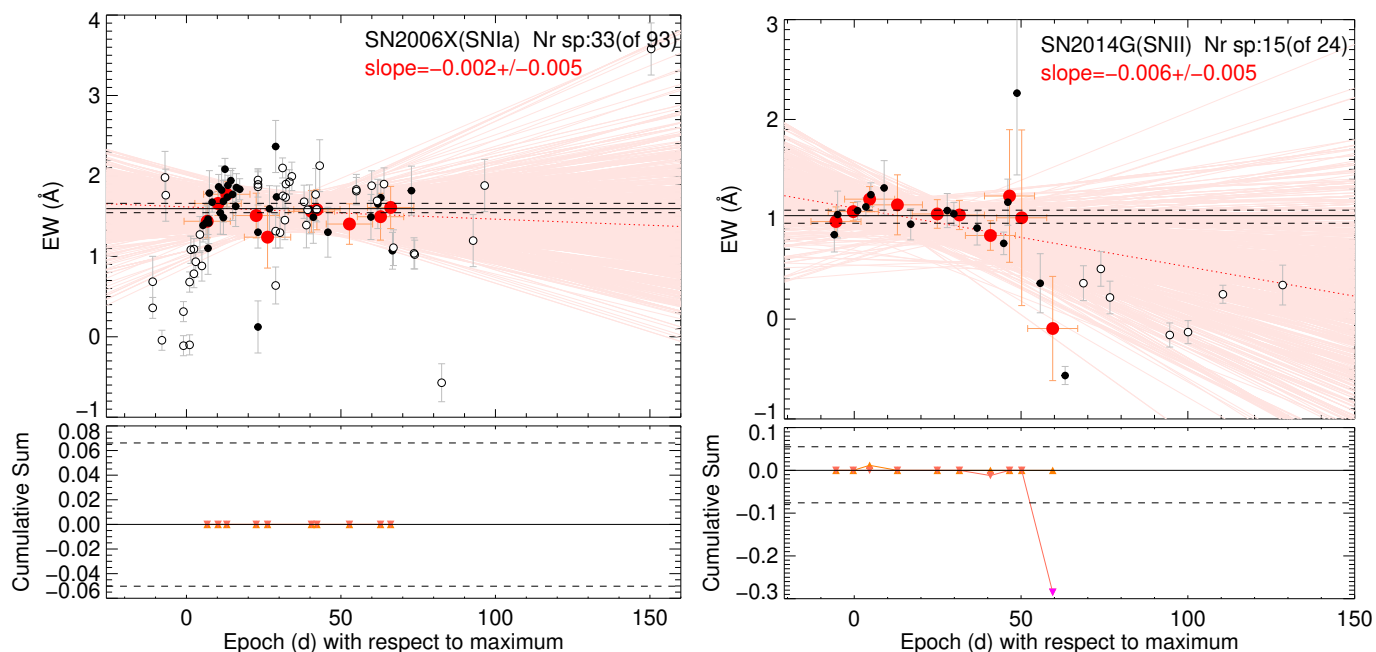


Fig. 23. Top: NaID EW evolution for SN 2006X (left) and SN 2014G (right) before/after cuts (empty/filled black points) and stacked measurements of points after culls in intervals of 15 days requiring minimum 2 spectra (red points). Horizontal lines indicate the stacked EW and error from all spectra that passed the cuts. A Bayesian linear fit to the red points is shown with light red lines (1000 realizations) and a corresponding median with a dotted red line. The resulting slope is negative with 68.7% and 93.7% probability, respectively for both SNe. **Bottom:** Cumulative deviation analysis above/below (upper/lower triangles) the stacked EW (corresponding to the zero horizontal line) and its associated errors (dashed lines). Significant points are shown in purple.

overlaps with the broad sodium from the SN ejecta, and in SNe Ia the narrow sodium overlaps with the P-Cygni profile of Si II. Indeed, we confirm this with simulations in which we input fake narrow lines into different locations of the broad SN P-Cygni lines and calculate the recovered EW. In our simulations of low-resolution spectra, we found large significant changes in the EW depending on the underlying profile. However, in our high-resolution simulations, the strength of the narrow lines was not affected by the interference of the broad SN P-Cygni profiles.

Based on these findings, we presented an easy way to detect and exclude cases of high contamination of the SN profile in the narrow line: when the normalized slope of the continuum is too high, i.e. $m_c > 0.002 \text{ \AA}^{-1}$, there is a broad component underneath blending with the narrow line. We show that excluding these cases with a steep continuum is essential in the study of narrow lines from intervening material in the line of sight. Not taking this into account may lead to important biases in the frequently used estimations of dust extinction through the $EW \propto A_V$ relation (Eq. 3) in low-resolution spectra, and it may lead to wrong inferences of the evolution of the lines and the presence of nearby material. Previous claims of the evolution of narrow lines in low-resolution spectra should be revisited in light of this study.

We also strongly encourage the use of more than one low-resolution spectrum in the estimation of the EW. Fluctuations of the S/N, the spectral resolution, and the morphology of the underlying P-Cygni profile over time can generate changes in these lines that are washed out with a larger number of spectra stacked to obtain a more accurate EW. We show that at least 2-3 spectra are needed to measure robust EWs with conservative uncertainties.

Finally, after considering all these effects, we analysed the temporal evolution of line-of-sight features in a large sample of nearby SNe to detect any possible statistical variation in their EWs. We found no overall evolution for three principal SN groups: SNe II, SNe Ia and SESNe, in all narrow lines considered. Significant individual SN variations were also ruled out based on our methodology and low-resolution spectra.

In this work, we have paved the way for robust measurement of narrow absorption lines in a variety of spectra from different instruments and resolutions. Armed with this methodology, we can now use a large sample to study the variations of the SN-averaged narrow lines according to SN type, to SN properties, and to host galaxy characteristics. A wealth of information on the pervading intervening material is contained in those lines providing essential clues to the immediate and farther vicinity of SNe and their progenitors, with far-reaching consequences for our understanding of the ISM cycle of galaxies and the persistent question of extinction in supernova cosmology.

Acknowledgements. We sincerely thank the referee for very useful comments that improved the quality of the paper. We heartily thank all the research groups and observers for making their data public. This research has made use of the Berkeley SNDB database as well as the CfA Supernova Archive, which is funded in part by the National Science Foundation through grant AST 0907903. S.G.G. acknowledges the financial support from the visitor and mobility program of the Finnish Centre for Astronomy with ESO (FINCA), funded by the Academy of Finland grant nr 306531. S.G.G. and A.M.M. acknowledge support by FCT under Project CRISP PTDC/FIS-AST-31546/2017 and Project No. UIDB/00099/2020. C.P.G. acknowledges financial support from the Secretary of Universities and Research (Government of Catalonia) and by the Horizon 2020 Research and Innovation Programme of the European Union under the Marie Skłodowska-Curie and the Beatriu de Pinós 2021 BP 00168 programme. C.P.G. and L.G. recognize the support from

the Spanish Ministerio de Ciencia e Innovación (MCIN) and the Agencia Estatal de Investigación (AEI) 10.13039/501100011033 under the PID2020-115253GA-I00 HOSTFLOWS project, from Centro Superior de Investigaciones Científicas (CSIC) under the PIE project 20215AT016, and the program Unidad de Excelencia María de Maeztu CEX2020-001058-M. L.G. also thanks the financial support from the European Social Fund (ESF) "Investing in your future" under the 2019 Ramón y Cajal program RYC2019-027683-I. J.P.A. acknowledges support by ANID, Millennium Science Initiative, ICN12_009. A.M.G. acknowledges financial support by the European Union under the 2014-2020 ERDF Operational Programme and by the Department of Economic Transformation, Industry, Knowledge, and Universities of the Regional Government of Andalusia through the FEDER-UCA18-107404 grant. S.M. acknowledges support from the Research Council of Finland project 350458.

References

- Ailawadhi, B., Dastidar, R., Misra, K., et al. 2023, *MNRAS*, 519, 248
- Appenzeller, I. 1986, in *European Southern Observatory Conference and Workshop Proceedings*, Vol. 24, *European Southern Observatory Conference and Workshop Proceedings*, ed. S. D'Odorico & J. P. Swings, 93–105
- Arbour, R., Li, W., Mostardi, R., et al. 2007, *IAU Circ.*, 8829, 2
- Arcavi, I., Gal-Yam, A., Yaron, O., et al. 2011, *ApJ*, 742, L18
- Aretxaga, I., Benetti, S., Terlevich, R. J., et al. 1999, *MNRAS*, 309, 343
- Barbon, R., Buondì, V., Cappellaro, E., & Turatto, M. 1999, *A&AS*, 139, 531
- Baron, D., Poznanski, D., Watson, D., Yao, Y., & Prochaska, J. X. 2015, *MNRAS*, 447, 545
- Baron, D., Stern, J., Poznanski, D., & Netzer, H. 2016, *ApJ*, 832, 8
- Benetti, S. 1991, in *European Southern Observatory Conference and Workshop Proceedings*, Vol. 37, *European Southern Observatory Conference and Workshop Proceedings*, 339
- Benetti, S., Cappellaro, E., Danziger, I. J., et al. 1998, *MNRAS*, 294, 448
- Benetti, S., Cappellaro, E., Turatto, M., et al. 1994, *A&A*, 285, 147
- Benetti, S., Chugai, N. N., Utrobin, V. P., et al. 2016, *MNRAS*, 456, 3296
- Benetti, S., Turatto, M., Balberg, S., et al. 2001, *MNRAS*, 322, 361
- Benetti, S., Turatto, M., Cappellaro, E., Danziger, I. J., & Mazzali, P. A. 1999, *MNRAS*, 305, 811
- Benetti, S., Turatto, M., Valenti, S., et al. 2011, *MNRAS*, 411, 2726
- Black, C. S., Milisavljevic, D., Margutti, R., et al. 2017, *ApJ*, 848, 5
- Blanco, V. M., Gregory, B., Hamuy, M., et al. 1987, *ApJ*, 320, 589
- Blanton, E. L., Schmidt, B. P., Kirshner, R. P., et al. 1995, *AJ*, 110, 2868
- Blaylock, M., Branch, D., Casebeer, D., et al. 2000, *PASP*, 112, 1439
- Blondin, S., Challis, P., & Kirshner, R. 2008, *Central Bureau Electronic Telegrams*, 1454, 1
- Blondin, S., Dessart, L., & Hillier, D. J. 2015, *MNRAS*, 448, 2766
- Blondin, S., Matheson, T., Kirshner, R. P., et al. 2012, *AJ*, 143, 126
- Blondin, S., Prieto, J. L., Patat, F., et al. 2009, *ApJ*, 693, 207
- Borish, H. J., Huang, C., Chevalier, R. A., et al. 2015, *ApJ*, 801, 7
- Bostroem, K. A. et al. 2023, *ApJ*, 956, L5
- Botticella, M. T. et al. 2009, *MNRAS*, 398, 1041
- Branch, D., Falk, S. W., Uomoto, A. K., et al. 1981, *ApJ*, 244, 780
- Branch, D. & Venkatakrisna, K. L. 1986, *ApJ*, 306, L21
- Bufano, F., Pignata, G., Bersten, M., et al. 2014, *MNRAS*
- Bufano, F. et al. 2012, *ApJ*, 753, 67
- Buscombe, W. & Kennedy, P. M. 1968, *MNRAS*, 139, 417
- Byrne, R. A., Fraser, M., Cai, Y. Z., Reguitti, A., & Valerin, G. 2023, *MNRAS*, 524, 2978
- Cappellaro, E., Danziger, I. J., della Valle, M., Gouiffes, C., & Turatto, M. 1995, *A&A*, 293, 723
- Casebeer, D., Branch, D., Blaylock, M., et al. 2000, *PASP*, 112, 1433
- Chakradhari, N. K., Sahu, D. K., Srivastav, S., & Anupama, G. C. 2014, *MNRAS*, 443, 1663
- Chen, Y.-M., Tremonti, C. A., Heckman, T. M., et al. 2010, *AJ*, 140, 445
- Childress, M. J., Hillier, D. J., Seitzzahl, I., et al. 2015, *MNRAS*, 454, 3816
- Childress, M. J., Tucker, B. E., Yuan, F., et al. 2016, *PASA*, 33, e055
- Ciabattari, F., Mazzoni, E., Rossi, M., et al. 2013, *Central Bureau Electronic Telegrams*, 3576, 1
- Clark, P., Maguire, K., Bulla, M., et al. 2021, *MNRAS*, 507, 4367
- Clocchiatti, A., Benetti, S., Wheeler, J. C., et al. 1996, *AJ*, 111, 1286
- Conley, A., Sullivan, M., Hsiao, E. Y., et al. 2008, *ApJ*, 681, 482
- Corsi, A., Ofek, E. O., Gal-Yam, A., et al. 2012, *ApJ*, 747, L5
- Cristiani, S., Cappellaro, E., Turatto, M., et al. 1992, *A&A*, 259, 63
- Dame, T. M., Hartmann, D., & Thaddeus, P. 2001, *ApJ*, 547, 792
- Davis, K., Johnson, J., Tinsyanont, S., et al. 2022, *Transient Name Server Classification Report*, 2022-362, 1
- de Jaeger, T., Anderson, J. P., Pignata, G., et al. 2015, *ApJ*, 807, 63
- de Jaeger, T., Zheng, W., Stahl, B. E., et al. 2019, *MNRAS*, 490, 2799
- D'Elia, V., Pian, E., Melandri, A., et al. 2015, *A&A*, 577, A116
- Deng, J. S., Qiu, Y. L., Hu, J. Y., Hatano, K., & Branch, D. 2000, *ApJ*, 540, 452
- DerKacy, J. M., Paugh, S., Baron, E., et al. 2023, *MNRAS*, 522, 3481
- Dessart, L., Gutierrez, C. P., Hamuy, M., et al. 2014, *MNRAS*, 440, 1856
- Dessart, L. & Hillier, D. J. 2011, *MNRAS*, 410, 1739
- Dessart, L., Yoon, S.-C., Aguilera-Dena, D. R., & Langer, N. 2020, *A&A*, 642, A106
- Draine, B. T. 2011, *Physics of the Interstellar and Intergalactic Medium* (Princeton University Press)
- Drake, A. J., Djorgovski, S. G., Graham, M. J., et al. 2013, *Central Bureau Electronic Telegrams*, 3494, 1
- Drout, M. R., Milisavljevic, D., Parrent, J., et al. 2016, *ApJ*, 821, 57
- Drout, M. R., Soderberg, A. M., Mazzali, P. A., et al. 2013, *ApJ*, 774, 58
- Dugas, A., Fremling, C., & Sharma, Y. 2019, *Transient Name Server Classification Report*, 2019-2840, 1
- Dunham, T., J. 1937, *PASP*, 49, 26
- Elias-Rosa, N., Pastorello, A., Maund, J. R., et al. 2013, *MNRAS*, 436, L109
- Elias-Rosa, N., Van Dyk, S. D., Li, W., et al. 2010, *ApJ*, 714, L254
- Elias-Rosa, N. et al. 2006, *MNRAS*, 369, 1880
- Ergon, M., Sollerman, J., Fraser, M., et al. 2014, *A&A*, 562, A17
- Evans, J. W. 1941, *ApJ*, 93, 275
- Faran, T., Poznanski, D., Filippenko, A. V., et al. 2014a, *MNRAS*, 442, 844
- Faran, T., Poznanski, D., Filippenko, A. V., et al. 2014b, *MNRAS*, 445, 554
- Fassia, A., Meikle, W. P. S., Chugai, N., et al. 2001, *MNRAS*, 325, 907
- Ferretti, R., Amanullah, R., Goobar, A., et al. 2016, *A&A*, 592, A40
- Filippenko, A. V. 1988, *AJ*, 96, 1941
- Filippenko, A. V. 1997, *ARA&A*, 35, 309
- Filippenko, A. V., Porter, A. C., & Sargent, W. L. W. 1990, *AJ*, 100, 1575
- Filippenko, A. V., Richmond, M. W., Branch, D., et al. 1992a, *AJ*, 104, 1543
- Filippenko, A. V., Richmond, M. W., Matheson, T., et al. 1992b, *ApJ*, 384, L15
- Filippenko, A. V. & Sargent, W. L. W. 1986, *AJ*, 91, 691
- Folatelli, G., Morrell, N., Phillips, M. M., et al. 2013, *ApJ*, 773, 53
- Foley, R. J. 2015, *MNRAS*, 452, 2463
- Foley, R. J., Filippenko, A. V., & Jha, S. W. 2008, *ApJ*, 686, 117
- Foley, R. J., Jha, S. W., Pan, Y.-C., et al. 2016a, *MNRAS*, 461, 433
- Foley, R. J., Pan, Y.-C., Brown, P., et al. 2016b, *MNRAS*, 461, 1308
- Foley, R. J., Smith, N., Ganeshalingam, M., et al. 2007, *ApJ*, 657, L105
- Foley, R. J., Van Dyk, S. D., Jha, S. W., et al. 2015, *ApJ*, 798, L37
- Foley, R. J. et al. 2012a, *ArXiv e-prints* [arXiv:1203.2916]
- Foley, R. J. et al. 2012b, *ApJ*, 744, 38
- Foley, R. J. et al. 2013, *ApJ*, 767, 57
- Förster, F., González-Gaitán, S., Anderson, J., et al. 2012, *ApJ*, 754, L21
- Förster, F., González-Gaitán, S., Folatelli, G., & Morrell, N. 2013, *ApJ*, 772, 19
- Fraser, M., Ergon, M., Eldridge, J. J., et al. 2011, *MNRAS*, 417, 1417
- Fraser, M. et al. 2013, *MNRAS*, 433, 1312
- Gagliano, R., Post, R., Weinberg, E., Newton, J., & Puckett, T. 2016, *Transient Name Server Discovery Report*, 2016-568, 1
- Gal-Yam, A., Arcavi, I., Ofek, E. O., et al. 2014, *Nature*, 509, 471
- Gal-Yam, A., Bruch, R., Schulze, S., et al. 2022, *Nature*, 601, 201
- Gal-Yam, A., Bufano, F., Barlow, T. A., et al. 2008, *ApJ*, 685, L117
- Gal-Yam, A., Kasliwal, M. M., Arcavi, I., et al. 2011, *ApJ*, 736, 159
- Gal-Yam, A., Leonard, D. C., Fox, D. B., et al. 2007, *ApJ*, 656, 372
- Galazutdinov, G. 2005, *Journal of Korean Astronomical Society*, 38, 215
- Galbany, L., Hamuy, M., Phillips, M. M., et al. 2016a, *AJ*, 151, 33
- Galbany, L., Moreno-Raya, M. E., Ruiz-Lapuente, P., et al. 2016b, *MNRAS*, 457, 525

- Gerardy, C. L., Meikle, W. P. S., Kotak, R., et al. 2007, *ApJ*, 661, 995
- Gomez, G. & Lopez, R. 1995, *AJ*, 109, 737
- Gómez, G. & López, R. 1998, *AJ*, 115, 1096
- Gómez, G. & López, R. 2000, *AJ*, 120, 367
- Gomez, G., Lopez, R., & Sanchez, F. 1996, *AJ*, 112, 2094
- Gorbikova, E., Gal-Yam, A., Ofek, E. O., et al. 2014, *MNRAS*, 443, 671
- Graham, M. L., Kumar, S., Hosseinzadeh, G., et al. 2017, *MNRAS*, 472, 3437
- Graham, M. L., Sand, D. J., Valenti, S., et al. 2014, *ApJ*, 787, 163
- Graham, M. L., Valenti, S., Fulton, B. J., et al. 2015, *ApJ*, 801, 136
- Green, D. W. E. 2007, *Central Bureau Electronic Telegrams*, 974, 2
- Guillochon, J., Parrent, J., Kelley, L. Z., & Margutti, R. 2017, *ApJ*, 835, 64
- Gutiérrez, C. P., Anderson, J. P., Hamuy, M., et al. 2017, *ApJ*, 850, 89
- Gutiérrez, C. P., Bersten, M. C., Orellana, M., et al. 2021, *MNRAS*, 504, 4907
- Gutiérrez, C. P., Cartier, R., & Yaron, O. 2017, *Transient Name Server Classification Report*, 2017-468, 1
- Gutiérrez, C. P., González-Gaitán, S., Folatelli, G., et al. 2016, *A&A*, 590, A5
- Hamuy, M., Maza, J., Pinto, P. A., et al. 2002, *AJ*, 124, 417
- Han, X., Zheng, W., Stahl, B. E., et al. 2020, *ApJ*, 892, 142
- Harutyunyan, A. H. et al. 2008, *A&A*, 488, 383
- Heckman, T. M. & Lehnert, M. D. 2000, *ApJ*, 537, 690
- Heger, M. L. 1919a, *PASP*, 31, 304
- Heger, M. L. 1919b, *Lick Observatory Bulletin*, 326, 59
- Heger, M. L. 1922, *Lick Observatory Bulletin*, 10, 141
- Hendry, M. A., Smartt, S. J., Crockett, R. M., et al. 2006, *MNRAS*, 369, 1303
- Herbig, G. H. 1995, *ARA&A*, 33, 19
- Hicken, M., Friedman, A. S., Blondin, S., et al. 2017, *ApJS*, 233, 6
- Hiramatsu, D., Arcavi, I., Burke, J., et al. 2019a, *Transient Name Server Classification Report*, 2019-1137, 1
- Hiramatsu, D., Burke, J., Arcavi, I., et al. 2019b, *Transient Name Server Classification Report*, 2019-738, 1
- Hobbs, L. M. 1974, *ApJ*, 191, 381
- Hosseinzadeh, G., Kilpatrick, C. D., Dong, Y., et al. 2022, *ApJ*, 935, 31
- Hosseinzadeh, G., Sand, D. J., Valenti, S., et al. 2017a, *ApJ*, 845, L11
- Hosseinzadeh, G., Valenti, S., Arcavi, I., et al. 2017b, *Transient Name Server Classification Report*, 2017-1514, 1
- Hosseinzadeh, G., Valenti, S., McCully, C., et al. 2018, *ApJ*, 861, 63
- Hosseinzadeh, G. et al. 2017c, *ApJ*, 836, 158
- Hsiao, E. Y., Conley, A., Howell, D. A., et al. 2007, *ApJ*, 663, 1187
- Humphreys, R. M., Davidson, K., Jones, T. J., et al. 2012, *ApJ*, 760, 93
- Inserra, C., Pastorello, A., Turatto, M., et al. 2013, *A&A*, 555, A142
- Inserra, C., Turatto, M., Pastorello, A., et al. 2012, *MNRAS*, 422, 1122
- Irani, I., Schulze, S., Gal-Yam, A., et al. 2019, *ApJ*, 887, 127
- Jacobson-Galán, W. V., Venkatraman, P., Margutti, R., et al. 2022, *ApJ*, 932, 58
- Jencson, J. E., Prieto, J. L., Kochanek, C. S., et al. 2016, *MNRAS*, 456, 2622
- Jha, S. & Brown, W. 2000, *IAU Circ.*, 7394, 2
- Jha, S., Challis, P., Kirshner, R., & Calkins, M. 2000, *IAU Circ.*, 7379, 1
- Jha, S., Garnavich, P., Challis, P., et al. 1999, *IAU Circ.*, 7107, 2
- Jones, D. O., Dimitriadis, G., Pan, Y. C., & Foley, R. J. 2017, *Transient Name Server Classification Report*, 2017-1464, 1
- Kangas, T. et al. 2016, *MNRAS*, 456, 323
- Karamahmetoglu, E., Fransson, C., Sollerman, J., et al. 2021, *A&A*, 649, A163
- Kelly, B. C. 2007, *ApJ*, 665, 1489
- Kessler, R., Narayan, G., Avelino, A., et al. 2019, *PASP*, 131, 094501
- Khazov, D., Yaron, O., Gal-Yam, A., et al. 2016, *ApJ*, 818, 3
- Kiewe, M., Gal-Yam, A., Arcavi, I., et al. 2012, *ApJ*, 744, 10
- Kilpatrick, C. D., Foley, R. J., Abramson, L. E., et al. 2017, *MNRAS*, 465, 4650
- Kos, J. & Zwitter, T. 2013, *ApJ*, 774, 72
- Kosugi, G., Mizumoto, Y., Kawai, N., et al. 2004, *PASJ*, 56, 61
- Krelowski, J., Galazutdinov, G., Godunova, V., & Bondar, A. 2019, *Acta Astron.*, 69, 159
- Kroto, H. W., Heath, J. R., O'Brien, S. C., Curl, R. F., & Smalley, R. E. 1985, *Nature*, 318, 162
- Kumar, B. et al. 2013, *MNRAS*, 431, 308
- Kumar, S., Hsiao, E. Y., Ashall, C., et al. 2023, *ApJ*, 945, 27
- Lan, T.-W., Ménard, B., & Zhu, G. 2015, *MNRAS*, 452, 3629
- Leonard, D. C., Filippenko, A. V., Barth, A. J., & Matheson, T. 2000, *ApJ*, 536, 239
- Leonard, D. C., Filippenko, A. V., Ganeshalingam, M., et al. 2006, *Nature*, 440, 505
- Leonard, D. C., Filippenko, A. V., Li, W., et al. 2002, *AJ*, 124, 2490
- Levanon, N. & Soker, N. 2019, *ApJ*, 872, L7
- Li, L., Wang, X., Zhang, J., et al. 2018, *MNRAS*, 478, 4575
- Lin, H., Xiang, D., Rui, L., et al. 2018, *The Astronomer's Telegram*, 11205, 1
- Lunnan, R., Kasliwal, M. M., Cao, Y., et al. 2017, *ApJ*, 836, 60
- Maeda, K., Tajitsu, A., Kawabata, K. S., et al. 2016, *ApJ*, 816, 57
- Maguire, K., Jerkstrand, A., Smartt, S. J., et al. 2012, *MNRAS*, 420, 3451
- Maguire, K., Sullivan, M., Pan, Y.-C., et al. 2014, *MNRAS*, 444, 3258
- Maguire, K., Sullivan, M., Patat, F., et al. 2013, *MNRAS*, 436, 222
- Mahabal, A. A., Drake, A. J., Djorgovski, S. G., et al. 2012, *Central Bureau Electronic Telegrams*, 3297, 1
- Margutti, R., Milisavljevic, D., Soderberg, A. M., et al. 2014, *ApJ*, 780, 21
- Marion, G. H., Brown, P. J., Vinkó, J., et al. 2016, *ApJ*, 820, 92
- Martinez, L., Bersten, M. C., Folatelli, G., Orellana, M., & Ertini, K. 2023, *arXiv e-prints*, arXiv:2310.08733
- Matheson, T., Challis, P., Kirshner, R., & Calkins, M. 2003a, *IAU Circ.*, 8203, 1
- Matheson, T., Challis, P., Kirshner, R., & Calkins, M. 2003b, *IAU Circ.*, 8228, 1
- Matheson, T., Filippenko, A. V., Chornock, R., Leonard, D. C., & Li, W. 2000, *AJ*, 119, 2303
- Matheson, T., Filippenko, A. V., Li, W., Leonard, D. C., & Shields, J. C. 2001, *AJ*, 121, 1648
- Matheson, T., Garnavich, P. M., Stanek, K. Z., et al. 2003c, *ApJ*, 599, 394
- Maund, J. R., Fraser, M., Smartt, S. J., et al. 2013, *MNRAS*, 431, L102
- Mazzali, P. A., Danziger, I. J., & Turatto, M. 1995, *A&A*, 297, 509
- Mazzali, P. A., Sullivan, M., Filippenko, A. V., et al. 2015, *MNRAS*, 450, 2631
- Mazzali, P. A., Sullivan, M., Hachinger, S., et al. 2014, *MNRAS*, 439, 1959
- Megier, A., Strobel, A., Galazutdinov, G. A., & Krelowski, J. 2009, *A&A*, 507, 833
- Meikle, W. P. S., Kotak, R., Farrah, D., et al. 2011, *ApJ*, 732, 109
- Melandri, A., Pian, E., Ferrero, P., et al. 2012, *A&A*, 547, A82
- Merrill, P. W. 1935, *ApJ*, 82, 413
- Merrill, P. W. 1937, *ApJ*, 86, 28
- Merrill, P. W. & Wilson, O. C. 1938, *ApJ*, 87, 9
- Milisavljevic, D., Margutti, R., Parrent, J. T., et al. 2015, *ApJ*, 799, 51
- Milisavljevic, D., Soderberg, A. M., Margutti, R., et al. 2013, *ApJ*, 770, L38
- Miller, A. A., Magee, M. R., Polin, A., et al. 2020, *ApJ*, 898, 56
- Miller, A. A. et al. 2010, *MNRAS*, 404, 305
- Modjaz, M., Blondin, S., Kirshner, R. P., et al. 2014, *AJ*, 147, 99
- Modjaz, M., Kirshner, R., Challis, P., Matheson, T., & Nutzman, P. 2005, *Central Bureau Electronic Telegrams*, 131, 1
- Modjaz, M., Kirshner, R. P., Blondin, S., Challis, P., & Matheson, T. 2008, *ApJ*, 687, L9
- Moore, K. & Bildsten, L. 2012, *ApJ*, 761, 182
- Morales-Garoffolo, A., Elias-Rosa, N., Bersten, M., et al. 2015, *MNRAS*, 454, 95
- Morton, D. C. 2003, *ApJS*, 149, 205
- Motylewski, T., Linnartz, H., Vaizert, O., et al. 2000, *ApJ*, 531, 312
- Munari, U. & Zwitter, T. 1997, *A&A*, 318, 269
- Murgia, M., Zhu, G., Ménard, B., & Lan, T.-W. 2015, *MNRAS*, 452, 511
- Nagao, T., Kuncarayakti, H., Maeda, K., et al. 2023, *A&A*, 673, A27
- Neill, J. 2016, *Transient Name Server Classification Report*, 2016-951, 1
- Nordin, J., Brinnel, V., Giomi, M., et al. 2019, *Transient Name Server Discovery Report*, 2019-1287, 1
- Nugent, P., Kim, A., & Perlmutter, S. 2002, *PASP*, 114, 803
- Nugent, P. E. et al. 2011, *Nature*, 480, 344
- Nyholm, A., Sollerman, J., Taddia, F., et al. 2017, *A&A*, 605, A6
- Oates, S. R., Bayless, A. J., Stritzinger, M. D., et al. 2012, *MNRAS*, 424, 1297
- Ochner, P., Benetti, S., Cappellaro, E., et al. 2015, *The Astronomer's Telegram*, 8205, 1
- Ofek, E. O., Cameron, P. B., Kasliwal, M. M., et al. 2007, *ApJ*, 659, L13

- Ofek, E. O. et al. 2010, ArXiv e-prints [arXiv:1009.5378]
- Östman, L., Nordin, J., Goobar, A., et al. 2011, *A&A*, 526, A28
- Page, E. S. 1954, *Biometrika*, 41, 100
- Pan, Y. C., Foley, R. J., Kromer, M., et al. 2015, *MNRAS*, 452, 4307
- Park, J., Jeong, H., & Yi, S. K. 2015, *ApJ*, 809, 91
- Parrent, J. T., Howell, D. A., Fesen, R. A., et al. 2016, *MNRAS*, 457, 3702
- Parrent, J. T., Howell, D. A., Friesen, B., et al. 2012, *ApJ*, 752, L26
- Pastorello, A., Baron, E., Branch, D., et al. 2005, *MNRAS*, 360, 950
- Pastorello, A., Benetti, S., Brown, P. J., et al. 2015a, *MNRAS*, 449, 1921
- Pastorello, A., Hadjijska, E., Rabinowitz, D., et al. 2015b, *MNRAS*, 449, 1954
- Pastorello, A., Kochanek, C. S., Fraser, M., et al. 2018, *MNRAS*, 474, 197
- Pastorello, A., Prieto, J. L., Elias-Rosa, N., et al. 2015c, *MNRAS*, 453, 3649
- Pastorello, A., Pumo, M. L., Navasardyan, H., et al. 2012, *A&A*, 537, A141
- Pastorello, A., Turatto, M., Benetti, S., et al. 2002, *MNRAS*, 333, 27
- Pastorello, A., Valenti, S., Zampieri, L., et al. 2009, *MNRAS*, 394, 2266
- Pastorello, A., Wyrzykowski, L., Valenti, S., et al. 2015d, *MNRAS*, 449, 1941
- Pastorello, A., Zampieri, L., Turatto, M., et al. 2004, *MNRAS*, 347, 74
- Pastorello, A. et al. 2008, *MNRAS*, 389, 113
- Pastorello, A. et al. 2015e, *MNRAS*, 454, 4293
- Patat, F., Benetti, S., Cappellaro, E., et al. 1996, *MNRAS*, 278, 111
- Patat, F., Cappellaro, E., Danziger, J., et al. 2001, *ApJ*, 555, 900
- Patat, F., Chandra, P., Chevalier, R., et al. 2007, *Science*, 317, 924
- Pellegrino, C., Hiramatsu, D., Arcavi, I., et al. 2023, *ApJ*, 954, 35
- Pellegrino, C., Howell, D. A., Terreran, G., et al. 2022, *ApJ*, 938, 73
- Penston, M. V. & Blades, J. C. 1980, *MNRAS*, 190, 51P
- Pereira, R., Thomas, R. C., Aldering, G., et al. 2013, *A&A*, 554, A27
- Pessi, T., Prieto, J. L., Monard, B., et al. 2022, *ApJ*, 928, 138
- Phillips, M. M., Heathcote, S. R., Hamuy, M., & Navarrete, M. 1988, *AJ*, 95, 1087
- Phillips, M. M. et al. 2013, *ApJ*, 779, 38
- Pignata, G. et al. 2011, *ApJ*, 728, 14
- Poidevin, F., Perez-Fournon, I., Angel, C. J., et al. 2020, *Transient Name Server Classification Report*, 2020-2512, 1
- Polshaw, J., Kotak, R., Chambers, K. C., et al. 2015, *A&A*, 580, L15
- Poznanski, D., Ganeshalingam, M., Silverman, J. M., & Filippenko, A. V. 2011, *MNRAS*, 415, L81
- Poznanski, D., Kostrzewa-Rutkowska, Z., Wyrzykowski, L., & Blagorodnova, N. 2015, *MNRAS*, 449, 1753
- Poznanski, D., Prochaska, J. X., & Bloom, J. S. 2012, *MNRAS*, 426, 1465
- Pozzo, M., Meikle, W. P. S., Fassia, A., et al. 2004, *MNRAS*, 352, 457
- Prentice, S. J., Ashall, C., James, P. A., et al. 2019a, *MNRAS*, 485, 1559
- Prentice, S. J., Maguire, K., Skillen, K., Magee, M. R., & Clark, P. 2019b, *Transient Name Server Classification Report*, 2019-1306, 1
- Pun, C. S. J., Kirshner, R. P., Sonneborn, G., et al. 1995, *ApJS*, 99, 223
- Quimby, R., Höflich, P., Kannappan, S. J., et al. 2006, *ApJ*, 636, 400
- Quimby, R. M., Wheeler, J. C., Höflich, P., et al. 2007, *ApJ*, 666, 1093
- Ransome, C. 2021, *Transient Name Server Classification Report*, 2021-2830, 1
- Raskin, C. & Kasen, D. 2013, *ApJ*, 772, 1
- Reguitti, A., Pastorello, A., Pignata, G., et al. 2019, *MNRAS*, 482, 2750
- Reguitti, A., Pastorello, A., Pignata, G., et al. 2022, *A&A*, 662, L10
- Reynolds, T. M., Fraser, M., Mattila, S., et al. 2020, *MNRAS*, 493, 1761
- Rich, D., Dennefeld, M., Pizzella, A., et al. 2012, *Central Bureau Electronic Telegrams*, 3227, 2
- Richardson, D., Thomas, R. C., Casebeer, D., et al. 2001, in *American Astronomical Society Meeting Abstracts*, Vol. 199, American Astronomical Society Meeting Abstracts, 84.08
- Richmond, M. W., Treffers, R. R., Filippenko, A. V., et al. 1994, *AJ*, 107, 1022
- Salama, F., Galazutdinov, G. A., Krelowski, J., Allamandola, L. J., & Musaev, F. A. 1999, *ApJ*, 526, 265
- Sanders, N. E., Soderberg, A. M., Valenti, S., et al. 2012, *ApJ*, 756, 184
- Sanford, R. F. 1937, *ApJ*, 86, 136
- Schlafly, E. F. & Finkbeiner, D. P. 2011, *ApJ*, 737, 103
- Schmidt, B. P., Kirshner, R. P., Schild, R., et al. 1993, *AJ*, 105, 2236
- Schulze, S., Yaron, O., Sollerman, J., et al. 2021, *ApJS*, 255, 29
- Shen, K. J., Guillochon, J., & Foley, R. J. 2013, *ApJ*, 770, L35
- Shivvers, I., Filippenko, A. V., Silverman, J. M., et al. 2019, *MNRAS*, 482, 1545
- Shivvers, I., Mazzali, P., Silverman, J. M., et al. 2013, *MNRAS*, 436, 3614
- Shivvers, I., Modjaz, M., Zheng, W., et al. 2017a, *PASP*, 129, 054201
- Shivvers, I. et al. 2016, *MNRAS*, 461, 3057
- Shivvers, I. et al. 2017b, *MNRAS*, 471, 4381
- Silverman, J. M., Foley, R. J., Filippenko, A. V., et al. 2012a, *MNRAS*, 425, 1789
- Silverman, J. M., Ganeshalingam, M., Cenko, S. B., et al. 2012b, *ApJ*, 756, L7
- Silverman, J. M., Ganeshalingam, M., & Filippenko, A. V. 2013a, *MNRAS*, 430, 1030
- Silverman, J. M., Ganeshalingam, M., Li, W., et al. 2011, *MNRAS*, 410, 585
- Silverman, J. M., Nugent, P. E., Gal-Yam, A., et al. 2013b, *ApJS*, 207, 3
- Silverman, J. M., Pickett, S., Wheeler, J. C., et al. 2017, *MNRAS*, 467, 369
- Silverman, J. M. et al. 2013c, *ApJS*, 207, 3
- Simon, J. D., Gal-Yam, A., Gnat, O., et al. 2009, *ApJ*, 702, 1157
- Singh, A., Srivastav, S., Kumar, B., Anupama, G. C., & Sahu, D. K. 2018, *MNRAS*, 480, 2475
- Smartt, S. J., Valenti, S., Fraser, M., et al. 2015, *A&A*, 579, A40
- Smith, N., Cenko, S. B., Butler, N., et al. 2012a, *MNRAS*, 420, 1135
- Smith, N., Chornock, R., Silverman, J. M., Filippenko, A. V., & Foley, R. J. 2010, *ApJ*, 709, 856
- Smith, N., Li, W., Silverman, J. M., Ganeshalingam, M., & Filippenko, A. V. 2011, *MNRAS*, 415, 773
- Smith, N., Mauerhan, J. C., Silverman, J. M., et al. 2012b, *MNRAS*, 426, 1905
- Smith, N., Silverman, J. M., Filippenko, A. V., et al. 2012c, *AJ*, 143, 17
- Sollerman, J., Cox, N., Mattila, S., et al. 2005, *A&A*, 429, 559
- Sparre, M., Sollerman, J., Fynbo, J. P. U., et al. 2011, *ApJ*, 735, L24
- Spiro, S., Pastorello, A., Pumo, M. L., et al. 2014, *MNRAS*, 439, 2873
- Spitzer, Lyman, J. 1948, *ApJ*, 108, 276
- Srivastav, S., Ninan, J. P., Kumar, B., et al. 2016, *MNRAS*, 457, 1000
- Srivastav, S., Smartt, S. J., Huber, M. E., et al. 2023, *ApJ*, 943, L20
- Stahl, B. E. et al. 2020, *MNRAS*, 492, 4325
- Sternberg, A., Gal-Yam, A., Simon, J. D., et al. 2011, *Science*, 333, 856
- Sternberg, A., Gal Yam, A., Simon, J. D., et al. 2013, *ArXiv e-prints* [arXiv:1311.3645]
- Stritzinger, M., Burns, C. R., Phillips, M. M., et al. 2010, *AJ*, 140, 2036
- Stritzinger, M. & Morrell, N. 2009, *Central Bureau Electronic Telegrams*, 2052, 1
- Stritzinger, M. et al. 2009, *ApJ*, 696, 713
- Stritzinger, M. D., Holmbo, S., Morrell, N., et al. 2023, *A&A*, 675, A82
- Stritzinger, M. D., Valenti, S., Hoefflich, P., et al. 2015, *A&A*, 573, A2
- Struve, O. 1928, *ApJ*, 67, 353
- Szalai, T., Vinkó, J., Könyves-Tóth, R., et al. 2019, *ApJ*, 876, 19
- Szalai, T., Vinkó, J., Nagy, A. P., et al. 2016, *MNRAS*, 460, 1500
- Taddia, F., Sollerman, J., Fremling, C., et al. 2019, *A&A*, 621, A71
- Taddia, F., Sollerman, J., Fremling, C., et al. 2016, *A&A*, 588, A5
- Taddia, F., Stritzinger, M. D., Fransson, C., et al. 2020, *A&A*, 638, A92
- Taddia, F. et al. 2013, *A&A*, 555, A10
- Takáts, K., Pignata, G., Pumo, M. L., et al. 2015, *MNRAS*, 450, 3137
- Takáts, K., Pumo, M. L., Elias-Rosa, N., et al. 2014, *MNRAS*, 438, 368
- Tartaglia, L., Elias-Rosa, N., Pastorello, A., et al. 2016, *ApJ*, 823, L23
- Tartaglia, L., Pastorello, A., Benetti, S., et al. 2015, *The Astronomer's Telegram*, 8291, 1
- Tartaglia, L., Pastorello, A., Sollerman, J., et al. 2020, *A&A*, 635, A39
- Tartaglia, L., Sand, D. J., Groh, J. H., et al. 2021, *ApJ*, 907, 52
- Taubenberger, S., Floers, A., Vogl, C., et al. 2019, *MNRAS*, 488, 5473
- Taubenberger, S., Valenti, S., Benetti, S., et al. 2009, *MNRAS*, 397, 677
- Teffs, J. J., Prentice, S. J., Mazzali, P. A., & Ashall, C. 2021, *MNRAS*, 502, 3829
- Terreran, G., Benetti, S., Cappellaro, E., et al. 2016, *The Astronomer's Telegram*, 9403, 1
- Tody, D. 1986, in *Society of Photo-Optical Instrumentation Engineers (SPIE) Conference Series*, Vol. 627, *Instrumentation in astronomy VI*, ed. D. L. Crawford, 733

- Tody, D. 1993, in *Astronomical Society of the Pacific Conference Series*, Vol. 52, *Astronomical Data Analysis Software and Systems II*, ed. R. J. Hanisch, R. J. V. Brissenden, & J. Barnes, 173
- Tomasella, L. 2013, *The Astronomer's Telegram*, 5005, 1
- Tomasella, L., Benetti, S., Pastorello, A., & Valenti, S. 2012, *Central Bureau Electronic Telegrams*, 3032, 2
- Tomasella, L., Cappellaro, E., Pumo, M. L., et al. 2018, *MNRAS*, 475, 1937
- Trundle, C. et al. 2009, *A&A*, 504, 945
- Tucker, M. A., Ashall, C., Shappee, B. J., et al. 2021, *ApJ*, 914, 50
- Turatto, M., Benetti, S., & Cappellaro, E. 2003, in *From Twilight to Highlight: The Physics of Supernovae*, ed. W. Hillebrandt & B. Leibundgut, 200
- Turatto, M., Benetti, S., Cappellaro, E., et al. 1996, *MNRAS*, 283, 1
- Turatto, M., Cappellaro, E., Benetti, S., & Danziger, I. J. 1993a, *MNRAS*, 265, 471
- Turatto, M., Cappellaro, E., Danziger, I. J., et al. 1993b, *MNRAS*, 262, 128
- Turatto, M., Suzuki, T., Mazzali, P. A., et al. 2000, *ApJ*, 534, L57
- Uno, K., Nagao, T., Maeda, K., et al. 2023, *ApJ*, 944, 204
- Valenti, S., Howell, D. A., Stritzinger, M. D., et al. 2016, *MNRAS*, 459, 3939
- Valenti, S., Sand, D., Stritzinger, M., et al. 2015, *MNRAS*, 448, 2608
- Valenti, S. et al. 2012, *ApJ*, 749, L28
- Valerin, G., Pumo, M. L., Pastorello, A., et al. 2022, *MNRAS*, 513, 4983
- Van Dyk, S. D., Zheng, W., Fox, O. D., et al. 2014, *AJ*, 147, 37
- Vinkó, J., Sárneczky, K., Balog, Z., et al. 2009, *ApJ*, 695, 619
- Wang, L. et al. 2003, *ApJ*, 591, 1110
- Wang, Q., Armstrong, P., Zenati, Y., et al. 2023, *ApJ*, 943, L15
- Wang, X., Chen, J., Wang, L., et al. 2019, *ApJ*, 882, 120
- Wilson, O. C. & Merrill, P. W. 1937, *ApJ*, 86, 44
- Xi, G., Wang, X., Li, W., et al. 2022, *MNRAS*, 517, 4098
- Yamanaka, M., Maeda, K., Kawabata, K. S., et al. 2015, *ApJ*, 806, 191
- Yamanaka, M., Maeda, K., Tanaka, M., et al. 2016, *PASJ*, 68, 68
- Yaron, O. & Gal-Yam, A. 2012, *PASP*, 124, 668
- Yaron, O., Perley, D. A., Gal-Yam, A., et al. 2017, *Nature Physics*, 13, 510
- Young, R. K. 1922, in *Publications of the American Astronomical Society*, Vol. 4, *Publications of the American Astronomical Society*, 194
- Zelaya, P., Clocchiatti, A., Baade, D., et al. 2017, *ApJ*, 836, 88
- Zhang, J., Wang, X., József, V., et al. 2020, *MNRAS*, 498, 84
- Zhang, J., Wang, X., Vinkó, J., et al. 2018, *ApJ*, 863, 109
- Zhang, K., Wang, X., Zhang, J., et al. 2016, *ApJ*, 820, 67
- Zhang, T. et al. 2012, *AJ*, 144, 131
- Zhang, Y., Zhang, T., Danzengluobu, et al. 2022, *PASP*, 134, 074201
- Zheng, W., Brink, T., & Filippenko, A. V. 2018, *Transient Name Server Classification Report*, 2018-1219, 1
- Zheng, W., Filippenko, A. V., Mauerhan, J., et al. 2017, *ApJ*, 841, 64
- Zheng, W., Silverman, J. M., Filippenko, A. V., et al. 2013, *ApJ*, 778, L15

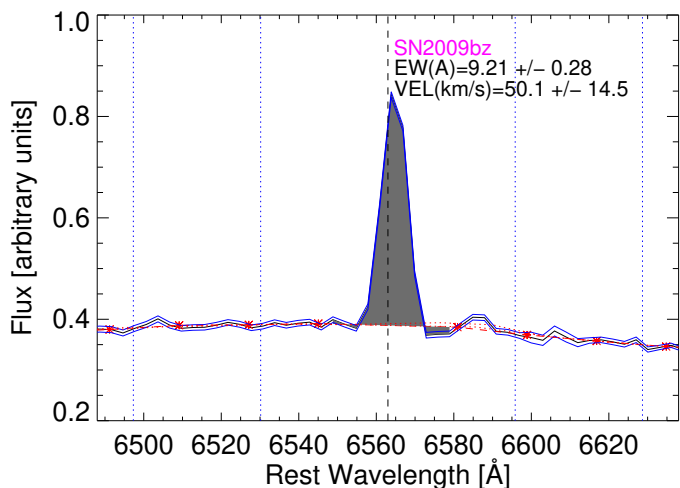


Fig. A.1. Spectrum of SN 2009bz around the emission line $H\alpha$ and automated measurement of EW and velocity. The quoted uncertainty in velocity does not include the wavelength calibration. The dispersion of the velocities of the three lines ($H\alpha$, $H\beta$ and $[OIII]$) for this spectrum is 33.2 km/s.

Appendix A: Wavelength calibration uncertainty

The heterogeneous dataset used in our analysis has been wavelength-calibrated by different groups for different instruments and observing conditions. Here we estimate an average uncertainty of the wavelength calibration for the entire sample. For this, we randomly take 1556 spectra of 180 core-collapse SNe from our sample and use our automated technique (see §4.2) around three narrow emission lines characteristic of gas-rich environments: $H\alpha$ (6563Å), $H\beta$ (4861Å) and $[OIII]$ (5007Å). We use the following integration windows: ± 750 km/s, ± 750 km/s and ± 900 km/s, respectively. An example measurement of $H\alpha$ for a spectrum of SN 2009bz is shown in Figure A.1. The dispersion of the three line velocities for this spectrum gives 33.2 km/s. Of the 1556 spectra, we select 696 that clearly show at least two of the three lines, i.e. requiring that $EW/\sigma_{EW} > 1.3$ and $EW > 0.5\text{Å}$; and we calculate the median dispersion for the sample finding 35.0 km/s. Doing the same analysis using Gaussian fits instead, we obtain proper fits with $EW > 0.5$ in at least two lines for 767 spectra for which the average of the velocity dispersion gives 36.6 km/s. This is in remarkable agreement with the automated value confirming that this dispersion is not dependent on the discussed methodologies. This value could reveal calibration uncertainties or real physical differences in the elements of the gas clouds, or a combination of both. We conservatively take it here as an intrinsic calibration uncertainty that is added in quadrature to other uncertainties of the method.

Appendix B: B-band maximum dates

To obtain the B-band maximum reference epochs used in section 6, we perform multi-band light-curve fits to every SN. We use a light-curve fitter commonly used for SNe Ia (Conley et al. 2008) but with different spectrophotometric templates for each type: the template by Hsiao et al. (2007) for SNe Ia, the template of Nugent et al. (2002) for SESNe and a model of SNe II used in the PLAsTiCC challenge (Kessler et al. 2019) based on empirical spectral energy dis-

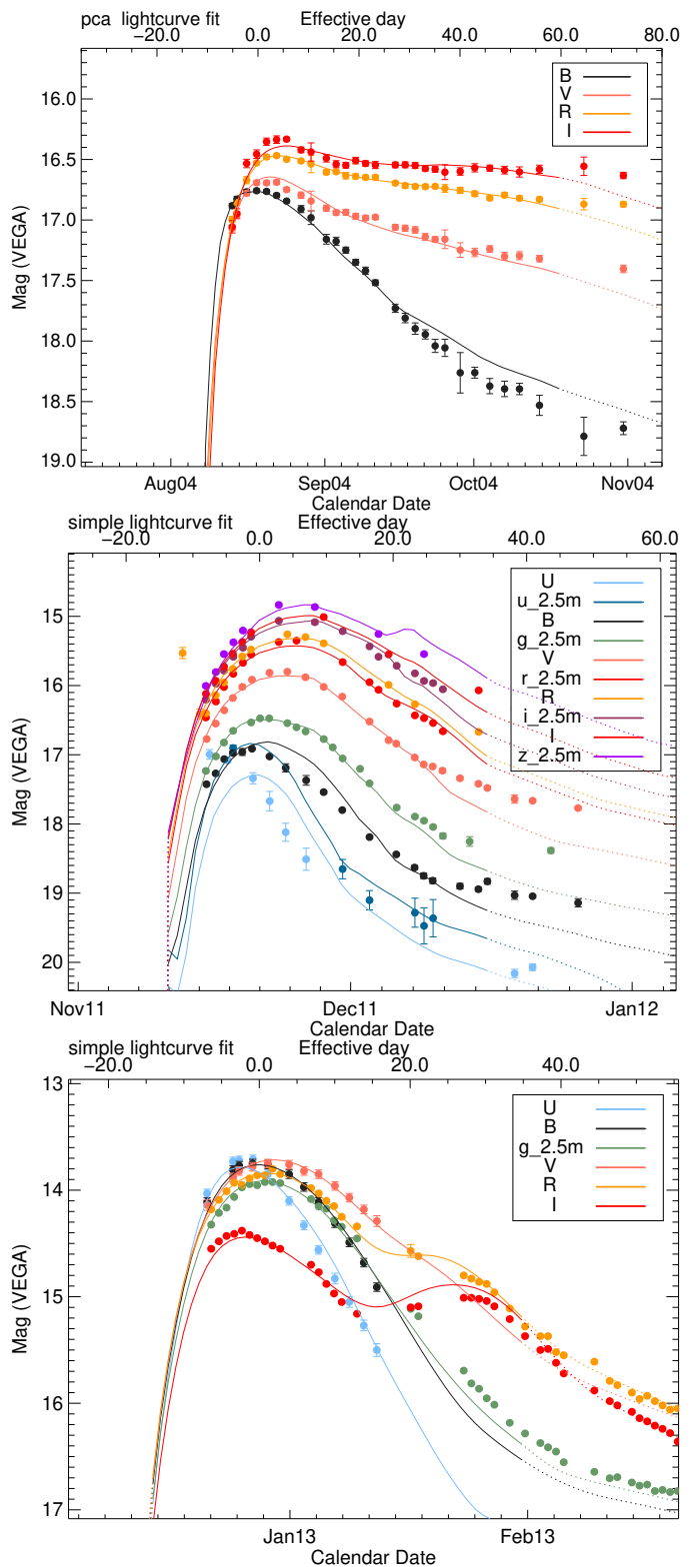


Fig. B.1. Example of multi-band light-curve fits with SiFTO (Conley et al. 2008) and different spectrophotometric templates to SN2004du (SN II, up), SN2011hs (SN IIb, middle) and SN2012hr (SN Ia, bottom).

tributions that are a linear combination of three ‘eigenvector’ components. For SNe-int, we try both, the template for SNe II and for SESNe, choosing visually the best obtained fit. Example fits are shown in Figure B.1. All fits are visually inspected, and SNe with poor data or bad fits are

discarded. Although core-collapse SNe are not as homogeneous as SNe Ia, and this fitter was devised for SNe Ia, this simple approach gets rough estimates that allow us to have epochs in the same reference system. We also attempted to use the explosion epochs as a reference for SNe II (Gutiérrez et al. 2017), confirming no general evolution of EW with time in all three SN types.

Appendix C: Figures

We present here additional figures: Figure C.1 shows the comparison of the EW measured from the stacked flux-to-continuum ratios of several spectra of a given SN (see §4.3) versus the median and the weighted average of individual spectra for a given SN (the uncertainties come from the median absolute deviation and the weighted error, respectively); Figure C.2 displays the impact of the continuum node separation on the EW measurement (see §4.1); Figures C.3 and C.4 shows how degrading the spectral resolution (§5.2) and the signal-to-noise (§5.3) affect the narrow line and its EW measurement; and Figure C.5 demonstrates that the narrow line at nebular times can emulate a blueshift in the line from the SN ejecta (see §5.4).

Appendix D: Tables

In table A1 we present all SNe used in this analysis with their type, redshift, number of spectra and the references for their spectra.

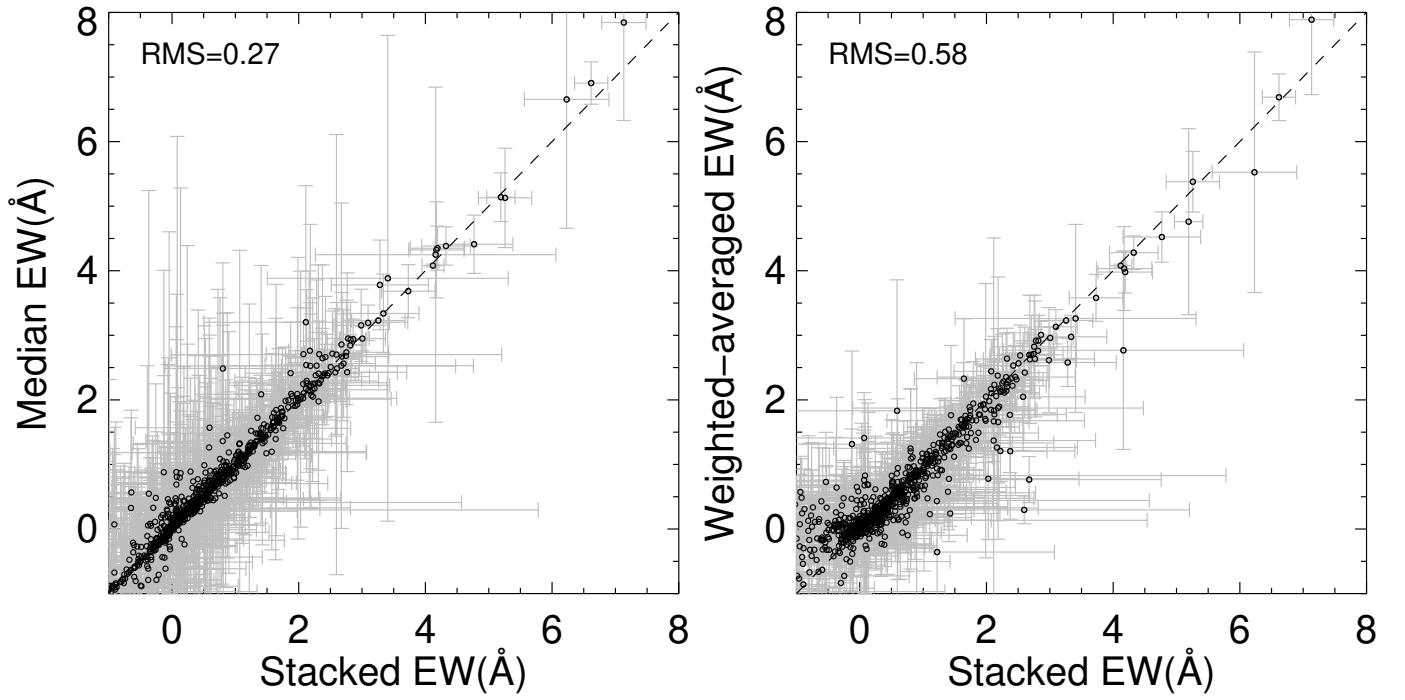


Fig. C.1. Comparison of Na I D EW measured from the stack of multiple spectra of each SN vs the median of individual EW (left) and the weighted average (right). The dashed lines indicate a $x = y$ relation.

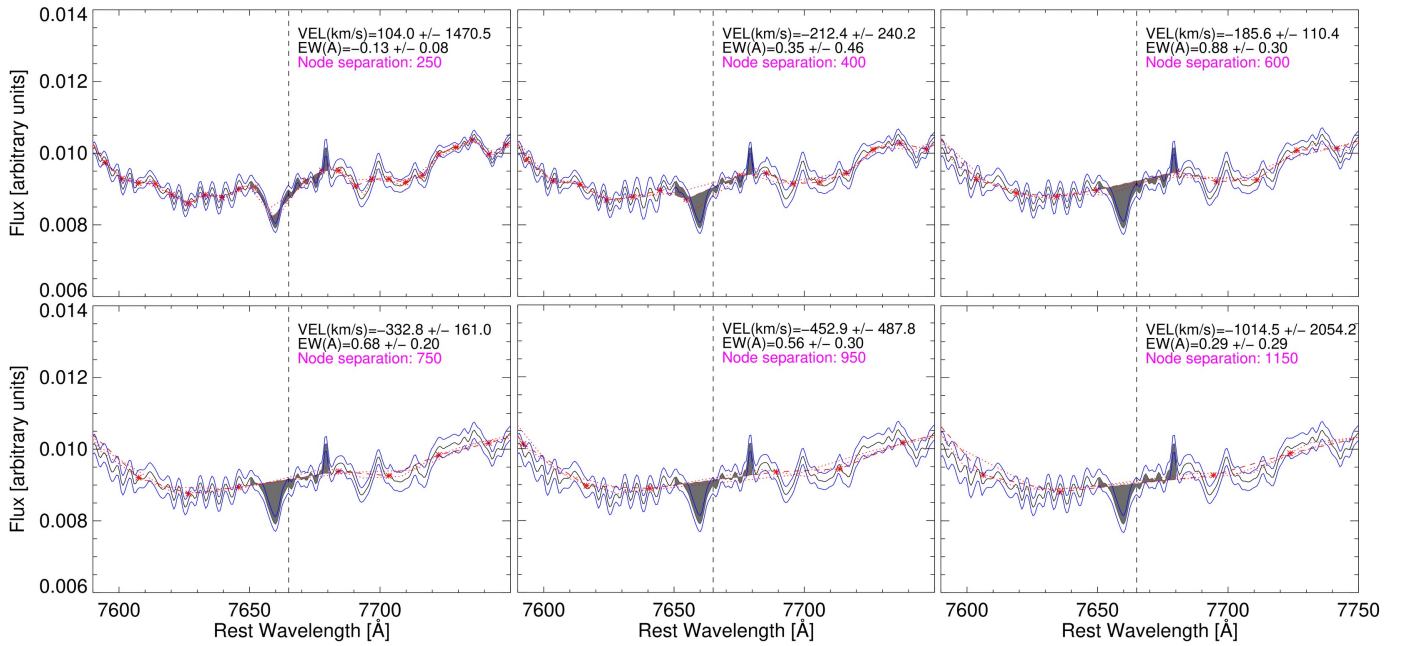


Fig. C.2. SN 2014J spectrum around the K I 7665 Å line showing different measured continua by increasing the node separation from top left to bottom right: 250, 400, 600, 750, 950 and 1150 km/s. The black line is the spectrum, the blue lines are the estimated flux errors, the red stars are the nodes and the red dashed line is the continuum crossing the nodes. Red dotted lines represent the continua at $\pm 25\%$ of the node separation being considered. The grey-shaded area is the integrated line within ± 600 km/s. The dashed vertical line is the central wavelength of the line.

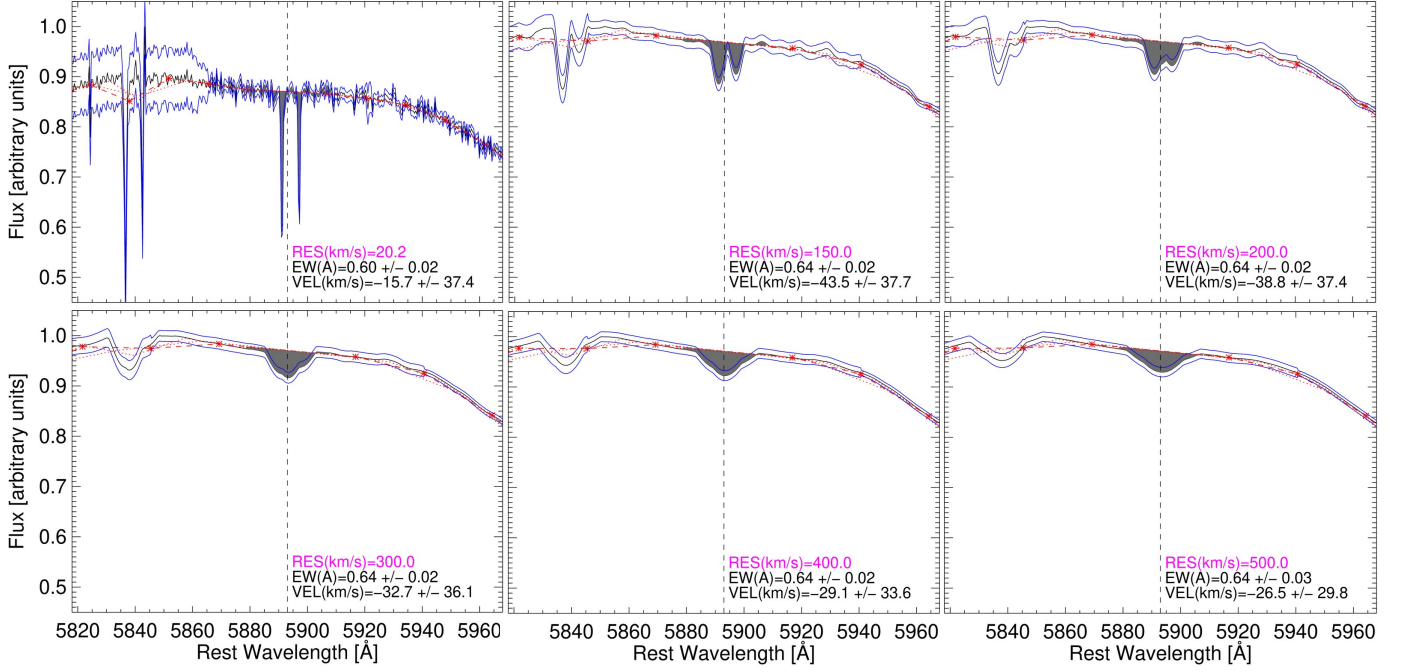


Fig. C.3. SN 2010ev high-resolution spectrum (top left) smoothed with decreasing kernel resolutions (increasing $\Delta v_{\text{res}} = 100 - 500$ km/s) around Na I D from left to right and top to bottom. The estimated error on the flux is shown in blue. The automated methodology outlined in section 4 calculates a continuum (shown in red) and integrates through a fixed spectral window (grey shading).

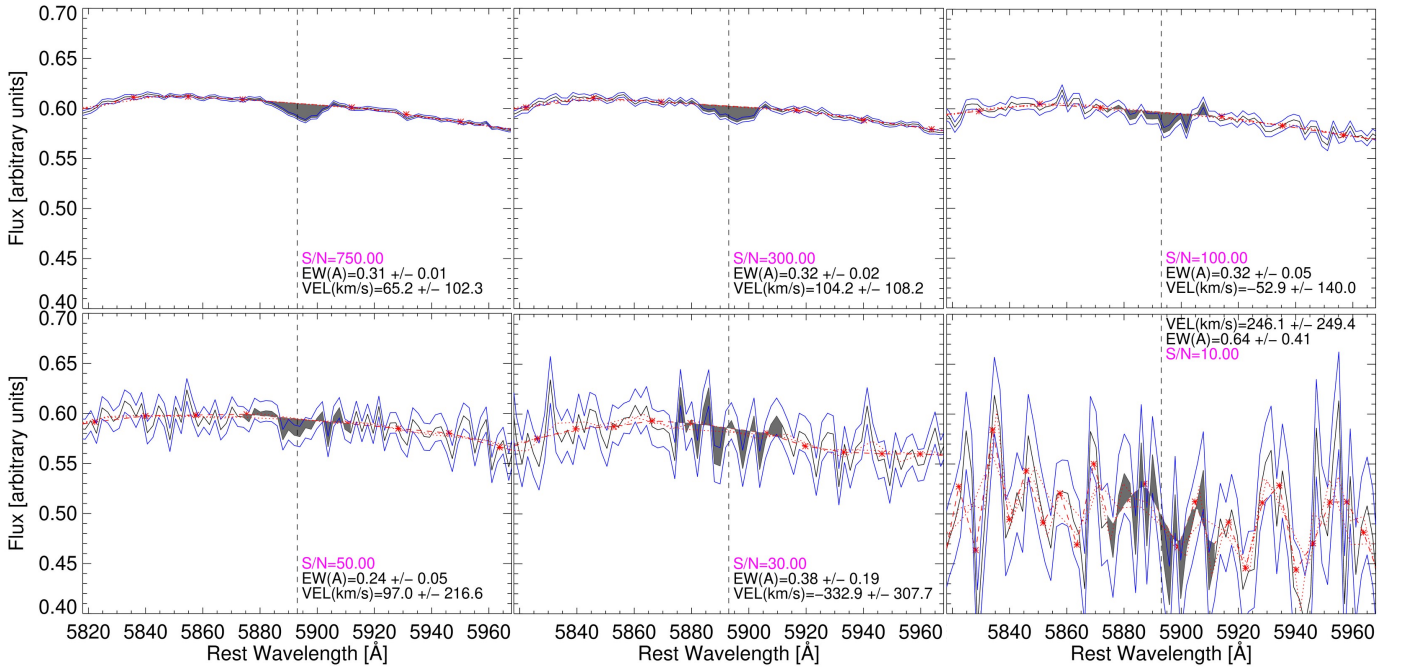


Fig. C.4. SN 2002an high-signal spectrum (top left) perturbed to various decreasing S/N around Na I D from left to right and top to bottom. The estimated error on the flux is shown in blue. The automated methodology outlined in section 4 calculates a continuum (shown in red) and integrates through a fixed spectral window (grey shading). The vertical dashed line shows the rest-frame central line of Na I D.

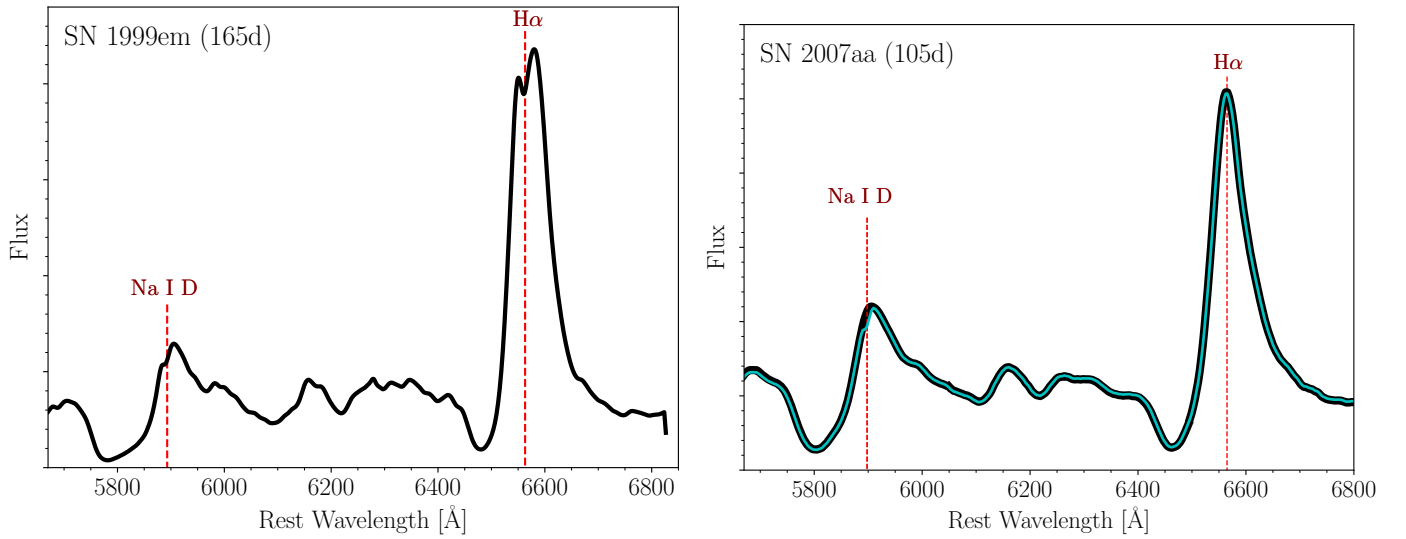


Fig. C.5. Observed spectra (black) of SN 1999em (**left**) and 2007aa (**right**) at 165 and 105 days from the explosion. The vertical dashed lines show the rest-frame position of the strongest lines. The simulated spectrum of SN 2007aa, where a fake Na I D narrow line was added at $\lambda = 5893 \text{ \AA}$ ($EW = 1.1 \text{ \AA}$), is presented on top of the observed spectrum (cyan). The peak of the Na I D seems redshifted in SN 1999em, compared to H α , which is at the rest-position. A comparable shift can be obtained when a narrow line is located on the top of the broad SN P-Cygni line of SN 2007aa.

Table A1. Sample of SNe initially included in our sample.

SN	Type	Redshift	# of spectra	References
		SNe Ia		
SN 1937C	Ia	0.001	2	Casebeer et al. 2000
SN 1937D	Ia	0.002	1	Casebeer et al. 2000
SN 1939A	Ia	0.003	2	Casebeer et al. 2000
SN 1954B	Ia	0.005	10	Casebeer et al. 2000
SN 1956A	Ia	0.004	8	Casebeer et al. 2000
SN 1957A	Ia	0.002	2	Casebeer et al. 2000
SN 1957B	Ia	0.004	7	Casebeer et al. 2000
SN 1959C	Ia	0.010	1	Casebeer et al. 2000
SN 1960F	Ia	0.006	8	Casebeer et al. 2000
SN 1960H	Ia	0.002	3	Casebeer et al. 2000
SN 1960R	Ia	0.002	2	Casebeer et al. 2000
SN 1962J	Ia	0.005	3	Casebeer et al. 2000
SN 1963I	Ia	0.001	1	Casebeer et al. 2000
SN 1964E	Ia	0.004	2	Casebeer et al. 2000
SN 1966J	Ia	0.002	1	Casebeer et al. 2000
SN 1968E	Ia	0.013	1	Casebeer et al. 2000
SN 1968I	Ia	0.006	1	Casebeer et al. 2000
SN 1971G	Ia	0.006	1	Casebeer et al. 2000
SN 1981B	Ia	0.006	13	Branch & Venkatakrisna 1986
SN 1983G	Ia	0.004	8	Foley et al. 2008
SN 1986G	Ia	0.002	39	Cristiani et al. 1992; Foley et al. 2008
SN 1989A	Ia	0.008	1	[2]
SN 1989B	Ia	0.002	12	[2]
SN 1989M	Ia	0.005	4	[2]
SN 1990G	Ia	0.036	2	[2]; Gomez et al. 1996
SN 1990M	Ia	0.009	6	[2]; Gomez et al. 1996
SN 1990N	Ia	0.003	11	[2]; Gomez et al. 1996
SN 1990O	Ia	0.031	4	[2]; Gomez et al. 1996
SN 1990R	Ia	0.016	6	[2]; Gomez et al. 1996
SN 1990Y	Ia	0.039	1	[2]
SN 1991ad	Ia	0.070	7	Gomez et al. 1996
SN 1991ak	Ia	0.010	3	[2]
SN 1991am	Ia	0.061	1	[2]
SN 1991as	Ia	0.011	1	[2]
SN 1991at	Ia	0.041	1	[2]
SN 1991ay	Ia	0.050	1	[2]
SN 1991B	Ia	0.009	5	[2]; Gomez et al. 1996
SN 1991bb	Ia	0.027	2	[2]
SN 1991bc	Ia	0.021	3	[2]; Gomez et al. 1996
SN 1991bd	Ia	0.013	2	[2]; Gomez et al. 1996
SN 1991bf	Ia	0.030	1	[2]
SN 1991bg	Ia	0.004	34	[2]; Filippenko et al. 1992a; Gomez et al. 1996; Turatto et al. 1996
SN 1991bh	Ia	0.028	1	[2]
SN 1991bj	Ia	0.018	2	[2]; Gomez et al. 1996
SN 1991F	Ia	0.006	3	Gomez & Lopez 1995
SN 1991K	Ia	0.017	6	Gomez et al. 1996; Matheson et al. 2001
SN 1991M	Ia	0.007	7	[2]; Gomez et al. 1996
SN 1991O	Ia	0.049	1	[2]
SN 1991S	Ia	0.055	2	[2]; Gomez et al. 1996
SN 1991T	Ia	0.006	30	[2]; Gomez et al. 1996; Filippenko et al. 1992b; Mazzali et al. 1995
SN 1991X	Ia	0.009	1	Gomez et al. 1996
SN 1992ac	Ia	0.052	3	Gomez et al. 1996; Gómez & López 1998
SN 1992ah	Ia	0.028	2	[2]; Gomez et al. 1996
SN 1992ap	Ia	0.030	1	[2]
SN 1992G	Ia	0.005	12	[2]; Gomez et al. 1996
SN 1992M	Ia	0.047	2	[2]
SN 1993aa	Ia	0.025	1	[2]
SN 1993ab	Ia	0.014	1	[2]
SN 1993ac	Ia	0.049	4	[2]; [3]
SN 1993ae	Ia	0.020	3	[2]; [3]
SN 1993ai	Ia	0.035	1	[2]
SN 1993aj	Ia	0.078	3	[2]
SN 1993C	Ia	0.013	3	[2]
SN 1993Y	Ia	0.020	1	[2]
SN 1993Z	Ia	0.004	9	[2]
SN 1994ab	Ia	0.034	1	[2]
SN 1994ae	Ia	0.004	21	[2]; [3]
SN 1994B	Ia	0.089	2	[2]
SN 1994D	Ia	0.001	77	[2]; [3]; Patat et al. 1996; Gomez et al. 1996
SN 1994E	Ia	0.064	1	[2]
SN 1994J	Ia	0.056	1	[2]
SN 1994M	Ia	0.023	10	[3]; Gomez et al. 1996
SN 1994Q	Ia	0.030	9	[2]; [3]; Gomez et al. 1996
SN 1994S	Ia	0.015	6	[2]; [3]; Gomez et al. 1996
SN 1994T	Ia	0.035	6	[2]; [3]
SN 1994U	Ia	0.004	2	[2]; Gomez et al. 1996
SN 1994X	Ia	0.056	1	[2]
SN 1995A	Ia	0.032	1	[2]
SN 1995ac	Ia	0.050	6	[2]; [3]
SN 1995ak	Ia	0.023	7	[2]; [3]
SN 1995al	Ia	0.005	15	[2]; [3]
SN 1995bd	Ia	0.015	9	[3]
SN 1995C	Ia	0.027	1	[2]

SN 1995D	Ia	0.007	18	[2]; [3]
SN 1995E	Ia	0.012	9	[2]; [3]
SN 1995L	Ia	0.024	1	[2]
SN 1995T	Ia	0.056	1	[2]
SN 1995Y	Ia	0.018	4	[3]
SN 1996ab	Ia	0.130	1	[3]
SN 1996ac	Ia	0.026	1	[3]
SN 1996ai	Ia	0.003	12	[2]; [3]
SN 1996bk	Ia	0.007	1	[3]
SN 1996bl	Ia	0.024	4	[3]
SN 1996bo	Ia	0.017	5	[3]
SN 1996bt	Ia	0.009	1	[3]
SN 1996bv	Ia	0.017	2	[2]; [3]
SN 1996by	Ia	0.014	6	[3]
SN 1996C	Ia	0.027	3	[3]
SN 1996ca	Ia	0.016	4	[3]
SN 1996O	Ia	0.037	1	[2]
SN 1996P	Ia	0.016	1	[2]
SN 1996V	Ia	0.024	1	[3]
SN 1996X	Ia	0.007	32	[3]
SN 1996Z	Ia	0.008	6	[3]
SN 1997bp	Ia	0.008	14	[2]; [3]
SN 1997bq	Ia	0.009	13	[3]
SN 1997br	Ia	0.007	27	[2]; [3]
SN 1997by	Ia	0.045	3	[3]
SN 1997bz	Ia	0.030	2	[3]
SN 1997C	Ia	0.023	1	Matheson et al. 2001
SN 1997cn	Ia	0.016	16	[2]; [3]
SN 1997ct	Ia	0.030	1	[3]
SN 1997cw	Ia	0.018	4	[2]; [3]
SN 1997do	Ia	0.010	16	[2]; [3]
SN 1997dt	Ia	0.007	8	[3]
SN 1997E	Ia	0.014	5	[2]; [3]
SN 1997fb	Ia	0.054	1	[2]
SN 1997fc	Ia	0.054	1	[2]
SN 1997T	Ia	0.042	1	[2]
SN 1997Y	Ia	0.016	5	[2]; [3]
SN 1998ab	Ia	0.027	13	[3]
SN 1998an	Ia	0.019	1	[3]
SN 1998aq	Ia	0.004	61	[2]; [3]
SN 1998bn	Ia	0.006	9	[2]; [3]
SN 1998bp	Ia	0.010	17	[2]; [3]
SN 1998bu	Ia	0.003	81	[2]; [3]
SN 1998cd	Ia	0.025	1	[2]
SN 1998cl	Ia	0.030	1	[2]
SN 1998cm	Ia	0.080	1	[2]
SN 1998cn	Ia	0.009	1	[3]
SN 1998co	Ia	0.018	8	[3]
SN 1998cs	Ia	0.033	7	[2]; [3]
SN 1998D	Ia	0.012	4	[3]
SN 1998de	Ia	0.016	10	[2]; [3]
SN 1998dh	Ia	0.009	14	[2]; [3]
SN 1998dj	Ia	0.014	1	[2]
SN 1998dk	Ia	0.013	14	[2]; [3]
SN 1998dm	Ia	0.007	15	[2]; [3]
SN 1998dw	Ia	0.049	1	[2]
SN 1998dx	Ia	0.054	9	[2]; [3]
SN 1998eb	Ia	0.013	2	[2]; [3]
SN 1998ec	Ia	0.020	7	[2]; [3]
SN 1998ef	Ia	0.018	9	[2]; [3]
SN 1998eg	Ia	0.025	7	[2]; [3]
SN 1998en	Ia	0.021	1	[2]
SN 1998es	Ia	0.011	33	[2]; [3]
SN 1998ex	Ia	0.037	1	[3]
SN 1998fc	Ia	0.107	1	[2]
SN 1998V	Ia	0.018	10	[2]; [3]
SN 1999aa	Ia	0.014	50	[2]; [3]
SN 1999ac	Ia	0.009	38	[2]; [3]
SN 1999aq	Ia	0.050	1	[2]
SN 1999be	Ia	0.019	3	[3]
SN 1999bh	Ia	0.017	2	[2]; [3]
SN 1999bt	Ia	0.050	2	[3]
SN 1999bv	Ia	0.019	3	[2]; [3]
SN 1999by	Ia	0.002	36	[2]; [3]
SN 1999C	Ia	0.125	1	[2]
SN 1999cb	Ia	0.029	1	[3]
SN 1999cc	Ia	0.031	7	[3]
SN 1999ce	Ia	0.077	1	[3]
SN 1999cf	Ia	0.025	3	[3]
SN 1999cl	Ia	0.008	15	[2]; [3]
SN 1999cm	Ia	0.045	2	[3]
SN 1999cp	Ia	0.009	5	[2]; [3]
SN 1999cw	Ia	0.012	7	[2]; [3]
SN 1999da	Ia	0.013	6	[2]; [3]
SN 1999dg	Ia	0.022	2	[2]
SN 1999dk	Ia	0.015	5	[2]
SN 1999do	Ia	0.022	1	[2]

SN 1999dq	Ia	0.014	27	[2]; [3]
SN 1999ee	Ia	0.011	26	[2]
SN 1999ef	Ia	0.039	3	[3]
SN 1999ej	Ia	0.014	5	[3]
SN 1999ek	Ia	0.018	5	[2]; [3]
SN 1999fz	Ia	0.022	1	[2]
SN 1999gd	Ia	0.019	6	[2]; [3]
SN 1999gf	Ia	0.044	1	[2]
SN 1999gh	Ia	0.008	19	[2]; [3]
SN 1999gj	Ia	0.017	1	[3]
SN 1999gm	Ia	0.042	5	[2]; [3]
SN 1999gp	Ia	0.027	10	[3]
SN 1999X	Ia	0.025	8	[2]; [3]
SN 2000A	Ia	0.030	1	[3]
SN 2000al	Ia	0.120	1	[2]
SN 2000B	Ia	0.020	7	[3]
SN 2000bh	Ia	0.023	1	[3]
SN 2000bk	Ia	0.025	4	[2]; [3]
SN 2000ce	Ia	0.016	5	[2]; [3]
SN 2000cf	Ia	0.036	6	[3]
SN 2000cm	Ia	0.007	2	[3]
SN 2000cn	Ia	0.023	12	[2]; [3]
SN 2000cp	Ia	0.034	5	[2]; [3]
SN 2000cu	Ia	0.020	3	[2]; [3]
SN 2000cv	Ia	0.020	2	[2]; [3]
SN 2000cw	Ia	0.030	3	[2]; [3]
SN 2000cx	Ia	0.008	66	[2]; [3]
SN 2000dd	Ia	0.042	1	[2]
SN 2000df	Ia	0.039	1	[2]
SN 2000dg	Ia	0.038	6	[2]; [3]
SN 2000dk	Ia	0.017	13	[2]; [3]
SN 2000dl	Ia	0.061	1	[3]
SN 2000dm	Ia	0.015	5	[2]; [3]
SN 2000dn	Ia	0.032	6	[2]; [3]
SN 2000dp	Ia	0.035	4	[2]; [3]
SN 2000dr	Ia	0.019	1	[2]
SN 2000dx	Ia	0.030	1	[2]
SN 2000E	Ia	0.005	9	[3]
SN 2000ej	Ia	0.030	1	[2]
SN 2000ey	Ia	0.020	4	[2]; [3]
SN 2000fa	Ia	0.021	17	[2]; [3]
SN 2000fd	Ia	0.016	2	[3]
SN 2000fo	Ia	0.024	5	[2]; [3]
SN 2000J	Ia	0.048	1	[2]
SN 2000K	Ia	0.055	1	[3]
SN 2000O	Ia	0.023	1	[3]
SN 2000Q	Ia	0.034	2	[2]
SN 2001A	Ia	0.007	1	[2]
SN 2001ah	Ia	0.058	5	[3]
SN 2001ay	Ia	0.030	17	[2]; [3]
SN 2001az	Ia	0.041	6	[2]; [3]
SN 2001ba	Ia	0.030	1	[2]
SN 2001bf	Ia	0.015	11	[2]; [3]
SN 2001bg	Ia	0.007	7	[2]; [3]
SN 2001bp	Ia	0.095	7	[2]; [3]
SN 2001br	Ia	0.021	7	[2]; [3]
SN 2001bs	Ia	0.029	3	[2]; [3]
SN 2001C	Ia	0.011	11	[2]; [3]
SN 2001cg	Ia	0.024	1	[2]
SN 2001cj	Ia	0.024	2	[2]; [3]
SN 2001ck	Ia	0.035	6	[2]; [3]
SN 2001cp	Ia	0.022	11	[2]; [3]
SN 2001da	Ia	0.017	9	[2]; [3]
SN 2001dd	Ia	0.019	1	[2]
SN 2001de	Ia	0.031	2	[2]; [3]
SN 2001dl	Ia	0.021	2	[2]
SN 2001dm	Ia	0.015	1	[2]
SN 2001dn	Ia	0.019	1	[2]
SN 2001ds	Ia	0.036	1	[2]
SN 2001dt	Ia	0.030	1	[2]
SN 2001dw	Ia	0.025	1	[2]
SN 2001E	Ia	0.019	5	[2]; [3]
SN 2001eb	Ia	0.013	1	[3]
SN 2001ec	Ia	0.045	4	[2]; [3]
SN 2001ed	Ia	0.017	2	[2]; [3]
SN 2001eg	Ia	0.013	1	[2]
SN 2001eh	Ia	0.037	22	[2]; [3]
SN 2001ei	Ia	0.028	2	[2]
SN 2001el	Ia	0.004	11	Wang et al. 2003; Foley et al. 2008
SN 2001en	Ia	0.016	12	[2]; [3]
SN 2001eo	Ia	0.068	1	[3]
SN 2001ep	Ia	0.013	30	[2]; [3]
SN 2001er	Ia	0.016	1	[2]
SN 2001es	Ia	0.067	3	[2]; [3]
SN 2001eu	Ia	0.136	1	[2]
SN 2001ew	Ia	0.018	1	[2]
SN 2001ex	Ia	0.026	2	[2]; [3]

SN 2001F	Ia	0.023	1	[3]
SN 2001fe	Ia	0.014	13	[2]; [3]
SN 2001fg	Ia	0.032	1	[2]
SN 2001fh	Ia	0.013	8	[2]; [3]
SN 2001fu	Ia	0.006	2	[2]; [3]
SN 2001G	Ia	0.017	16	[2]; [3]
SN 2001gb	Ia	0.026	5	[3]
SN 2001gc	Ia	0.019	10	[2]; [3]
SN 2001ib	Ia	0.019	4	[2]; [3]
SN 2001ic	Ia	0.044	4	[2]; [3]
SN 2001ie	Ia	0.031	8	[3]
SN 2001if	Ia	0.038	2	[3]
SN 2001iq	Ia	0.019	6	[2]; [3]
SN 2001L	Ia	0.015	3	[2]; [3]
SN 2001N	Ia	0.021	10	[2]; [3]
SN 2001P	Ia	0.021	3	[2]; [3]
SN 2001U	Ia	0.029	2	[2]; [3]
SN 2001V	Ia	0.015	82	[2]; [3]
SN 2002ar	Ia	0.030	7	[2]; [3]
SN 2002av	Ia	0.049	6	[2]; [3]
SN 2002aw	Ia	0.026	5	[2]; [3]
SN 2002bf	Ia	0.024	15	[2]; [3]
SN 2002bg	Ia	0.043	2	[2]; [3]
SN 2002bi	Ia	0.023	2	[2]; [3]
SN 2002bk	Ia	0.055	1	[2]
SN 2002bn	Ia	0.026	1	[3]
SN 2002bo	Ia	0.004	66	[2]; [3]
SN 2002bp	Ia	0.021	1	[2]
SN 2002br	Ia	0.034	2	[3]
SN 2002bs	Ia	0.010	7	[2]; [3]
SN 2002bt	Ia	0.060	1	[3]
SN 2002bw	Ia	0.017	1	[3]
SN 2002bz	Ia	0.037	11	[2]; [3]
SN 2002cc	Ia	0.066	2	[2]; [3]
SN 2002cd	Ia	0.010	18	[2]; [3]
SN 2002cf	Ia	0.015	3	[2]; [3]
SN 2002ci	Ia	0.022	2	[2]; [3]
SN 2002ck	Ia	0.030	9	[2]; [3]
SN 2002cr	Ia	0.009	12	[2]; [3]
SN 2002cs	Ia	0.016	13	[2]; [3]
SN 2002cu	Ia	0.023	5	[2]; [3]
SN 2002cv	Ia	0.004	2	[2]
SN 2002cx	Ia	0.024	13	[2]; [3]
SN 2002db	Ia	0.036	2	[2]; [3]
SN 2002de	Ia	0.028	13	[2]; [3]
SN 2002df	Ia	0.029	2	[2]; [3]
SN 2002di	Ia	0.036	2	[2]; [3]
SN 2002dj	Ia	0.009	24	[2]; [3]
SN 2002dk	Ia	0.019	3	[2]; [3]
SN 2002dl	Ia	0.016	4	[3]
SN 2002do	Ia	0.016	6	[2]; [3]
SN 2002dp	Ia	0.012	12	[2]; [3]
SN 2002dr	Ia	0.022	1	[2]
SN 2002dx	Ia	0.024	1	[2]
SN 2002eb	Ia	0.028	3	[2]
SN 2002ec	Ia	0.041	2	[2]
SN 2002ef	Ia	0.024	3	[2]; [3]
SN 2002eh	Ia	0.018	1	[2]
SN 2002el	Ia	0.029	3	[2]
SN 2002ep	Ia	0.056	1	[2]
SN 2002er	Ia	0.009	31	[2]; [3]
SN 2002es	Ia	0.018	6	[3]
SN 2002et	Ia	0.028	2	[2]; [3]
SN 2002eu	Ia	0.038	12	[2]; [3]
SN 2002ey	Ia	0.039	5	[2]; [3]
SN 2002fb	Ia	0.016	10	[2]; [3]
SN 2002fi	Ia	0.057	1	[2]
SN 2002fk	Ia	0.007	29	[2]; [3]
SN 2002G	Ia	0.034	3	[2]; [3]
SN 2002gb	Ia	0.074	1	[2]
SN 2002gc	Ia	0.021	4	[2]
SN 2002gf	Ia	0.086	1	[2]
SN 2002gg	Ia	0.110	1	[2]
SN 2002gx	Ia	0.080	1	[2]
SN 2002H	Ia	0.022	1	[3]
SN 2002ha	Ia	0.014	11	[2]; [3]
SN 2002hd	Ia	0.030	5	[2]; [3]
SN 2002he	Ia	0.025	9	[2]; [3]
SN 2002hl	Ia	0.007	1	[2]
SN 2002hu	Ia	0.030	6	[2]; [3]
SN 2002hv	Ia	0.023	2	[2]; [3]
SN 2002hw	Ia	0.018	7	[2]; [3]
SN 2002I	Ia	0.023	1	[3]
SN 2002jg	Ia	0.015	5	[2]; [3]
SN 2002jm	Ia	0.018	4	[2]; [3]
SN 2002jo	Ia	0.009	1	[2]
SN 2002jy	Ia	0.020	13	[2]; [3]

SN 2002kf	Ia	0.019	12	[2]; [3]
SN 2003ae	Ia	0.033	6	[2]; [3]
SN 2003af	Ia	0.021	3	[2]; [3]
SN 2003ag	Ia	0.023	2	[3]
SN 2003ah	Ia	0.030	1	[2]
SN 2003ai	Ia	0.036	3	[2]; [3]
SN 2003an	Ia	0.037	1	[2]
SN 2003ar	Ia	0.025	1	[3]
SN 2003au	Ia	0.031	1	[2]
SN 2003av	Ia	0.140	1	[2]
SN 2003ax	Ia	0.058	1	[2]
SN 2003ay	Ia	0.073	1	[2]
SN 2003bf	Ia	0.034	1	[2]
SN 2003bh	Ia	0.089	1	[2]
SN 2003bi	Ia	0.092	1	[2]
SN 2003bt	Ia	0.027	1	[3]
SN 2003cg	Ia	0.004	43	[3]
SN 2003ch	Ia	0.029	13	[3]
SN 2003cq	Ia	0.033	9	[2]; [3]
SN 2003D	Ia	0.022	5	[2]; [3]
SN 2003de	Ia	0.038	1	[3]
SN 2003dt	Ia	0.014	1	[3]
SN 2003du	Ia	0.006	82	[2]; [3]
SN 2003dw	Ia	0.030	1	[2]
SN 2003eh	Ia	0.025	6	[3]
SN 2003ek	Ia	0.036	12	[2]; [3]
SN 2003ep	Ia	0.016	5	[3]
SN 2003ez	Ia	0.048	2	[3]
SN 2003F	Ia	0.017	4	[2]; [3]
SN 2003fa	Ia	0.040	23	[2]; [3]
SN 2003fd	Ia	0.060	11	[2]; [3]
SN 2003ge	Ia	0.034	2	[3]
SN 2003gj	Ia	0.035	2	[2]; [3]
SN 2003gn	Ia	0.034	3	[2]; [3]
SN 2003gq	Iax	0.021	3	[2]; [3]
SN 2003gs	Ia	0.005	2	[2]
SN 2003gt	Ia	0.016	2	[2]
SN 2003he	Ia	0.025	2	[2]
SN 2003hj	Ia	0.076	1	[2]
SN 2003hm	Ia	0.014	2	[2]; [3]
SN 2003hs	Ia	0.054	1	[2]
SN 2003hu	Ia	0.055	6	[3]
SN 2003hv	Ia	0.006	15	[2]; [3]
SN 2003hw	Ia	0.064	4	[2]; [3]
SN 2003hx	Ia	0.007	2	[2]; [3]
SN 2003hz	Ia	0.020	1	[3]
SN 2003ia	Ia	0.030	3	[3]
SN 2003ic	Ia	0.056	8	[3]
SN 2003if	Ia	0.006	2	[3]
SN 2003ij	Ia	0.018	1	[2]
SN 2003ik	Ia	0.024	1	[2]
SN 2003im	Ia	0.019	2	[2]; [3]
SN 2003in	Ia	0.021	3	[2]; [3]
SN 2003it	Ia	0.025	15	[3]
SN 2003iu	Ia	0.018	14	[3]
SN 2003iv	Ia	0.034	10	[2]; [3]
SN 2003iz	Ia	0.048	2	[2]; [3]
SN 2003jz	Ia	0.016	1	[3]
SN 2003K	Ia	0.022	3	[2]; [3]
SN 2003kc	Ia	0.033	8	[2]; [3]
SN 2003kd	Ia	0.030	9	[2]; [3]
SN 2003kf	Ia	0.007	28	[2]; [3]
SN 2003kg	Ia	0.026	2	[2]; [3]
SN 2003kh	Ia	0.033	3	[2]; [3]
SN 2003kz	Ia	0.050	1	[3]
SN 2003lb	Ia	0.018	1	[2]
SN 2003lc	Ia	0.035	3	[2]; [3]
SN 2003lq	Ia	0.024	2	[2]; [3]
SN 2003ls	Ia	0.043	1	[2]
SN 2003M	Ia	0.024	5	[2]; [3]
SN 2003P	Ia	0.034	1	[2]
SN 2003S	Ia	0.040	2	[2]; [3]
SN 2003U	Ia	0.028	4	[2]; [3]
SN 2003V	Ia	0.045	1	[2]
SN 2003W	Ia	0.020	20	[2]; [3]
SN 2003X	Ia	0.023	1	[2]
SN 2003Y	Ia	0.017	5	[2]; [3]
SN 2004ab	Ia	0.006	1	[3]
SN 2004ap	Ia	0.024	1	[3]
SN 2004as	Ia	0.031	19	[2]; [3]
SN 2004av	Ia	0.024	1	[3]
SN 2004az	Ia	0.029	1	[3]
SN 2004B	Ia	0.016	2	[3]
SN 2004bc	Ia	0.024	1	[3]
SN 2004bd	Ia	0.009	8	[2]; [3]
SN 2004bg	Ia	0.021	7	[2]; [3]
SN 2004bj	Ia	0.050	2	[2]; [3]

SN 2004bk	Ia	0.023	3	[2]; [3]
SN 2004bl	Ia	0.017	2	[2]
SN 2004bo	Ia	0.024	1	[3]
SN 2004bp	Ia	0.030	2	[2]; [3]
SN 2004bq	Ia	0.028	1	[2]
SN 2004br	Ia	0.023	3	[2]
SN 2004bv	Ia	0.011	7	[2]
SN 2004bw	Ia	0.021	2	[2]
SN 2004bz	Ia	0.034	1	[2]
SN 2004ca	Ia	0.018	3	[2]; [3]
SN 2004cb	Ia	0.014	1	[2]
SN 2004ct	Ia	0.034	2	[3]
SN 2004cu	Ia	0.025	1	[3]
SN 2004cv	Ia	0.037	1	[2]
SN 2004da	Ia	0.016	4	[2]; [3]
SN 2004db	Ia	0.011	2	[2]; [3]
SN 2004di	Ia	0.020	2	[2]
SN 2004dt	Ia	0.020	46	[1]; [2]; [3]
SN 2004E	Ia	0.030	1	[2]
SN 2004ef	Ia	0.031	29	[1]; [2]; [3]
SN 2004eo	Ia	0.016	25	[1]; [2]
SN 2004eq	Ia	0.009	1	[2]
SN 2004ev	Ia	0.031	1	[2]
SN 2004ey	Ia	0.016	7	[1]; [2]
SN 2004fa	Ia	0.019	1	[2]
SN 2004fd	Ia	0.017	3	[2]; [3]
SN 2004fg	Ia	0.030	1	[2]
SN 2004fu	Ia	0.009	12	[2]; [3]
SN 2004fw	Ia	0.019	1	[2]
SN 2004fy	Ia	0.035	2	[2]
SN 2004fz	Ia	0.017	4	[2]; [3]
SN 2004gc	Ia	0.032	6	[1]; [2]; [3]
SN 2004gl	Ia	0.174	1	[2]
SN 2004go	Ia	0.029	1	[2]
SN 2004gs	Ia	0.027	13	[1]; [2]; [3]
SN 2004gu	Ia	0.046	2	[1]; [2]
SN 2004gw	Ia	0.017	2	[2]
SN 2004gz	Ia	0.015	2	[2]; [3]
SN 2004H	Ia	0.032	1	[3]
SN 2004J	Ia	0.025	1	[3]
SN 2004K	Ia	0.036	1	[3]
SN 2004L	Ia	0.032	13	[3]
SN 2004P	Ia	0.024	1	[3]
SN 2004S	Ia	0.009	11	[2]
SN 2004W	Ia	0.004	1	[2]
SN 2004Y	Ia	0.068	1	[2]
SN 2005A	Ia	0.019	9	[1]; [2]; [3]
SN 2005ag	Ia	0.080	5	[1]; [2]
SN 2005al	Ia	0.012	7	[1]
SN 2005am	Ia	0.008	32	[1]; [2]; [3]
SN 2005ao	Ia	0.038	5	[2]; [3]
SN 2005as	Ia	0.013	1	[2]
SN 2005bc	Ia	0.012	4	[2]; [3]
SN 2005bd	Ia	0.037	1	[3]
SN 2005be	Ia	0.034	7	[1]; [2]; [3]
SN 2005bg	Ia	0.023	3	[1]
SN 2005bl	Ia	0.024	14	[1]; [2]; [3]
SN 2005bo	Ia	0.014	5	[1]; [2]; [3]
SN 2005bu	Ia	0.029	1	[2]
SN 2005bv	Ia	0.036	2	[3]
SN 2005cc	Iax	0.008	12	[3]
SN 2005cf	Ia	0.006	116	[2]; [3]
SN 2005cg	Ia	0.032	6	Quimby et al. 2006
SN 2005ch	Ia	0.027	1	[3]
SN 2005cn	Ia	0.007	1	[3]
SN 2005cr	Ia	0.021	1	[3]
SN 2005de	Ia	0.015	4	[2]
SN 2005df	Ia	0.004	1	Gerardy et al. 2007
SN 2005dh	Ia	0.015	2	[2]
SN 2005di	Ia	0.025	1	[2]
SN 2005dm	Ia	0.017	1	[2]
SN 2005do	Ia	0.030	1	[2]
SN 2005dv	Ia	0.010	1	[2]
SN 2005ec	Ia	0.029	1	[2]
SN 2005ej	Ia	0.038	6	[2]; [3]
SN 2005el	Ia	0.015	17	[1]; [2]; [3]
SN 2005eq	Ia	0.029	20	[1]; [2]; [3]
SN 2005er	Ia	0.026	3	[2]
SN 2005eu	Ia	0.034	11	[2]; [3]
SN 2005ew	Ia	0.003	2	[2]
SN 2005F	Ia	0.029	1	[2]
SN 2005G	Ia	0.023	2	[2]; [3]
SN 2005gj	Ia	0.062	5	[2]
SN 2005hc	Ia	0.046	6	[1]; [2]; [3]
SN 2005hf	Ia	0.043	7	[3]
SN 2005hj	Ia	0.057	11	[2]
SN 2005hk	Iax	0.013	44	[2]; [3]

SN 2005iq	Ia	0.034	4	[1]; [2]; [3]
SN 2005kc	Ia	0.015	12	[1]; [2]; [3]
SN 2005ke	Ia	0.005	30	[1]; [2]; [3]
SN 2005ki	Ia	0.019	9	[1]; [2]; [3]
SN 2005ls	Ia	0.021	5	[2]; [3]
SN 2005lt	Ia	0.020	1	[2]
SN 2005lu	Ia	0.032	12	[1]; [2]; [3]
SN 2005lz	Ia	0.041	2	[2]; [3]
SN 2005M	Ia	0.025	24	[1]; [2]; [3]
SN 2005mc	Ia	0.025	4	[2]; [3]
SN 2005ms	Ia	0.025	2	[2]
SN 2005mz	Ia	0.018	5	[3]
SN 2005na	Ia	0.026	27	[1]; [2]; [3]
SN 2005P	Ia	0.009	2	[2]
SN 2005W	Ia	0.009	4	[1]; [2]
SN 2005X	Ia	0.074	1	[2]
SN 2006ac	Ia	0.023	14	[2]; [3]
SN 2006ak	Ia	0.038	2	[2]; [3]
SN 2006al	Ia	0.068	6	[3]
SN 2006ap	Ia	0.022	1	[3]
SN 2006ax	Ia	0.017	19	[1]; [2]; [3]
SN 2006ay	Ia	0.015	1	[2]
SN 2006az	Ia	0.031	3	[2]; [3]
SN 2006B	Ia	0.016	1	[3]
SN 2006bb	Ia	0.025	1	[3]
SN 2006bd	Ia	0.026	1	[1]
SN 2006bh	Ia	0.011	6	[1]
SN 2006bk	Ia	0.050	2	[3]
SN 2006bm	Ia	0.068	1	[3]
SN 2006bq	Ia	0.022	5	[2]; [3]
SN 2006br	Ia	0.025	4	[2]; [3]
SN 2006bt	Ia	0.032	14	[2]; [3]
SN 2006bu	Ia	0.084	2	[2]; [3]
SN 2006bw	Ia	0.030	3	[2]; [3]
SN 2006bz	Ia	0.028	4	[2]; [3]
SN 2006cc	Ia	0.033	2	[2]; [3]
SN 2006ce	Ia	0.005	3	[2]
SN 2006cf	Ia	0.042	10	[2]; [3]
SN 2006ch	Ia	0.017	2	[2]
SN 2006cj	Ia	0.068	9	[2]; [3]
SN 2006cm	Ia	0.016	6	[2]; [3]
SN 2006cp	Ia	0.022	12	[2]; [3]
SN 2006cq	Ia	0.048	2	[2]; [3]
SN 2006cs	Ia	0.024	2	[2]; [3]
SN 2006ct	Ia	0.031	2	[2]
SN 2006cz	Ia	0.042	8	[2]; [3]
SN 2006D	Ia	0.009	29	[1]; [2]; [3]
SN 2006da	Ia	0.041	6	[2]; [3]
SN 2006dd	Ia	0.006	6	Stritzinger et al. 2010
SN 2006dh	Ia	0.060	1	[2]
SN 2006di	Ia	0.019	1	[2]
SN 2006dm	Ia	0.022	5	[2]
SN 2006do	Ia	0.028	4	[2]
SN 2006dt	Ia	0.026	3	[3]
SN 2006dv	Ia	0.033	6	[2]; [3]
SN 2006dw	Ia	0.027	4	[2]
SN 2006dy	Ia	0.008	5	[2]
SN 2006E	Ia	0.003	4	[2]; [3]
SN 2006eb	Ia	0.017	2	[2]
SN 2006ef	Ia	0.018	4	[1]; [2]
SN 2006ej	Ia	0.020	7	[1]; [2]
SN 2006em	Ia	0.019	4	[2]; [3]
SN 2006eq	Ia	0.049	3	[1]; [3]
SN 2006es	Ia	0.041	2	[2]
SN 2006et	Ia	0.023	11	[1]; [2]; [3]
SN 2006eu	Ia	0.024	3	[2]; [3]
SN 2006ev	Ia	0.029	7	[1]; [2]; [3]
SN 2006fw	Ia	0.084	3	[1]
SN 2006gj	Ia	0.028	9	[1]; [2]; [3]
SN 2006gr	Ia	0.035	20	[2]; [3]
SN 2006gt	Ia	0.045	9	[1]; [2]; [3]
SN 2006gz	Ia-supCh	0.024	27	[3]
SN 2006H	Ia	0.014	15	[2]; [3]
SN 2006ha	Ia	0.031	1	[2]
SN 2006hb	Ia	0.015	14	[1]; [2]; [3]
SN 2006hn	Iax	0.017	1	[2]
SN 2006hx	Ia	0.045	2	[1]
SN 2006is	Ia	0.031	13	[1]
SN 2006je	Ia	0.038	3	[2]; [3]
SN 2006ke	Ia	0.017	4	[2]; [3]
SN 2006kf	Ia	0.021	9	[1]; [2]; [3]
SN 2006le	Ia	0.017	26	[2]; [3]
SN 2006lf	Ia	0.013	24	[2]; [3]
SN 2006lu	Ia	0.068	3	[1]
SN 2006mo	Ia	0.037	2	[2]; [3]
SN 2006mp	Ia	0.021	1	[2]
SN 2006mr	Ia	0.006	15	[1]

SN 2006N	Ia	0.014	16	[2]; [3]
SN 2006nr	Ia	0.018	1	[2]
SN 2006nz	Ia	0.044	1	[3]
SN 2006oa	Ia	0.060	7	[3]
SN 2006ob	Ia	0.059	2	[1]; [2]
SN 2006oq	Ia	0.021	1	[3]
SN 2006or	Ia	0.021	3	[2]; [3]
SN 2006os	Ia	0.033	4	[1]; [2]
SN 2006ot	Ia	0.053	6	[1]; [2]; [3]
SN 2006ou	Ia	0.013	1	[3]
SN 2006ow	Ia	0.039	1	[2]
SN 2006py	Ia	0.058	1	[1]
SN 2006qo	Ia	0.030	1	[2]
SN 2006R	Ia	0.034	1	[3]
SN 2006S	Ia	0.032	12	[2]; [3]
SN 2006sr	Ia	0.024	8	[2]; [3]
SN 2006su	Ia	0.041	2	[2]; [3]
SN 2006td	Ia	0.016	1	[2]
SN 2006te	Ia	0.032	4	[2]; [3]
SN 2006X	Ia	0.005	93	[1]; [2]; [3]
SN 2007A	Ia	0.018	10	[1]; [2]; [3]
SN 2007ae	Ia	0.064	2	[3]
SN 2007af	Ia	0.005	55	[1]; [2]; [3]
SN 2007ai	Ia	0.032	9	[1]
SN 2007aj	Ia	0.011	2	[2]
SN 2007al	Ia	0.012	15	[1]; [2]; [3]
SN 2007ao	Ia	0.025	5	[2]; [3]
SN 2007ap	Ia	0.016	5	[2]; [3]
SN 2007as	Ia	0.018	4	[1]
SN 2007at	Ia	0.054	2	[3]
SN 2007au	Ia	0.021	6	[2]; [3]
SN 2007ax	Ia	0.007	8	[1]; [2]; [3]
SN 2007B	Ia	0.021	7	[2]; [3]
SN 2007ba	Ia	0.039	12	[1]; [2]; [3]
SN 2007bc	Ia	0.021	10	[2]; [3]
SN 2007bd	Ia	0.031	16	[1]; [2]; [3]
SN 2007bj	Ia	0.017	10	[2]; [3]
SN 2007bk	Ia	0.032	1	[3]
SN 2007bm	Ia	0.006	15	[2]; [3]
SN 2007bz	Ia	0.022	2	[2]; [3]
SN 2007ca	Ia	0.014	18	[1]; [2]; [3]
SN 2007cb	Ia	0.037	1	[3]
SN 2007cc	Ia	0.029	1	[3]
SN 2007cf	Ia	0.033	3	[2]; [3]
SN 2007cg	Ia	0.033	4	[2]; [3]
SN 2007ci	Ia	0.018	15	[2]; [3]
SN 2007cj	Ia	0.008	1	[3]
SN 2007co	Ia	0.027	25	[2]; [3]
SN 2007cp	Ia	0.037	5	[2]; [3]
SN 2007cq	Ia	0.026	8	[2]; [3]
SN 2007cs	Ia	0.018	4	[2]
SN 2007E	Ia	0.023	2	[2]
SN 2007F	Ia	0.024	17	[2]; [3]
SN 2007fb	Ia	0.018	18	[2]; [3]
SN 2007fc	Ia	0.034	4	[2]; [3]
SN 2007fq	Ia	0.042	1	[2]
SN 2007fr	Ia	0.051	2	[2]
SN 2007fs	Ia	0.017	14	[2]; [3]
SN 2007ge	Ia	0.060	1	[2]
SN 2007gi	Ia	0.005	5	[2]
SN 2007gk	Ia	0.027	2	[2]
SN 2007H	Ia	0.044	1	[3]
SN 2007hj	Ia	0.014	22	[1]; [2]; [3]
SN 2007hu	Ia	0.035	4	[2]; [3]
SN 2007if	Ia	0.074	21	[1]; [2]; [3]
SN 2007ir	Ia	0.035	3	[2]; [3]
SN 2007is	Ia	0.030	4	[2]; [3]
SN 2007jd	Ia	0.073	6	[1]
SN 2007jg	Ia	0.037	10	[1]; [3]
SN 2007kd	Ia	0.024	2	[2]; [3]
SN 2007kf	Ia	0.044	2	[2]; [3]
SN 2007kg	Ia	0.006	2	[2]; [3]
SN 2007ki	Ia	0.017	2	[3]
SN 2007kk	Ia	0.041	17	[2]; [3]
SN 2007le	Ia	0.007	58	[1]; [2]; [3]
SN 2007M	Ia	0.021	1	[2]
SN 2007N	Ia	0.013	11	[1]; [2]
SN 2007nq	Ia	0.045	16	[1]; [3]
SN 2007O	Ia	0.036	2	[2]
SN 2007ob	Ia	0.034	2	[3]
SN 2007on	Ia	0.006	32	[1]; [2]
SN 2007oo	Ia	0.030	1	[3]
SN 2007qd	Ia	0.043	1	[2]
SN 2007qe	Ia	0.024	13	[2]; [3]
SN 2007R	Ia	0.031	1	[2]
SN 2007rx	Ia	0.029	3	[2]; [3]
SN 2007ry	Ia	0.040	1	[2]

SN 2007S	Ia	0.014	21	[1]; [2]; [3]
SN 2007sa	Ia	0.005	1	[2]
SN 2007so	Ia	0.030	5	[1]; [3]
SN 2007sr	Ia	0.005	35	[1]; [2]; [3]
SN 2007ss	Ia	0.016	2	[3]
SN 2007st	Ia	0.021	7	[1]
SN 2007su	Ia	0.028	5	[2]; [3]
SN 2007sw	Ia	0.025	5	[3]
SN 2007ux	Ia	0.031	8	[1]; [2]; [3]
SN 2007V	Ia	0.030	1	[2]
SNF20071021-000	Ia	0.025	2	[2]
SN 2008A	Iax	0.016	20	[2]; [3]
SN 2008ae	Iax	0.030	10	[1]; [3]
SN 2008af	Ia	0.034	3	[2]; [3]
SN 2008ai	Ia	0.035	3	[2]; [3]
SN 2008ar	Ia	0.026	35	[1]; [2]; [3]
SN 2008as	Ia	0.020	1	[3]
SN 2008at	Ia	0.035	1	[3]
SN 2008bc	Ia	0.015	14	[1]
SN 2008bd	Ia	0.030	4	[1]
SN 2008bf	Ia	0.025	28	[1]; [2]; [3]
SN 2008bi	Ia	0.013	6	[1]
SN 2008bq	Ia	0.034	4	[1]
SN 2008bt	Ia	0.015	2	[2]
SN 2008bv	Ia	0.056	1	[2]
SN 2008bw	Ia	0.033	1	[2]
SN 2008bz	Ia	0.060	1	[2]
SN 2008C	Ia	0.017	16	[1]; [2]; [3]
SN 2008ca	Ia	0.132	1	[2]
SN 2008cb	Ia	0.165	1	[2]
SN 2008cd	Ia	0.007	1	[2]
SN 2008cf	Ia	0.046	1	[2]
SN 2008cl	Ia	0.063	1	[2]
SN 2008ct	Ia	0.025	1	[2]
SN 2008db	Ia	0.019	3	[2]
SN 2008dh	Ia	0.037	2	Sternberg et al. 2011
SN 2008dr	Ia	0.041	5	[2]
SN 2008ds	Ia	0.021	11	[2]
SN 2008dt	Ia	0.035	3	[2]
SN 2008dx	Ia	0.023	4	[2]
SN 2008E	Ia	0.034	1	[3]
SN 2008ec	Ia	0.016	7	[2]
SN 2008ee	Ia	0.013	3	[2]
SN 2008eg	Ia	0.034	1	[9]
SN 2008ei	Ia	0.038	4	[2]
SN 2008ek	Ia	0.034	1	Blondin et al. 2008
SN 2008er	Ia	0.017	1	[2]
SN 2008ey	Ia	0.018	1	[2]
SN 2008ez	Ia	0.023	1	[2]
SN 2008ff	Ia	0.019	7	[1]
SN 2008fg	Ia	0.011	1	[2]
SN 2008fj	Ia	0.027	1	[2]
SN 2008fl	Ia	0.020	5	[1]
SN 2008fp	Ia	0.006	4	[1]
SN 2008fr	Ia	0.048	5	[1]; [2]
SN 2008fu	Ia	0.052	2	[1]
SN 2008fv	Ia	0.009	3	[1]
SN 2008fx	Ia	0.055	1	[2]
SN 2008ge	Iax	0.004	1	[2]
SN 2008gh	Ia	0.034	2	[2]
SN 2008gl	Ia	0.034	6	[1]
SN 2008go	Ia	0.062	4	[1]
SN 2008gp	Ia	0.033	4	[1]
SN 2008gs	Ia	0.063	1	[2]
SN 2008gt	Ia	0.067	2	[2]
SN 2008gw	Ia	0.068	1	[2]
SN 2008gy	Ia	0.029	1	[2]
SN 2008ha	Ia	0.005	3	[2]
SN 2008hj	Ia	0.038	11	[1]; [2]
SN 2008hk	Ia	0.036	1	[2]
SN 2008hm	Ia	0.020	1	[5]
SN 2008hq	Ia	0.068	1	[2]
SN 2008hr	Ia	0.076	1	[2]
SN 2008hs	Ia	0.017	1	[2]
SN 2008hu	Ia	0.050	5	[1]; [2]
SN 2008hv	Ia	0.013	15	[1]; [5]
SN 2008hy	Ia	0.008	2	[2]; [5]
SN 2008hz	Ia	0.072	1	[2]
SN 2008ia	Ia	0.022	11	[1]
SN 2008L	Ia	0.019	2	[2]; [3]
SN 2008Q	Ia	0.008	9	[2]; [3]
SN 2008R	Ia	0.013	9	[1]; [3]
SN 2008Y	Ia	0.070	2	[3]
SN 2008Z	Ia	0.021	18	[2]; [3]
SN 2009aa	Ia	0.027	16	[1]
SN 2009ab	Ia	0.011	8	[1]
SN 2009ad	Ia	0.028	9	[1]

SN 2009ae	Ia	0.031	1	[5]
SN 2009ag	Ia	0.009	7	[1]
SN 2009al	Ia	0.022	6	[1]
SN 2009an	Ia	0.009	2	[5]
SN 2009bp	Ia	–	1	[5]
SN 2009bs	Ia	0.030	2	[5]
SN 2009bv	Ia	0.037	1	[5]
SN 2009cz	Ia	0.021	5	[1]; [5]
SN 2009D	Ia	0.025	7	[1]; [5]
SN 2009dc	Ia-supCh	0.021	18	[1]; Silverman et al. 2011
SN 2009do	Ia	0.227	1	[5]
SN 2009ds	Ia	0.019	2	[5]
SN 2009en	Ia	0.047	2	[5]
SN 2009ep	Ia	0.024	2	[5]
SN 2009eq	Ia	0.024	3	[5]
SN 2009eu	Ia	0.030	1	[5]
SN 2009ew	Ia	0.090	2	[5]
SN 2009F	Ia	0.013	6	[1]
SN 2009fl	Ia	0.029	2	[5]
SN 2009ft	Ia	0.057	1	[5]
SN 2009fu	Ia	0.017	1	[5]
SN 2009fv	Ia	0.029	3	[5]
SN 2009fw	Ia	0.028	4	[5]
SN 2009fx	Ia	0.048	1	[5]
SN 2009fy	Ia	0.041	2	[5]
SN 2009gf	Ia	0.019	3	[5]
SN 2009gq	Ia	–	1	[5]
SN 2009gs	Ia	–	3	[5]
SN 2009he	Ia	0.031	1	[5]
SN 2009hi	Ia	0.041	3	[5]
SN 2009hk	Ia	0.020	1	[5]
SN 2009hl	Ia	0.050	2	[5]
SN 2009hn	Ia	0.022	1	[5]
SN 2009ho	Ia	0.062	1	[5]
SN 2009hp	Ia	0.021	1	[5]
SN 2009hr	Ia	0.017	1	[5]
SN 2009hs	Ia	0.027	1	[5]
SN 2009I	Ia	0.026	4	[1]
SN 2009ig	Ia	0.009	16	[5]; Foley et al. 2012b
SN 2009ih	Ia	0.033	1	[5]
SN 2009ix	Ia	–	2	[5]
SN 2009jb	Ia	0.023	3	[5]
SN 2009jg	Ia	–	1	[5]
SN 2009jp	Ia	0.056	1	[5]
SN 2009jr	Ia	0.017	2	[5]
SN 2009kk	Ia	0.013	2	[5]
SN 2009ko	Ia	0.016	2	[5]
SN 2009kq	Ia	0.012	4	[5]
SN 2009le	Ia	0.018	4	[5]; [9]
SN 2009lg	Ia	0.058	1	[5]
SN 2009li	Ia	0.040	1	[5]
SN 2009lr	Ia	–	2	[5]
SN 2009lu	Ia	0.022	1	[5]
SN 2009lv	Ia	–	2	[5]
SN 2009me	Ia	–	2	[5]
SN 2009mh	Ia	0.020	1	[5]
SN 2009mj	Ia	0.020	1	[5]
SN 2009mv	Ia	–	1	[5]
SN 2009mz	Ia	0.009	3	[5]; [9]
SN 2009na	Ia	0.021	3	[5]
SN 2009nk	Ia	0.020	2	[5]
SN 2009nq	Ia	0.016	1	[5]
SN 2009nr	Ia	0.011	4	[5]; [9]
SN 2009P	Ia	0.025	10	[1]
SN 2009V	Ia	0.093	1	[5]
SN 2009Y	Ia	0.009	22	[1]; [5]
SN 2010A	Ia	0.021	2	[5]; [9]
SN 2010ag	Ia	0.034	3	[5]
SN 2010ai	Ia	0.018	1	[5]
SN 2010an	Ia	0.030	3	[5]
SN 2010ao	Ia	0.023	1	[5]
SN 2010at	Ia	0.047	1	[5]
SN 2010au	Ia	0.061	2	[5]
SN 2010ax	Ia	0.051	1	[5]
SN 2010B	Ia	0.010	4	[5]
SN 2010ba	Ia	–	3	[5]
SN 2010bn	Ia	0.053	1	[5]
SN 2010bu	Ia	0.039	2	[5]
SN 2010cp	Ia	0.016	1	[5]
SN 2010cr	Ia	0.022	2	[5]
SN 2010cs	Ia	0.042	1	[5]
SN 2010dl	Ia	0.030	1	[5]
SN 2010eb	Ia	0.008	1	[5]
SN 2010ev	Ia	0.009	14	Gutiérrez et al. 2016
SN 2010gj	Ia	0.037	1	[5]
SN 2010gl	Ia	0.019	2	[5]
SN 2010gv	Ia	–	1	[5]

SN 2010gz	Ia	0.018	1	[5]
SN 2010H	Ia	0.015	3	[5]
SN 2010hh	Ia	0.019	1	[5]
SN 2010hs	Ia	0.041	4	[9]; Maguire et al. 2014
SN 2010hz	Ia	0.026	1	[5]
SN 2010ii	Ia	0.027	2	[5]
SN 2010iw	Ia	0.021	1	[5]
SN 2010ju	Ia	0.015	4	[5]; [9]
SN 2010kg	Ia	0.017	2	[5]
SN 2010N	Ia	0.021	2	[5]
SN 2010V	Ia	–	3	[5]
SN 2010Y	Ia	0.011	4	[5]
SN 2011ae	Ia	0.006	2	Zelaya et al. 2017
SN 2011ao	Ia	0.011	3	[5]
SN 2011ay	Ia	0.021	9	Foley et al. 2013
SN 2011by	Ia	0.003	22	[9]; Silverman et al. 2013a
SN 2011dm	Ia	0.005	1	[5]
SN 2011dn	Ia	0.025	1	[5]
SN 2011dz	Ia	0.024	1	Maguire et al. 2014
SN 2011ek	Ia	0.005	9	Maguire et al. 2014
SN 2011fe	Ia	0.001	79	[5]; Nugent et al. 2011; Parrent et al. 2012; Pereira et al. 2013 Maguire et al. 2014; Mazzali et al. 2014, 2015; Zhang et al. 2016
SN 2011fg	Ia	0.045	2	[5]
SN 2011fk	Ia	0.020	1	[5]
SN 2011fs	Ia	0.021	4	[5]; [9]
SN 2011gy	Ia	0.017	1	[5]
SN 2011H	Ia	0.022	1	[5]
SN 2011hb	Ia	0.029	1	[5]
SN 2011iv	Ia	0.006	2	[5]
SN 2011jh	Ia	0.008	3	[5]
SN 2011jn	Ia	0.047	1	[5]
SN 2011jr	Ia	0.023	2	[5]
SN 2011jt	Ia	0.028	2	[5]
SN 2011K	Ia	0.015	1	[5]
SN 2011U	Ia	0.013	1	[5]
SN 2012B	Ia	0.017	1	[5]
SN 2012cg	Ia	0.001	36	[5]; [9]; Silverman et al. 2012b; Maguire et al. 2013; Marion et al. 2016
SN 2012cu	Ia	0.003	3	[5]
SN 2012de	Ia	0.090	1	[5]
SN 2012dn	Ia	0.010	70	[5]; Childress et al. 2016; Parrent et al. 2016; Yamanaka et al. 2016
SN 2012dv	Ia	0.070	1	[5]
SN 2012E	Ia	0.020	2	[5]; [9]
SN 2012ea	Ia	0.010	2	[5]
SN 2012et	Ia	0.025	4	Rich et al. 2012; [9]
SN 2012fw	Ia	0.019	7	[8]; Maguire et al. 2013
SN 2012gh	Ia	0.070	1	Mahabal et al. 2012
SN 2012gl	Ia	0.009	1	[5]
SN 2012gx	Ia	0.014	1	[5]
SN 2012hd	Ia	0.012	15	[8]; Maguire et al. 2013
SN 2012hr	Ia	0.008	15	[8]; Maguire et al. 2013; Childress et al. 2015, 2016
SN 2012ht	Ia	0.004	49	[5]; [8]; Maguire et al. 2013; Yamanaka et al. 2015
SN 2012ij	Ia	0.010	4	[5]
SN 2012Z	Ia	0.007	37	Foley et al. 2013; Stritzinger et al. 2015; Yamanaka et al. 2015
SN 2013aa	Ia	0.004	25	Maguire et al. 2013; Childress et al. 2015, 2016; Kumar et al. 2023
SN 2013aj	Ia	0.009	12	[8]; Maguire et al. 2013; Childress et al. 2016
SN 2013ao	Ia	0.030	24	[8]; Maguire et al. 2013; Childress et al. 2016
SN 2013bs	Ia	0.028	1	Drake et al. 2013
SN 2013ct	Ia	0.004	1	[5]
SN 2013dh	Ia	0.013	18	[5]; Childress et al. 2016
SN 2013di	Ia	0.024	2	[5]
SN 2013dj	Ia	–	1	[5]
SN 2013dr	Ia	0.017	1	Ciabattari et al. 2013
SN 2013dy	Ia	0.004	14	Zheng et al. 2013; Pan et al. 2015
SN 2013E	Ia	0.009	5	[5]
SN 2013fa	Ia	0.015	1	[5]
SN 2013fw	Ia	0.017	2	[5]; Childress et al. 2016
SN 2013gh	Ia	0.009	8	[5]; Childress et al. 2016
SN 2013gq	Ia	0.014	7	[5]; Childress et al. 2016
SN 2013gs	Ia	0.017	2	[5]
SN 2013gy	Ia	0.014	5	[5]; Childress et al. 2015; Mazzali et al. 2015
SN 2013hs	Ia	0.019	1	[5]
SN 2013Q	Ia	0.017	2	[5]
SN 2013S	Ia	0.019	1	[5]
SN 2013U	Ia	0.034	8	[8]; Maguire et al. 2013
SN 2014ag	Ia	0.032	1	[5]
SN 2014ao	Ia	0.014	5	[5]; Childress et al. 2016
SN 2014ck	Ia	0.005	2	[5]
SN 2014da	Ia	0.014	1	[5]
SN 2014dg	Ia	0.004	11	[5]
SN 2014dl	Ia	0.033	1	[5]
SN 2014dm	Ia	0.033	1	[5]
SN 2014dt	Ia	0.005	13	[5]; Foley et al. 2015, 2016a
SN 2014ek	Iax	0.023	10	Li et al. 2018
SN 2014J	Ia	0.001	141	[5]; Childress et al. 2015; Galbany et al. 2016b; Srivastav et al. 2016; Maeda et al. 2016
SN 2015ac	Ia-91bg	0.017	1	[5]
SN 2015bd	Ia	0.019	5	[5]
SN 2015bp	Ia	0.004	3	[5]

SN 2015F	Ia	0.005	45	[8]; Foley et al. 2016b; Graham et al. 2017
SN 2015H	Ia	0.012	1	[5]
SN 2015N	Ia	0.019	11	[5]
SN 2016aew	Ia	0.025	1	[8]
SN 2016aqt	Ia-pec	0.050	3	[5]
SN 2016blh	Ia	0.024	1	[5]
SN 2016bln	Ia	0.023	3	[5]
SN 2016bsa	Ia	0.014	1	[5]
SN 2016ccj	Ia-pec	0.030	1	[5]
SN 2016cmn	Ia	0.018	1	[5]
SN 2016coj	Ia	0.004	22	[5]; Zheng et al. 2017
SN 2016F	Ia	0.016	1	[5]
SN 2016fbk	Ia	0.036	1	Gagliano et al. 2016
SN 2016ffh	Ia	0.018	2	Terreran et al. 2016
SN 2016flv	Ia	–	2	[5]
SN 2016hvl	Ia	0.013	3	[5]; [8]
SN 2016ije	Ia-91bg	0.040	1	[5]
SN 2016zc	Ia	0.034	1	[5]
SN 2017cbv	Ia	0.004	26	[8]; Hosseinzadeh et al. 2017a; Kumar et al. 2023
SN 2017cfd	Ia	0.012	12	[5]; Han et al. 2020
SN 2017drh	Ia	0.006	8	[5]
SN 2017dwp	Ia	0.033	3	[5]
SN 2017dws	Ia	0.082	1	[5]
SN 2017erp	Ia	0.006	17	[5]
SN 2017fgc	Ia	0.008	12	[5]
SN 2017glx	Ia	0.011	5	[5]
SN 2017hbi	Ia	0.040	6	[5]
SN 2017hou	Ia	0.017	3	[5]
SN 2017hpa	Ia	0.016	5	[5]
SN 2017igr	Ia	0.025	1	[5]
SN 2017iji	Ia	0.013	3	[5]
SN 2017iws	Ia	0.091	1	[5]
SN 2017ixg	Ia	0.028	2	[5]
SN 2018aae	Ia	0.029	1	[5]
SN 2018aoz	Ia	0.006	2	[5]
SN 2018bsn	Ia	0.059	1	[5]
SN 2018cni	Ia-pec	0.032	1	[5]
SN 2018dem	Ia	0.060	1	Zheng et al. 2018
SN 2018eqq	Ia	0.016	1	[5]
SN 2018evt	Ia-CSM	0.025	8	[8]
SN 2018feb	Ia	0.015	6	[5]
SN 2018gl	Ia	0.018	1	[5]
SN 2018gv	Ia	0.005	2	[5]
SN 2018hfp	Ia	0.029	3	[5]
SN 2018hfr	Ia-91T	0.023	3	[5]
SN 2018hhn	Ia	0.029	3	[5]
SN 2018htt	Ia	0.009	1	[5]
SN 2018hzg	Ia	0.022	1	[5]
SN 2018jaz	Ia	0.023	1	[5]
SN 2018oh	Ia	0.011	1	[5]
SN 2018pc	Ia	0.009	1	[5]
SN 2018pv	Ia	0.003	1	[5]
SN 2019ein	Ia	0.008	55	Xi et al. 2022
SN 2019yvv	Ia	0.009	27	Miller et al. 2020; Tucker et al. 2021
SN 2020rea	Ia-pec	0.029	1	Poidevin et al. 2020
SN 2021fxy	Ia	0.009	12	DerKacy et al. 2023
SN 2021gno	Ia-Ca-rich	0.006	17	Jacobson-Galán et al. 2022
SN 2021hpr	Ia	0.009	9	Zhang et al. 2022
SN 2021inl	Ia-Ca-rich	0.018	4	Jacobson-Galán et al. 2022
SN 2022ilv	Ia-supCh	0.026	21	Srivastav et al. 2023
SNhunt276	Ia	–	1	[5]
SNF20080514-002	Ia	0.022	20	[2]; [6]
SNF20080522-000	Ia	0.045	13	[3]
SNF20080522-011	Ia	0.038	12	[3]
SNF20080623-001	Ia	0.043	3	[3]
SNF20080720-001	Ia	0.021	5	[3]
SNF20080825-006	Ia	0.042	1	[2]
SNF20080825-010	Ia	0.042	1	[2]
SNF20080909-030	Ia	0.034	3	[2]
SNF20080920-000	Ia	0.034	2	[2]
ROTSE3125642	Ia	0.024	2	[2]
LSQ12dbr	Ia	0.020	2	[9]; Maguire et al. 2013
LSQ12fhe	Ia	–	1	[5]
LSQ12fuk	Ia	0.020	1	Maguire et al. 2013
LSQ12fxd	Ia	0.031	19	[8]; Maguire et al. 2013
LSQ12gdj	Ia	0.030	34	[8]; Maguire et al. 2013; Childress et al. 2016
LSQ12hzj	Ia	0.029	2	Maguire et al. 2013
PTF09dlc	Ia	0.068	2	[5]
PTF09dnp	Ia	0.037	2	[5]
PTF12iiq	Ia	0.029	1	Maguire et al. 2013
PTF12jgb	Ia	0.028	1	Maguire et al. 2013
iPTF13dge	Ia	0.016	19	[8]; Childress et al. 2016
GAlA15aba	Ia	–	1	[5]
GAlA15abu	Ia	–	1	[5]
GAlA15aby	Ia	–	1	[5]
PS-15cku	Ia	–	1	[5]
PS-15cut	Ia	–	1	[5]

PS-15cwx	Ia	–	1	[5]
PS-16ud	Ia	–	1	[5]
PSNJ09100885+500	Ia-pec	0.026	7	[5]
SNe II				
SN 1948B	II	–	18	Casebeer et al. 2000
SN 1961F	II	0.005	3	Blaylock et al. 2000
SN 1961I	II	0.005	6	Blaylock et al. 2000
SN 1961V	II	0.002	3	Blaylock et al. 2000
SN 1964F	II	0.005	1	Blaylock et al. 2000
SN 1964H	II	0.003	1	Blaylock et al. 2000
SN 1969L	II	0.002	7	Benetti 1991; Barbon et al. 1999
SN 1970A	II	-0.001	1	Blaylock et al. 2000
SN 1979C	II	0.005	4	Branch et al. 1981
SN 1986E	II	0.004	2	Cappellaro et al. 1995
SN 1986L	II	0.004	31	[4]
SN 1987A	II	0.000	55	Blanco et al. 1987; Phillips et al. 1988; Pun et al. 1995
SN 1988A	II	0.005	9	[4]; Turatto et al. 1993a
SN 1988H	II	0.007	3	Turatto et al. 1993a
SN 1988Z	II	0.023	21	Turatto et al. 1993b; Aretxaga et al. 1999
SN 1989C	II	0.006	3	Turatto et al. 1993a
SN 1990ae	II	0.025	1	Gómez & López 2000
SN 1990ag	II	0.054	1	Gómez & López 2000
SN 1990E	II	0.004	29	[4]; Gómez & López 2000
SN 1990H	II	0.005	1	Gómez & López 2000
SN 1990K	II	0.005	32	[4]; Gómez & López 2000
SN 1990Q	II	0.006	2	Gómez & López 2000
SN 1990V	II	0.034	1	Gómez & López 2000
SN 1990X	II	0.028	3	Gómez & López 2000
SN 1991al	II	0.010	8	[4]
SN 1991ao	II	0.016	1	Gómez & López 2000
SN 1991C	II	0.028	1	Gómez & López 2000
SN 1991G	II	0.003	2	Blanton et al. 1995
SN 1991H	II	0.018	1	Gómez & López 2000
SN 1991J	II	0.011	1	Gómez & López 2000
SN 1992aa	II	0.033	3	Gómez & López 2000
SN 1992ab	II	0.010	3	Gómez & López 2000
SN 1992af	II	0.018	5	[4]
SN 1992am	II	0.048	2	[4]
SN 1992ba	II	0.004	10	[4]
SN 1992C	II	0.010	2	Gómez & López 2000
SN 1992H	II	0.006	32	Clocchiatti et al. 1996; Filippenko 1997; Gómez & López 2000
SN 1993A	II	0.029	2	[4]
SN 1993K	II	0.009	17	[4]
SN 1993S	II	0.033	4	[4]
SN 1994aj	II	0.032	28	Benetti et al. 1998
SN 1994N	II	0.010	4	Pastorello et al. 2004
SN 1995ad	II	0.006	11	Inserra et al. 2013
SN 1996al	II	0.007	37	Benetti et al. 2016
SN 1996W	II	0.006	12	Inserra et al. 2013
SN 1997ab	II	0.012	1	Gómez & López 2000
SN 1997cy	II	0.059	15	Turatto et al. 2000
SN 1997D	II	0.004	16	Benetti et al. 2001
SN 1998A	II	0.007	10	Pastorello et al. 2005
SN 1998dn	II	0.004	1	Gómez & López 2000
SN 1999bg	II	0.004	1	Faran et al. 2014a
SN 1999br	II	0.003	8	[4]
SN 1999ca	II	0.009	4	[4]
SN 1999co	II	0.031	1	Faran et al. 2014b
SN 1999cr	II	0.020	6	[4]
SN 1999D	II	0.010	4	Faran et al. 2014a
SN 1999eg	II	0.022	2	[4]
SN 1999em	II	0.002	59	[4]; [6]
SN 1999eu	II	0.004	4	Pastorello et al. 2004
SN 1999ga	II	0.005	4	Pastorello et al. 2009
SN 1999gi	II	0.002	51	Leonard et al. 2002; Shivvers et al. 2017a
SN 2000bs	II	0.028	2	Faran et al. 2014a
SN 2000cb	II	0.006	8	[4]
SN 2000dc	II	0.010	3	Faran et al. 2014b
SN 2000dj	II	0.015	5	Faran et al. 2014a
SN 2001bq	II	0.009	3	Faran et al. 2014a
SN 2001cm	II	0.006	5	Faran et al. 2014a
SN 2001cy	II	0.015	6	Faran et al. 2014b
SN 2001dc	II	–	3	Pastorello et al. 2004
SN 2001do	II	0.010	5	Faran et al. 2014b
SN 2001ez	II	0.013	1	Hicken et al. 2017
SN 2001hg	II	0.009	4	Faran et al. 2014a
SN 2001X	II	0.005	12	Faran et al. 2014a
SN 200210	II	0.051	8	[4]
SN 2002an	II	0.013	5	Faran et al. 2014a
SN 2002bx	II	0.008	4	Faran et al. 2014a
SN 2002ca	II	0.011	4	Faran et al. 2014a
SN 2002ew	II	0.030	7	[4]
SN 2002fa	II	0.060	6	[4]
SN 2002gd	II	0.009	29	[4]; Faran et al. 2014a
SN 2002gw	II	0.010	11	[4]
SN 2002hh	II	–	9	Faran et al. 2014a
SN 2002hj	II	0.024	8	[4]

SN 2002hx	II	0.031	9	[4]
SN 2002ig	II	0.077	5	[4]
SN 2003B	II	0.004	9	[4]
SN 2003bj	II	0.012	10	[4]
SN 2003bl	II	0.014	8	[4]
SN 2003bn	II	0.013	12	[4]
SN 2003ci	II	0.030	7	[4]
SN 2003cn	II	0.018	5	[4]
SN 2003cx	II	0.037	6	[4]
SN 2003dq	II	0.046	3	[4]
SN 2003E	II	0.015	9	[4]
SN 2003ef	II	0.014	6	[4]
SN 2003eg	II	0.025	5	[4]
SN 2003ej	II	0.017	3	[4]
SN 2003fb	II	0.018	4	[4]
SN 2003gd	II	0.002	9	[4]; Faran et al. 2014a
SN 2003hd	II	0.040	9	[4]
SN 2003hf	II	0.031	3	Faran et al. 2014b
SN 2003hg	II	0.014	7	[4]
SN 2003hk	II	0.023	5	[4]; Faran et al. 2014b
SN 2003hl	II	0.008	11	[4]; Faran et al. 2014a
SN 2003hn	II	0.004	10	[4]
SN 2003ho	II	0.014	5	[4]
SN 2003ib	II	0.025	5	[4]
SN 2003ie	II	0.002	2	Harutyunyan et al. 2008
SN 2003ip	II	0.018	4	[4]
SN 2003iq	II	0.008	9	[4];Faran et al. 2014a
SN 2003T	II	0.028	6	[4]
SN 2003Z	II	0.004	11	Faran et al. 2014a
SN 2004A	II	0.003	2	Hendry et al. 2006; Silverman et al. 2017
SN 2004dj	II	0.0004	13	Vinkó et al. 2009; Silverman et al. 2017; Meikle et al. 2011; Leonard et al. 2006
SN 2004du	II	0.017	3	Faran et al. 2014a
SN 2004dy	II	0.031	3	[4]
SN 2004eg	II	0.008	2	Spiro et al. 2014
SN 2004ej	II	0.009	9	[4]
SN 2004ek	II-87A	0.017	6	Taddia et al. 2016
SN 2004em	II-87A	0.015	5	Taddia et al. 2016
SN 2004er	II	0.015	10	[4]
SN 2004et	II	-	39	Faran et al. 2014a
SN 2004fb	II	0.020	4	[4]
SN 2004fc	II	0.006	10	[4]
SN 2004fx	II	0.009	10	[4]
SN 2005af	II	0.002	9	[4]
SN 2005an	II	0.011	7	[4]
SN 2005au	II	0.019	1	Modjaz et al. 2005
SN 2005ay	II	0.003	10	Gal-Yam et al. 2008; Faran et al. 2014a
SN 2005ci	II-87A	0.008	4	Taddia et al. 2016
SN 2005cs	II	0.002	40	Faran et al. 2014a
SN 2005dk	II	0.016	7	[4]
SN 2005dn	II	0.011	8	[4]
SN 2005dq	II	0.022	3	Faran et al. 2014b
SN 2005dr	II	0.038	1	[4]
SN 2005dt	II	0.026	1	[4]
SN 2005dw	II	0.018	3	[4]
SN 2005dx	II	0.027	1	[4]
SN 2005dz	II	0.019	9	[4]
SN 2005es	II	0.038	1	[4]
SN 2005gn	II	0.040	2	[4]
SN 2005gz	II	0.028	1	[4]
SN 2005J	II	0.014	11	[4]
SN 2005K	II	0.027	2	[4]
SN 2005kh	II	0.008	5	[4]
SN 2005lw	II	0.026	16	[4]
SN 2005me	II	0.022	1	[4]
SN 2005Z	II	0.019	9	[4]
SN 2006ai	II	0.015	17	[4]
SN 2006at	II	0.015	1	Hicken et al. 2017
SN 2006au	II	0.022	13	[4]
SN 2006bc	II	0.005	6	[4]
SN 2006be	II	0.007	10	[4]; Hicken et al. 2017
SN 2006bl	II	0.032	7	[4]; Hicken et al. 2017
SN 2006bp	II	0.004	16	Quimby et al. 2007
SN 2006ca	II	0.009	4	Sternberg et al. 2011; Hicken et al. 2017
SN 2006cd	II	0.037	1	Hicken et al. 2017
SN 2006ee	II	0.015	11	[4]; de Jaeger et al. 2019
SN 2006ek	II	0.020	1	de Jaeger et al. 2019
SN 2006it	II	0.016	6	[4]
SN 2006iw	II	0.031	6	[4]
SN 2006ms	II	0.015	2	[4]
SN 2006ov	II	0.005	8	Spiro et al. 2014; Silverman et al. 2017
SN 2006qr	II	0.015	11	[4]
SN 2006V	II	0.016	16	[4]
SN 2006Y	II	0.034	16	[4]
SN 2007aa	II	0.005	12	[4]
SN 2007ab	II	0.024	5	[4]
SN 2007ad	II	0.028	1	Hicken et al. 2017
SN 2007ah	II	0.019	1	Hicken et al. 2017

SN 2007am	II	0.010	3	[4]
SN 2007av	II	0.005	5	[4]; Hicken et al. 2017
SN 2007ay	II	0.015	3	[4]; [7]
SN 2007be	II	0.013	1	Hicken et al. 2017
SN 2007bf	II	0.018	5	[4]; Hicken et al. 2017
SN 2007ck	II	0.027	7	Hicken et al. 2017; de Jaeger et al. 2019
SN 2007ct	II	0.014	1	Hicken et al. 2017
SN 2007fz	II	0.014	4	Faran et al. 2014b
SN 2007hm	II	0.020	8	[4]
SN 2007hv	II	0.017	1	Hicken et al. 2017
SN 2007il	II	0.021	12	[4]
SN 2007it	II	0.004	13	[4]
SN 2007ld	II	0.023	9	[4]
SN 2007oc	II	0.007	19	[4]
SN 2007od	II	0.006	32	[4]; Hicken et al. 2017; de Jaeger et al. 2019
SN 2007P	II	0.041	9	[4]
SN 2007Q	II	0.029	2	Hicken et al. 2017
SN 2007rw	II	0.009	4	[6]
SN 2007sq	II	0.015	9	[4]
SN 2007U	II	0.026	7	[4]
SN 2007W	II	0.010	7	[4]
SN 2007X	II	0.009	12	[4]
SN 2007Z	II	0.018	2	[4]
SN 2008ag	II	0.015	22	[4]
SN 2008aw	II	0.010	21	[4]; de Jaeger et al. 2019
SN 2008bh	II	0.014	6	[4]
SN 2008bj	II	0.019	19	Hicken et al. 2017
SN 2008bk	II	0.001	38	[4]
SN 2008bm	II	0.032	5	[4]
SN 2008bn	II	0.024	12	Hicken et al. 2017
SN 2008bp	II	0.009	7	[4]
SN 2008br	II	0.010	4	[4]
SN 2008bu	II	0.022	8	[4]
SN 2008bx	II	0.008	7	Hicken et al. 2017; de Jaeger et al. 2019
SN 2008cn	II	0.009	1	Maguire et al. 2012
SN 2008ea	II	0.014	5	de Jaeger et al. 2019
SN 2008ex	II	0.013	2	de Jaeger et al. 2019
SN 2008F	II	0.018	3	[4]
SN 2008fq	III/L/n	0.011	11	[4]; Faran et al. 2014b
SN 2008ga	II	0.015	3	[4]
SN 2008gi	II	0.024	8	[4]; de Jaeger et al. 2019
SN 2008gq	II	0.012	2	[4]
SN 2008gr	II	0.023	6	[4]
SN 2008H	II	0.014	1	[4]
SN 2008hg	II	0.019	7	[4]
SN 2008ho	II	0.010	3	[4]
SN 2008if	II	0.011	24	[4]; de Jaeger et al. 2019
SN 2008il	II	0.021	3	[4]
SN 2008in	II	0.005	17	[4]; de Jaeger et al. 2019
SN 2008K	II	0.027	15	[4]
SN 2008M	II	0.008	12	[4]
SN 2008N	II	0.008	2	[4]
SN 2008V	II	0.014	3	[4]
SN 2008W	II	0.019	12	[4]
SN 2009A	II	0.017	5	[4]
PTF09ij	II	0.124	1	Khazov et al. 2016
SN 2009ah	II	0.014	1	[4]
SN 2009aj	II	0.010	14	[4]
SN 2009ao	II	0.011	9	[4]
SN 2009at	II	0.005	3	de Jaeger et al. 2019
SN 2009au	II	0.009	11	[4]
SN 2009ay	II	0.022	2	de Jaeger et al. 2019
SN 2009bu	II	0.012	6	[4]
SN 2009bw	II	0.004	20	Inserra et al. 2012
SN 2009bz	II	0.011	6	[4]
SN 2009dd	II	0.003	7	Inserra et al. 2013
SN 2009E	II	0.006	13	Pastorello et al. 2012
SN 2009hz	II	0.025	1	de Jaeger et al. 2019
SN 2009ib	II	0.004	12	Takáts et al. 2015
SN 2009js	II	0.005	4	de Jaeger et al. 2019
SN 2009kr	II	0.006	8	Elias-Rosa et al. 2010
SN 2009lq	II	0.044	1	Stritzinger & Morrell 2009
SN 2009md	II	0.004	10	Fraser et al. 2011
SN 2009N	II	0.003	64	[4]; Maguire et al. 2012; Takáts et al. 2014; de Jaeger et al. 2019
SN 2009W	II	0.017	1	[4]
PTF10abyy	II	0.030	1	Khazov et al. 2016
PTF10gva	II	0.028	1	Khazov et al. 2016
PTF10uls	II	0.044	1	Khazov et al. 2016
SN 2010aj	II	0.021	5	Inserra et al. 2013
SN 2010id	II	0.016	5	Gal-Yam et al. 2011; de Jaeger et al. 2019
PTF11iqb	II	0.013	1	Khazov et al. 2016
SN 2011cj	II	0.007	5	de Jaeger et al. 2019
SN 2011cl	II	0.025	1	Schulze et al. 2021
SN 2011ef	II	0.013	3	de Jaeger et al. 2019
SN 2011fd	II	0.007	6	de Jaeger et al. 2019
CSS120416	II	0.065	2	[8]
SSS120807	II	0.030	1	[8]

LSQ12blb	II	0.052	1	[8]
PTF12gmn	II	0.031	1	Khazov et al. 2016
PTF12krf	II	0.062	1	Khazov et al. 2016
SN 2012A	II	0.002	3	de Jaeger et al. 2019
SN 2012ak	II	0.041	1	Tomasella et al. 2012
SN 2012aw	II	0.003	52	de Jaeger et al. 2019
SN 2012ck	II	0.042	4	de Jaeger et al. 2019
SN 2012ec	II	0.005	87	[8]; Maund et al. 2013; Childress et al. 2016
SN 2012fs	II	0.015	1	[8]
SN 2012fy	II	0.020	1	[8]
SNhunt141	II	0.004	1	[8]
ASASSN-13co	II	0.023	3	Childress et al. 2016
LSQ13cuw	II	0.250	11	[8]
LSQ13fn	II	0.064	29	[8]
OGLE2013-SN-011	II	0.050	1	Poznanski et al. 2015
OGLE2013-SN-045	II	0.100	1	Poznanski et al. 2015
OGLE2013-SN-046	II	0.070	1	Poznanski et al. 2015
OGLE2013-SN-047	II	0.060	1	Poznanski et al. 2015
OGLE2013-SN-048	II	0.060	1	Poznanski et al. 2015
OGLE2013-SN-135	II	0.057	1	Poznanski et al. 2015
OGLE2013-SN-144	II	0.040	1	Poznanski et al. 2015
PTF13dkk	II	0.009	1	Khazov et al. 2016
SN 2013ab	II	0.005	14	de Jaeger et al. 2019
SN 2013ai	II	0.009	23	[8]; Childress et al. 2016
SN 2013am	II	0.003	31	Tomasella et al. 2018; de Jaeger et al. 2019
SN 2013bu	II	0.003	1	Tomasella 2013
SN 2013by	II	0.004	15	Valenti et al. 2015; Childress et al. 2016; Black et al. 2017
SN 2013ej	II	0.002	34	de Jaeger et al. 2019
SN 2013fp	II	0.012	1	de Jaeger et al. 2019
SN 2013fs	II	0.012	42	[8]; Childress et al. 2016; Yaron et al. 2017; Childress et al. 2016
SN 2013ft	II	0.010	3	Childress et al. 2016; Khazov et al. 2016
SN 2013gd	II	0.013	2	de Jaeger et al. 2019
SN 2013hj	II	0.007	5	Childress et al. 2016
SN 2013K	II	0.008	32	Tomasella et al. 2018
ASASSN-14dq	II	0.010	7	Singh et al. 2018
ASASSN-14ha	II	0.005	11	Childress et al. 2016
ASASSN-14jb	II	0.006	11	Childress et al. 2016
ASASSN-14kg	II	0.014	7	Valenti et al. 2016
LSQ14gv	II	0.026	2	[8]
OGLE2014-SN-004	II	0.030	1	Poznanski et al. 2015
OGLE2014-SN-009	II	0.056	2	Poznanski et al. 2015
OGLE2014-SN-018	II	0.030	1	Poznanski et al. 2015
PTF14bag	II	0.116	1	Khazov et al. 2016
SN 2014bc	II	0.001	3	Polshaw et al. 2015
SN 2014bi	II	0.002	1	Khazov et al. 2016
SN 2014ce	II	0.011	1	de Jaeger et al. 2019
SN 2014cx	II	0.005	40	[8]; Childress et al. 2016
SN 2014cy	II	0.006	10	de Jaeger et al. 2019
SN 2014dq	II	0.006	4	de Jaeger et al. 2019
SN 2014G	II	0.004	24	de Jaeger et al. 2019
SN 2015be	II	0.009	6	de Jaeger et al. 2019
SN 2015C	II	0.010	4	de Jaeger et al. 2019
SN 2015O	II	0.056	2	de Jaeger et al. 2019
SN 2015V	II	0.005	14	de Jaeger et al. 2019
SN 2015W	II	0.013	3	de Jaeger et al. 2019
SN 2015X	II	0.011	1	de Jaeger et al. 2019
SN 2016adg	II	0.013	6	de Jaeger et al. 2019
SN 2016bkv	II-LL	0.002	22	Hosseinzadeh et al. 2018
SN 2016cok	II	0.002	1	de Jaeger et al. 2019
SN 2016cyx	II	0.014	1	de Jaeger et al. 2019
SN 2016fqr	II	0.012	7	de Jaeger et al. 2019
SN 2016gsd	II	0.067	11	Reynolds et al. 2020
SN 2016hil	II	0.061	4	Irani et al. 2019
SN 2016ija	II	0.003	23	Hosseinzadeh et al. 2017b; Neill 2016
SN 2016X	II	0.004	10	de Jaeger et al. 2019
SN 2017ahn	II	0.009	31	Tartaglia et al. 2021
SN 2017eaw	II	0.0001	43	Szalai et al. 2019
SN 2017faf	II	0.029	6	de Jaeger et al. 2019
SN 2017hta	II	0.006	1	de Jaeger et al. 2019
SN 2017iit	II	0.017	1	de Jaeger et al. 2019
SN 2017jbj	II	0.013	1	de Jaeger et al. 2019
SN 2018hde	II	0.034	1	de Jaeger et al. 2019
SN 2018zd	II	0.003	39	Zhang et al. 2020
SN 2020cxd	II	0.004	9	Valerin et al. 2022
SN 2020jfo	II	0.005	47	Ailawadhi et al. 2023
SN 2021aai	II	0.007	1	Valerin et al. 2022
SN 2021yja	II	0.005	68	Hosseinzadeh et al. 2022
SESNe				
SN 1983V	Ic	0.005	4	[6]
SN 1985F	Ib	0.002	1	Filippenko & Sargent 1986
SN 1987K	Ib	0.003	7	Filippenko 1988
SN 1987M	Ic	0.004	8	Filippenko et al. 1990
SN 1988L	Ic	0.006	7	Matheson et al. 2001
SN 1990aa	Ic	0.017	7	Matheson et al. 2001
SN 1990aj	Ibc	0.005	4	Matheson et al. 2001; Taubenberger et al. 2009
SN 1990U	Ibc	0.008	21	Matheson et al. 2001; Taubenberger et al. 2009
SN 1991A	Ic	0.011	12	Matheson et al. 2001

SN 1991ar	Ib	0.015	4	Matheson et al. 2001
SN 1991D	Ib	0.042	5	Matheson et al. 2001
SN 1991L	SE	0.031	2	Matheson et al. 2001
SN 1991N	Ic	0.003	9	Matheson et al. 2001
SN 1993J	IIfb	—	45	[6]
SN 1994ai	Ibc	0.005	1	[7]
SN 1994I	Ic	0.002	24	[6]
SN 1995bb	SE	0.006	3	[6]
SN 1995F	Ibc	0.005	5	[6]
SN 1996cb	IIfb	0.002	25	[6]
SN 1997B	Ic	0.010	4	[7]; Taubenberger et al. 2009
SN 1997dc	Ib	0.012	2	Matheson et al. 2001
SN 1997dd	IIfb	0.015	2	Matheson et al. 2001
SN 1997dq	Ibc	0.003	7	[6]
SN 1997ef	Ibc	0.012	30	[6]; Matheson et al. 2001
SN 1997ei	Ic	0.011	5	Matheson et al. 2001
SN 1997X	Ibc	0.004	6	[6]
SN 1998bw	Ic	0.009	31	Patat et al. 2001
SN 1998dt	Ib	0.015	7	[6]
SN 1998fa	Ibc	0.025	11	[6]
SN 1998T	Ib	0.010	4	Matheson et al. 2001
SN 1999di	Ib	0.016	6	Matheson et al. 2001
SN 1999dn	Ib	0.009	15	Deng et al. 2000 ; Matheson et al. 2001 ; Benetti et al. 2011
SN 1999ex	Ic	0.011	9	Hamuy et al. 2002
SN 1999P	Ib/c	0.060	5	Matheson et al. 2001
SN 2000cr	Ic	0.012	7	[7]
SN 2000ds	Ib/c	0.005	1	[7]
SN 2000dt	Ib	0.023	6	[7]
SN 2000dv	Ib	0.012	1	[7]
SN 2000ew	Ic	0.004	2	[7]; Taubenberger et al. 2009
SN 2000fn	Ib	0.015	1	[5]
SN 2000H	Ibc	0.013	13	[6]
SN 2001ai	Ib	0.025	2	[6]
SN 2001B	Ib	0.005	10	[7]
SN 2001bb	Ic	0.016	2	[7]
SN 2001cf	IIfb	0.020	1	[7]
SN 2001ch	Ic	0.010	1	[7]
SN 2001ci	Ic	0.004	3	Shivvers et al. 2017a
SN 2001co	Ib/c	0.017	4	[7]
SN 2001dq	Ic	0.031	1	[7]
SN 2001ef	Ic	0.008	4	[7]
SN 2001ej	Ib	0.014	8	[6]
SN 2001em	Ib	0.020	3	[7]
SN 2001eq	Ib	0.025	1	[7]
SN 2001fw	Ib	0.030	3	[7]
SN 2001fx	Ib	0.027	1	[7]
SN 2001gd	IIfb	0.003	3	[6]
SN 2001ig	IIfb	0.003	14	[6]
SN 2001ih	Ib	0.025	1	[7]
SN 2001ii	Ic	0.035	1	[7]
SN 2001is	Ib	0.013	8	Shivvers et al. 2017a
SN 2001M	Ic	0.012	5	Shivvers et al. 2017a
SN 2002ap	SE	0.002	36	[6]
SN 2002au	IIfb	0.018	3	[7]
SN 2002bl	Ic	0.016	4	[7]
SN 2002cg	Ic	0.032	2	[7]
SN 2002cj	Ic	0.023	2	[7]
SN 2002cp	Ib/c	0.017	7	[7]
SN 2002dz	Ib	0.018	1	[7]
SN 2002eg	IIfb	0.026	3	[7]
SN 2002ex	IIfb	0.038	1	[7]
SN 2002gy	IIfb	0.024	1	[7]
SN 2002gz	Ic	0.085	1	[7]
SN 2002hf	Ic	0.019	5	[7]
SN 2002hn	Ic-BL	0.018	3	[7]
SN 2002ho	Ic	0.009	1	[7]
SN 2002hy	Ib-pec	0.012	2	[7]; Harutyunyan et al. 2008
SN 2002hz	Ic	0.018	1	[7]
SN 2002J	Ic	0.012	4	Shivvers et al. 2017a
SN 2002ji	Ibc	0.005	12	[6]
SN 2002jj	Ic	0.014	6	Shivvers et al. 2017a
SN 2002jp	Ic	0.012	2	[7]
SN 2002jz	Ib/c	0.005	6	Shivvers et al. 2017a
SN 2003A	Ib/c	0.022	2	[7]
SN 2003aa	Ic	0.010	9	Shivvers et al. 2017a
SN 2003bg	IIfb	0.005	27	[4]
SN 2003cr	Ic	0.036	3	[7]
SN 2003cv	SE	0.028	4	[4]
SN 2003dg	Ic	0.018	1	[7]
SN 2003dh	Ic-pec	0.169	16	[6]; [7]; Matheson et al. 2003c ; Kosugi et al. 2004
SN 2003ds	Ic	0.030	1	[7]
SN 2003ed	IIfb	0.005	13	Shivvers et al. 2017a
SN 2003ev	Ic	0.024	1	[7]
SN 2003fc	IIfb	0.035	1	[7]
SN 2003gf	Ic	0.009	7	[7]
SN 2003gu	Ib/Ic	0.019	4	[7]
SN 2003H	Ib-pec	0.009	5	Shivvers et al. 2017a

SN 2003hp	Ic	0.021	1	[7]
SN 2003I	Ib	0.018	3	[7]
SN 2003id	Ic	0.008	4	Shivvers et al. 2017a
SN 2003ig	Ic	0.020	1	[7]
SN 2003ih	Ic	0.017	1	[7]
SN 2003is	Ic	0.018	3	[7]
SN 2003iw	Ic	0.016	1	Matheson et al. 2003b
SN 2003jd	Ic-BL	0.019	25	[6]
SN 2003jg	IIB	0.004	1	[7]
SN 2003kb	Ic	0.017	5	[7]
SN 2003ki	IIB	0.025	3	[7]
SN 2003L	Ic	0.021	5	[7]
SN 2004ao	Ib	0.006	30	[6]
SN 2004aw	SE	0.016	15	[6]
SN 2004bf	Ic	0.017	5	[7]
SN 2004bi	IIB	0.022	7	[7]
SN 2004bm	IIB	0.004	2	Shivvers et al. 2017a
SN 2004bs	Ib	0.017	1	Harutyunyan et al. 2008
SN 2004bu	IIB	0.019	4	[7]
SN 2004C	Ic	0.006	17	Shivvers et al. 2017a
SN 2004cc	Ic	0.008	5	Harutyunyan et al. 2008; Shivvers et al. 2017a
SN 2004dc	IIB	0.021	1	[7]
SN 2004dk	Ibc	0.005	3	[6]
SN 2004dn	Ic	0.013	4	[6]
SN 2004dx	IIB	0.030	1	[7]
SN 2004eh	Ic-BL	0.033	1	[7]
SN 2004eu	Ibc	0.022	6	[6]
SN 2004ex	IIB	0.018	7	[4]; [7]
SN 2004fe	Ic	0.018	12	[6]
SN 2004ff	Ibc	0.023	1	[6]
SN 2004ge	Ibc	0.016	1	[6]
SN 2004gj	Ic	0.020	1	[7]
SN 2004gk	Ic	0.0004	31	[6]
SN 2004gn	Ic	0.006	2	[7]
SN 2004gq	Ib	0.006	24	[6]
SN 2004gt	Ic	0.005	19	[6]; [7]; Modjaz et al. 2008; Taubenberger et al. 2009
SN 2004gv	Ib	0.020	4	[6]
SN 2005aj	Ic	0.009	1	[7]
SN 2005ar	Ibc	0.025	2	[6]
SN 2005az	Ic	0.008	22	[6]
SN 2005bf	Ibc	0.019	23	[6]
SN 2005bh	Ic	0.022	6	[7]
SN 2005bj	Ic	0.022	3	Stritzinger et al. 2023
SN 2005bk	Ic	0.024	1	[7]
SN 2005C	Ic	0.046	1	[7]
SN 2005ct	Ic	0.013	3	[7]
SN 2005D	Ic	0.028	1	[7]
SN 2005da	Ibc	0.015	3	[6]
SN 2005ek	Ic	0.017	10	[7]; Drout et al. 2013
SN 2005em	IIB	0.025	2	[4]; [7]
SN 2005eo	Ic	0.017	7	[6]
SN 2005hg	Ib	0.021	18	[6]
SN 2005kf	Ic	0.015	5	[6]
SN 2005kl	Ic	0.003	4	[6]
SN 2005kz	Ic	0.027	1	[7]
SN 2005mf	Ic	0.027	4	[6]
SN 2005nb	Ic	0.024	1	[6]
SN 2005Q	IIB	0.022	2	[4]
SN 2005U	IIB	0.010	4	[6]
SN 2006ab	Ic	0.017	1	[7]
SN 2006aj	Ic	0.033	13	[6]
SN 2006ba	IIB	0.019	6	[4]
SN 2006bf	IIB	0.024	5	[4]
SN 2006ck	Ic	0.024	9	[6]
SN 2006dg	Ic	0.014	1	[7]
SN 2006ea	Ic	0.025	2	[7]
SN 2006ec	Ic	0.026	1	[7]
SN 2006eg	Ib/c	0.013	2	Shivvers et al. 2017a
SN 2006ei	Ib	0.015	2	[7]
SN 2006el	IIB	0.017	7	[6]
SN 2006ep	Ib	0.015	5	[6]
SN 2006fo	Ib	0.021	4	[6]
SN 2006ir	Ic	–	1	[7]
SN 2006iv	Ib	0.008	1	[7]
SN 2006jo	Ib	0.077	1	Östman et al. 2011
SN 2006lc	Ib	0.016	4	[6]
SN 2006ld	Ib	0.014	7	[6]; [7]; Taubenberger et al. 2009
SN 2006lv	Ib	0.008	6	[6]
SN 2006nx	Ic	0.050	3	Östman et al. 2011
SN 2006P	Ib	0.015	1	[7]
SN 2006qk	Ib	0.060	2	Östman et al. 2011
SN 2006qp	Ic	0.012	1	[7]
SN 2006T	IIB	0.008	25	[4]; [6]
SN 2007ag	Ib	0.021	4	[6]; [7]
SN 2007az	IIB	0.007	1	[7]
SN 2007bg	Ic	0.034	2	[6]; [7]
SN 2007C	Ib	0.006	12	[6]

SN 2007ce	Ic	0.046	10	[6]
SN 2007cl	Ic	0.022	6	[6]; [7]
SN 2007D	Ic-bl	0.023	4	[6]; [7]
SN 2007fn	Ic	0.017	1	[7]
SN 2007fo	Ib	0.009	3	[7]
SN 2007go	Ic	0.023	1	[7]
SN 2007gr	Ic	0.002	17	[6]
SN 2007hb	Ic	0.022	2	[6]
SN 2007I	Ic	0.022	4	[6]
SN 2007iq	Ic-bl	0.013	1	[6]
SN 2007jy	Ib	0.182	1	Östman et al. 2011
SN 2007ke	Ib	0.017	1	[7]
SN 2007kj	Ib	0.018	3	[6]
SN 2007ms	Ic	0.039	3	Östman et al. 2011
SN 2007nc	Ib	0.087	1	Östman et al. 2011
SN 2007qx	Ic	0.080	1	Östman et al. 2011
SN 2007ru	Ic-bl	0.015	3	[6]
SN 2007rz	Ic	0.013	2	[6]
SN 2007uy	Ib	0.006	10	[6]
SN 2007Y	Ibc	0.005	11	[7]; Stritzinger et al. 2009
SN 2008an	Ic	0.027	2	[6]
SN 2008ao	Ic	0.015	2	[7]
SN 2008aq	Ib	0.008	24	[4]; [6]
SN 2008ax	Ib	0.002	32	[6]
SN 2008ay	Ib	0.034	1	[7]
SN 2008bo	Ib	0.005	12	[6]
SN 2008cw	Ib	0.032	5	[6]
SN 2008cx	Ib	0.019	1	[7]
SN 2008D	Ib	0.006	12	[6]
SN 2008dq	Ic	0.031	2	[7]
SN 2008du	Ic	0.016	1	[7]
SN 2008dv	Ic	0.007	1	[7]
SN 2008eb	Ib	0.008	2	[7]
SN 2008em	Ic	0.033	1	[7]
SN 2008ew	Ic	0.020	4	[7]
SN 2008fd	Ib	0.018	1	[7]
SN 2008fi	Ib	-	3	[7]
SN 2008fs	Ib	0.039	1	[7]
SN 2008gj	Ib	0.024	2	[7]
SN 2008ht	Ib	0.022	1	[7]
SN 2008ie	Ib	0.014	3	[4]
SN 2008im	Ib	0.008	1	[7]
SN 2009bb	Ic-BL	0.010	11	Pignata et al. 2011
SN 2009C	Ib	0.023	2	[5]; [7]
SN 2009dq	Ib	0.005	2	[4]
SN 2009er	Ib-pec	0.035	9	[6]
SN 2009gi	Ib	0.013	3	[7]
SN 2009gk	Ic	0.026	2	[7]
SN 2009gl	Ic	0.024	1	[7]
SN 2009ha	Ic	0.015	1	[7]
SN 2009hy	Ic	0.025	1	[7]
SN 2009iz	Ib	0.014	10	[6]
SN 2009jf	Ib	0.008	16	[6]
SN 2009jv	Ib	0.016	2	[7]
SN 2009K	Ib	0.012	9	[4]
SN 2009ka	Ib	0.015	2	[7]
SN 2009lj	Ic	0.015	1	[7]
SN 2009lw	Ic	0.017	1	[7]
SN 2009mg	Ib	0.008	10	Oates et al. 2012
SN 2009mi	Ic	0.010	3	[7]
SN 2009np	Ic	0.025	2	[7]
SN 2009Z	Ib	0.025	11	[4]
PTF10vgv	Ic-BL	0.015	13	Corsi et al. 2012 ; Taddia et al. 2019
SN 2010ak	Ic	0.037	1	[7]
SN 2010am	Ic	0.020	1	[7]
SN 2010av	Ib	0.030	1	[7]
SN 2010ay	Ic-BL	0.067	3	[7]; Sanders et al. 2012
SN 2010bh	Ic-BL	0.059	16	Bufano et al. 2012
SN 2010cn	Ib	0.026	3	[7]
SN 2010do	Ib	0.014	1	[7]
SN 2010ei	Ib	0.019	1	[7]
SN 2010ej	Ib	0.052	1	[7]
SN 2010ek	Ib	0.032	1	[7]
SN 2010gk	Ib	0.015	1	[7]
SN 2010gr	Ic	0.017	1	[7]
SN 2010if	Ic	0.039	1	[7]
SN 2010kc	Ib	0.014	1	[7]
SN 2010ma	Ic-BL	0.552	7	Sparre et al. 2011
SN 2010O	Ib	0.010	2	[7]
PTF11kmb	Ib-Ca-rich	0.017	8	Foley 2015 ; Lunnan et al. 2017
SN 2011bm	Ic	0.022	17	Valenti et al. 2012
SN 2011bp	Ib	0.027	1	[7]
SN 2011br	Ib	0.022	1	[7]
SN 2011D	Ib	0.023	1	[7]
SN 2011dh	Ib	0.002	76	[7]; Arcavi et al. 2011 ; Shivvers et al. 2013 ; Ergon et al. 2014
SN 2011ft	Ib	0.017	2	[7]
SN 2011fu	Ib	0.018	44	[7]; Kumar et al. 2013 ; Morales-Garoffolo et al. 2015

SN 2011gd	Ib	0.010	1	[7]
SN 2011hs	I Ib	0.006	23	Bufano et al. 2014
SN 2011jm	I Ib	0.003	1	[7]
SN 2012aa	I Ib	0.080	4	[7]
SN 2012ap	Ic	0.012	20	Milisavljevic et al. 2015
SN 2012au	Ib	0.004	10	[7]; Milisavljevic et al. 2013
SN 2012bz	Ic-GRB	0.280	5	Melandri et al. 2012
SN 2012fh	Ib	0.002	3	[7]
SN 2013bb	I Ib	0.018	16	[8]
SN 2013bn	Ic-BL	0.054	5	[7]; Taddia et al. 2019
SN 2013cu	I Ib	0.025	5	Gal-Yam et al. 2014
SN 2013df	I Ib	0.002	25	[7]; Van Dyk et al. 2014; Childress et al. 2016; Szalai et al. 2016
SN 2013dk	Ic	0.005	4	[7]; Elias-Rosa et al. 2013
SN 2013dx	Ic-GRB	0.145	27	Taddia et al. 2019; D'Elia et al. 2015
SN 2013ek	Ib	0.016	21	[7]; Childress et al. 2016
SN 2013el	Ib-pec	0.018	1	[7]
SN 2013F	I Ib	0.005	2	[8]
SN 2013ge	I Ib	0.004	40	[7]; Drout et al. 2016
SN 2013gl	Ib	0.020	3	[7]
SN 2014as	Ib	0.012	1	[7]
SN 2014bl	Ic	–	1	[7]
SN 2014C	Ib	0.003	18	[7]
SN 2014cp	Ic-BL	0.016	10	[7]; Childress et al. 2016
SN 2014dj	Ic	0.018	3	[7]
SN 2014dp	Ib	0.018	2	Childress et al. 2016
SN 2014ds	I Ib	0.014	3	[7]
SN 2014eh	Ic	0.011	8	[7]; Childress et al. 2016
SN 2014ei	Ib	0.014	8	[7]; Childress et al. 2016
SN 2014L	Ic	0.008	34	[7]; Childress et al. 2016; Zhang et al. 2018
SN 2015ag	Ic	0.016	2	[7]
SN 2015ah	Ib	0.016	16	[7]
SN 2015ap	Ib/c	0.011	34	[7]; Prentice et al. 2019a
SN 2015as	I Ib	0.004	1	Tartaglia et al. 2015
SN 2015bi	I Ib	0.016	2	[7]
SN 2015dj	I Ib	0.009	15	[7]
SN 2015Q	Ib	0.008	6	[7]
SN 2015Y	I Ib	0.008	6	[7]; Childress et al. 2016
SN 2016frp	Ib	0.027	12	[8]; Prentice et al. 2019a
SN 2016gkg	I Ib	0.005	2	Kilpatrick et al. 2017
SN 2016iae	Ib	0.004	23	[8]; Prentice et al. 2019a
SN 2016jdw	Ib	0.019	14	Prentice et al. 2019a
SN 2016P	Ic	0.015	19	[8]; Prentice et al. 2019a
SN 2017bgu	Ib	0.008	14	Prentice et al. 2019a
SN 2017dcc	Ic-BL	0.025	9	[8]; Gutiérrez et al. 2017
SN 2017ein	Ic	0.003	19	Teffs et al. 2021
SN 2017hyh	I Ib	0.012	5	Prentice et al. 2019a
SN 2017ifh	Ic-BL	0.042	5	Prentice et al. 2019a
SN 2017ixz	I Ib	0.024	3	Jones et al. 2017
SN 2018cbz	Ic	0.022	5	Prentice et al. 2019a
SN 2018ie	Ic	0.014	1	Lin et al. 2018
SN 2019cad	Ic	0.027	10	Gutiérrez et al. 2021
SN 2020bio	I Ib	0.008	12	Pellegrino et al. 2023
SN 2021zby	I Ib	0.026	11	Wang et al. 2023
ASASSN-14az	I Ib	0.007	10	[7]
ASASSN-15bd	I Ib	0.008	3	[7]
ASASSN-15ed	Ib	0.049	16	[7]; Pastorello et al. 2015c
ASASSN-15mj	Ib	0.034	3	[7]
ASASSN-15re	Ic-pec	0.030	1	Ochner et al. 2015
iPTF13bvn	Ib	0.004	3	[7]
PS-15cjr	I Ib	0.023	5	[7]
PSNJ0110+3313	I Ib	0.018	1	[7]
PSNJ2241-2147	Ib	0.015	5	[7]
iPTF16asu	Ic-BL	0.187	7	Taddia et al. 2019
Interacting SNe				
SN 1994ak	I In	0.008	3	Ransome 2021
SN 1994Y	I In	0.008	7	Ransome 2021
SN 1995G	I In	0.016	11	Pastorello et al. 2002
SN 1996L	I In	0.033	14	Benetti et al. 1999
SN 1998S	I In	0.003	43	Leonard et al. 2000; Fassia et al. 2001; Pozzo et al. 2004
SN 1999cq	Ibn	0.026	4	Matheson et al. 2000
SN 1999E	I In	0.026	19	Schmidt et al. 1993; Benetti et al. 1994; Gómez & López 2000; Silverman et al. 2013b, 2017
SN 1999eb	I In	0.018	6	Ransome 2021
SN 1999el	I In	0.005	7	Ransome 2021
SN 1999Z	I In	0.051	5	Jha et al. 1999
SN 2000eo	I In	0.010	16	[2]; [9]; Hicken et al. 2017
SN 2000P	I In	0.007	9	Jha et al. 2000; Ransome 2021
SN 2000bg	I In	0.024	5	Jha & Brown 2000, [9]
SN 2001fa	I In	0.017	6	Faran et al. 2014b
SN 2002ao	Ibn	0.005	13	Pastorello et al. 2008; Foley et al. 2007
SN 2002bu	Impostor	0.002	11	Smith et al. 2011
SN 2003G	I In	0.012	11	Shivvers et al. 2017a; Ransome 2021
SN 2003hy	I In	0.024	11	Matheson et al. 2003a, [9]
SN 2005cl	I In	0.026	3	Kiewe et al. 2012
SN 2005cp	I In	0.022	7	Kiewe et al. 2012
SN 2005db	I In	0.015	12	Kiewe et al. 2012
SN 2005gl	I In	0.015	6	Gal-Yam et al. 2007
SN 2005ip	I In	0.007	22	[4]

SN 2005kj	IIn	0.017	20	[4]
SN 2005la	Ib/IIn	0.002	5	[6]
SN 2006aaa	IIn	0.021	9	[4]
SN 2006bo	IIn	0.015	3	[4]
SN 2006bv	IIn?	0.008	1	[9]
SN 2006gy	IIn	0.019	17	Ofek et al. 2007; Smith et al. 2010
SN 2006jc	Ibn	0.006	22	[6]
SN 2006jd	IIn	0.019	19	[4]
SN 2006qq	IIn	0.029	11	[4]
SN 2007ak	IIn	0.016	1	[4]
SN 2007bb	IIn	0.021	1	Arbour et al. 2007
SN 2007cm	IIn	0.016	1	Green 2007
SN 2007pk	IIn-P	0.017	10	Inserra et al. 2013
SN 2007rt	IIn	0.022	7	Trundle et al. 2009
SN 2008aj	IIn	0.025	1	[9]
SN 2008B	IIn	0.019	3	[9]
SN 2008cg	Ia-CSM	0.036	5	Silverman et al. 2013c
SN 2008fq	IIn	0.011	18	Taddia et al. 2013; Faran et al. 2014b
SN 2008ip	IIn	0.015	11	[9]
SN 2008iy	IIn	0.041	2	Miller et al. 2010
SN 2008J	Ia-CSM	0.016	24	[1]
SN 2008S	IIn	0.0002	13	Botticella et al. 2009
SN 2009ip	IIn	0.006	50	Margutti et al. 2014; Fraser et al. 2013; Graham et al. 2014; Childress et al. 2016
SN 2009kn	IIn	0.016	8	Ransome 2021, [9]
SN 2010al	IIn	0.017	13	[7]; Pastorello et al. 2015a
SN 2010jl	IIn	0.011	36	Smith et al. 2012c; Zhang et al. 2012; Borish et al. 2015; Jencson et al. 2016
SN 2010jp	IIn	0.009	10	Smith et al. 2012a; Ransome 2021, [9]
SN 2010mc	IIn	0.035	4	Khazov et al. 2016
SN 2011A	IIn	0.009	11	de Jaeger et al. 2015
SN 2011ap	IIn	0.024	9	[9]
SN 2011fh	IIn	0.008	9	Pessi et al. 2022
SN 2011ht	IIn	0.004	12	Humphreys et al. 2012
SN 2011hw	IIn/Ibn	0.023	21	Smith et al. 2012b; Pastorello et al. 2015a
SN 2011jb	Ia-CSM	0.127	3	Silverman et al. 2013b
SN 2012ca	IIn	0.019	27	[8]
SN 2012y	IIn	0.083	3	Schulze et al. 2021
SN 2013dn	IIn	0.056	12	[8]
SN 2013fc	IIn	0.019	30	[8]; Kangas et al. 2016
SN 2013ff	Impostor	0.005	8	Tartaglia et al. 2016
SN 2013gc	IIn	0.003	8	Reguitti et al. 2019
SN 2013L	IIn	0.017	7	Taddia et al. 2020
SN 2014ab	IIn	0.023	1	[8]
SN 2014es	IIn	0.020	14	[8]
SN 2015da	IIn	0.007	50	Tartaglia et al. 2020
SN 2015G	Ibn	0.005	56	Shivvers et al. 2017b; Hosseinzadeh et al. 2017c
SN 2015J	IIn	0.005	6	Childress et al. 2016
SN 2015U	Ibn	0.014	34	Pastorello et al. 2015e; Shivvers et al. 2016; Hosseinzadeh et al. 2017c
SN 2016aiy	IIn	0.010	8	[8]
SN 2016drl	IIn	0.061	7	[8]
SN 2016eso	IIn	0.016	2	[8]
SN 2016ieq	IIn	0.066	3	[8]
SN 2016jbu	IIn	0.005	31	[8]
SN 2017ben	IIn	0.036	3	[8]
SN 2017cfq	IIn	0.022	4	[8]
SN 2017gir	IIn	0.164	6	[8]
SN 2017hcc	IIn	0.017	6	[8]
SN 2017ijn	IIn	0.050	24	[8]
SN 2018bcc	Ibn	0.064	5	Karamehmetoglu et al. 2021
SN 2018cnf	IIn	0.024	3	[8]
SN 2018khh	IIn	0.023	6	[8]
SN 2019bwb	IIn	0.020	4	[8]
SN 2019esa	IIn	0.009	1	Hiramatsu et al. 2019b
SN 2019hgp	Icn	0.064	33	Gal-Yam et al. 2022; Pellegrino et al. 2022
SN 2019jc	Icn	0.019	4	Pellegrino et al. 2022
SN 2019kbj	Ibn	0.048	2	Hiramatsu et al. 2019a
SN 2019lkr	IIn	0.035	2	Prentice et al. 2019b; Dugas et al. 2019; Nordin et al. 2019
SN 2020uem	Ia-CSM	0.041	9	Uno et al. 2023
SN 2021ckj	Icn	0.143	3	Nagao et al. 2023
SN 2021csp	Icn	0.084	4	Pellegrino et al. 2022
SN 2021foa	IIn	0.008	17	Reguitti et al. 2022
SN 2022ann	Icn	0.049	1	Davis et al. 2022
ASASSN-14il	IIn	0.022	9	Childress et al. 2016
ASASSN-15og	IIn	0.068	7	Stahl et al. 2020
iPTF13beo	Ibn	0.091	2	Gorbikov et al. 2014
iPTF13z	IIn	0.033	10	Nyholm et al. 2017
iPTF14aki	Ibn	0.064	13	Hosseinzadeh et al. 2017c, [8]
iPTF15akq	Ibn	0.109	5	Hosseinzadeh et al. 2017c
iPTF15ul	Ibn	0.066	4	Hosseinzadeh et al. 2017c
LSQ12heq	IIn	0.148	11	[8]
LSQ12hxg	IIn	0.039	15	[8]
LSQ13bxv	IIn	0.125	3	[8]
LSQ13ccw	Ibn	0.060	4	Pastorello et al. 2015b
LSQ13sd	IIn	0.039	2	[8]
LSQ13zm	Impostor	0.029	12	Tartaglia et al. 2016
LSQ14pt	IIn	0.059	17	[8]
OGLE-2012-SN-006	Ibn	0.006	10	Pastorello et al. 2015d, [8]
OGLE-2013-SN-016	IIn	0.074	17	[8]

PTF10gvf	IIn	0.081	3	Khazov et al. 2016
PTF11rfh	Ibn	0.060	4	Hosseinzadeh et al. 2017c
PTF12efc	IIn	0.234	5	Silverman et al. 2013b
PTF12ldy	Ibn	0.106	6	Hosseinzadeh et al. 2017c
SSS130221-133330-194457	IIn	0.096	13	[8]

Additional references: [1] [Folatelli et al. 2013](#); [2] [Silverman et al. 2012a](#); [3] [Blondin et al. 2012](#); [4] [Gutiérrez et al. 2017](#); [5] [Stahl et al. 2020](#); [6] [Modjaz et al. 2014](#); [7] [Shivvers et al. 2019](#); [8] PESSO data release: [Smartt et al. 2015](#); [9] Publically available from WISEREP: [Yaron & Gal-Yam 2012](#).